National Library of Canada
Bibliothèque nationale du Canada

Canadian Theses Service
Services des thèses canadiennes

Ottawa, Canada
K1A 0N4

CANADIAN THESES

THÈSES CANADIENNES

NOTICE

The quality of this microfiche is heavily dependent upon the quality of the original thesis submitted for microfilming. Every effort has been made to ensure the highest quality of reproduction possible.

If pages are missing, contact the university which granted the degree.

Some pages may have indistinct print especially if the original pages were typed with a poor typewriter ribbon or if the university sent us an inferior photocopy.

Previously copyrighted materials (journal articles, published tests, etc.) are not filmed.

Reproduction in full or in part of this film is governed by the Canadian Copyright Act, R.S.C. 1970, c. C-30.

AVIS

La qualité de cette microfiche dépend grandement de la qualité de la thèse soumise au microfilmage. Nous avons tout fait pour assurer une qualité supérieure de reproduction.

S'il manque des pages, veuillez communiquer avec l'université qui a conféré le grade.

La qualité d'impression de certaines pages peut laisser à désirer, surtout si les pages originales ont été dactylographiées à l'aide d'un ruban usé ou si l'université nous a fait parvenir une photocopie de qualité inférieure.

Les documents qui font déjà l'objet d'un droit d'auteur (articles de revue, examens publiés, etc.) ne sont pas microfilmés.

La reproduction, même partielle, de ce microfilm est soumise à la Loi canadienne sur le droit d'auteur, SRC 1970, c. C-30.

THIS DISSERTATION
HAS BEEN MICROFILMED
EXACTLY AS RECEIVED

LA THÈSE A ÉTÉ
MICROFILMÉE TELLE QUE
NOUS L'AVONS REÇUE

NL-339 (r.86/06)

Canada

THE UNIVERSITY OF ALBERTA

Ultramafic Xenoliths from British Columbia, Canada: Petrological and Dissolution studies

by

M. Brearley

A THESIS

SUBMITTED TO THE FACULTY OF GRADUATE STUDIES AND RESEARCH

IN PARTIAL FULFILMENT OF THE REQUIREMENTS FOR THE DEGREE

OF Doctor of Philosophy

Department of Geology

EDMONTON, ALBERTA

Spring, 1986

Permission has been granted to the National Library of Canada to microfilm this thesis and to lend or sell copies of the film.

The author (copyright owner) has reserved other publication rights, and neither the thesis nor extensive extracts from it may be printed or otherwise reproduced without his/her written permission.

L'autorisation a été accordée à la Bibliothèque nationale du Canada de microfilmer cette thèse et de prêter ou de vendre des exemplaires du film.

L'auteur (titulaire du droit d'auteur) se réserve les autres droits de publication; ni la thèse ni de longs extraits de celle-ci ne doivent être imprimés ou autrement reproduits sans son autorisation écrite.

ISBN 0-315-30190-2

THE UNIVERSITY OF ALBERTA

RELEASE FORM

NAME OF AUTHOR M. Brearley

TITLE OF THESIS Ultramafic Xenoliths from British Columbia, Canada: Petrological and Dissolution studies

DEGREE FOR WHICH THESIS WAS PRESENTED Doctor of Philosophy

YEAR THIS DEGREE GRANTED Spring, 1986

Permission is hereby granted to THE UNIVERSITY OF ALBERTA LIBRARY to reproduce single copies of this thesis and to lend or sell such copies for private, scholarly or scientific research purposes only.

The author reserves other publication rights, and neither the thesis nor extensive extracts from it may be printed or otherwise reproduced without the author's written permission.

(SIGNED) M. Brearley

PERMANENT ADDRESS:

3 HOLME GROVE

BURLEY-IN-WHARFEDALE, ILKLEY

WEST YORKSHIRE, ENGLAND

DATED January 20th 1986

THE UNIVERSITY OF ALBERTA

FACULTY OF GRADUATE STUDIES AND RESEARCH

The undersigned certify that they have read, and recommend to the Faculty of Graduate Studies and Research, for acceptance, a thesis entitled Ultramafic Xenoliths from British Columbia: Petrological and Dissolution studies submitted by M. Brearley in partial fulfilment of the requirements for the degree of Doctor of Philosophy.

.....

Supervisor

.....

.....

.....

.....

External Examiner

Date.....January 20th 1986.....

Abstract

The results of three independent studies of the petrology of ultramafic xenoliths from British Columbia and western Alaska are presented and integrated to determine the nature of the upper mantle beneath the Canadian Cordillera. A fourth study is concerned with an experimental investigation of the dissolution rates of ultramafic xenoliths in alkali basalt magmas at high pressure.

Approximately 200 upper mantle xenoliths from Summit Lake, near Prince George, British Columbia, were collected from a basanitoid flow of Late Cenozoic (possibly post-glacial) age. The most abundant xenolith type is spinel lherzolite. Xenoliths have granular textures and both green chrome diopside-bearing and black aluminous augite-bearing xenoliths are present. About 5% of the xenoliths are banded on a centimeter scale, suggesting that the upper mantle beneath north-central British Columbia is heterogeneous on a scale of centimeters to meters.

Electron microprobe data on the mineral phases indicate that the xenoliths are generally well equilibrated. Typically in spinel lherzolite, olivines are Fo_{91}, orthopyroxenes are En_{91} and chrome diopside is $Wo_{45}En_{50}Fs_5$. Spinels vary in composition from xenolith to xenolith.

Using element partition geothermometers, equilibration temperatures are calculated to be between 1080-1100°C. Pressures, estimated from a Cordilleran geotherm, are between 18-20 kbar.

Pargasitic amphibole has been observed for the first time in an ultramafic xenolith from British Columbia. The xenolith is a chrome diopside-bearing spinel lherzolite trapped within an alkali basaltic lava flow at Lightning Peak, near Vernon, British Columbia. Amphibole (<5%) occurs within the xenolith as small grains, interstitial between other xenolith mineral phases and always shows evidence of melting. Microprobe analyses of the amphibole reveal that it is a pargasite rich in MgO (MgO = 17.1-17.7 wt%; $Mg/(Mg+Fe^{2+}) = 0.89$) and CaO (CaO = 10.4-10.7 wt%). The pargasite probably crystallized within the spinel stability field of the upper mantle from a volatile-rich metasomatic fluid which was produced by dehydration of subducted material. Melting in the amphibole may have been caused by one of three processes: superheating by the host alkali basalt, decompression as the magma ascended, or by in situ partial melting within the upper mantle.

The petrography, mineralogy and mineral chemistry of a suite of 25 ultramafic xenoliths from the Seward Peninsula, western Alaska have been studied. The xenoliths are predominantly chrome diopside-bearing spinel lherzolite exhibiting well developed equigranular and protogranular textures. The majority of the xenoliths contain olivine (Fo_{90}), orthopyroxene (En_{90}), clinopyroxene ($Wo_{47}En_{47}Fs_{6}$) and aluminous spinel (Mg/(Mg+Fe) = 0.81-0.82). Two of the xenoliths studied contain the same mineral phases but with significantly more iron-rich compositions.

Equilibration temperatures of the Fo_{90}-bearing xenoliths range from 910-950°C using the Wells (1977) two-pyroxene geothermometer, indicating that the geotherm beneath this locality is similar to other areas in North America. The more iron-rich xenoliths are interpreted to be either high pressure cumulates or a product of exchange of the upper mantle with an iron-rich metasomatic fluid.

The dissolution rates of the major upper mantle minerals: olivine, orthopyroxene, clinopyroxene, spinel and garnet have been determined in an alkali basalt melt at superliquidus temperatures and 5, 12 and 30 kbar. The relative rates of dissolution of the minerals at each pressure are governed by their relative stabilities in the melt. Olivine has a slower dissolution rate than clinopyroxene at low pressure, whereas clinopyroxene has a slower dissolution rate than olivine at higher pressure. Spinel has the slowest dissolution rate at each pressure and garnet dissolves very rapidly at low pressure.

A simple model has been constructed that predicts the survival of ultramafic xenoliths in alkali basalt magmas as a function of xenolith radius, magma ascent time and superheating. The experimentally determined dissolution rates of olivine and clinopyroxene were used to calculate the digestion of peridotite and pyroxenite in an ascending alkali basalt magma. The

pressure-integrated dissolution rates of olivine and clinopyroxene are similar, unless the magma is generated at low pressure, in which case preferential dissolution of clinopyroxene may occur. The results of the model suggest that the relative proportions of peridotite and pyroxenite xenoliths brought to the surface in alkali basalts are generally representative of their proportions as constituents of the upper mantle.

Acknowledgements

There are many people I wish to thank for their advice and counsel during the course of the work involved in this thesis. Firstly, my sincerest thanks are due to Dr. Chris Scarfe who supervised this project and helped me immensely on numerous occasions with his expertise and friendship. Drs. Don Dingwell, Jim Dickinson and Todd Dunn are also thanked for their advice throughout. Without them, I feel this thesis would not have progressed as it did. They are also thanked for their sincere friendship during my tenure at the University of Alberta. I would also like to thank Drs. D.I. Gough, B.E, Nesbitt, J. Nicholls and D.G.W. Smith for serving on my committee, and Steve Launspach for his friendship and advice while using the electron microprobe.

Finally, I would like to thank my fellow graduate students Simon Hook, Kevin Ansdell, Mike Dufresne and especially Chris Sayer for all they did for me when things were not going as they might have.

Table of Contents

Chapter — Page

I. Introduction 1

A. Opening comments 1

B. Background 2

C. Objectives 4

II. The petrology of ultramafic xenoliths from Summit Lake, near Prince George, British Columbia 6

A. Introduction 6

B. Geological Setting 7

C. Analytical methods 7

D. Host basalt 8

E. Ultramafic xenoliths 10

Petrography 11

Mineral Chemistry 15

F. Discussion 26

Xenoliths with chrome diopside 26

Xenoliths with aluminous augite 29

Estimation of Equilibration Temperatures and Pressures 30

G. Summary 34

III. Amphibole in a spinel lherzolite xenolith: evidence for volatiles and partial melting in the upper mantle beneath southern British Columbia 35

A. Introduction 35

B. Field setting and petrography 37

C. Analytical methods 38

D. Ultramafic xenoliths 39

Amphibole mineral chemistry 41

E. Discussion 43

F. Conclusions 47

IV. The petrology of ultramafic xenoliths from the Seward Peninsula, western Alaska: a preliminary investigation 48

A. Introduction 48

B. Petrography 49

C. Mineral chemistry 51

Analytical methods 51

D. Results 51

E. Discussion 57

Geothermometry 59

F. Comparison with other ultramafic xenoliths from western Alaska 61

G. Conclusions 62

V. The nature of the upper mantle beneath the Canadian Cordillera: an overview 64

A. Introduction 64

B. Geothermometry and Discussion 66

C. Conclusions 71

VI. Dissolution rates of upper mantle minerals in an alkali basalt melt at high pressure: an experimental study and implications for ultramafic xenolith survival 72

A. Introduction 72

B. Theory of dissolution kinetics 74

Molecular diffusion 75

Natural convection 78

C. Experimental procedure 79

Dissolution experiments 79

Phase equilibrium experiments 82

D. Analytical method 83

E. Results of experiments 84

Liquidus phase equilibria 84

Dissolution experiments 84

Crystal/melt textural relationships 84

Dissolution rates 91

Cation diffusivities 105

F. Discussion 114

Crystal/melt textural relationships ...114

Dissolution rates 119

Cation diffusivities 127

G. The dissolution of ultramafic xenoliths in alkali basalt magmas: a model 130

Magma generation at 30 kbar 136

Magma generation at 20 kbar 136

Magma generation at 10 kbar 137

H. Conclusions 139

VII. Summary and Conclusions 141

A. Summary of Results 141

B. Conclusions 143

The nature of the Cordilleran upper mantle 143

Ultramafic xenolith survival 145

Bibliography 147

List of Figures

1. Distribution of xenolith types at Summit Lake...12
2. Estimates of ultramafic xenolith mineralogy at Summit Lake in terms of modal olivine, orthopyroxene and clinopyroxene.....13
3. Compositions of pyroxenes from Summit Lake ultramafic xenoliths.....23
4. Variation of $Cr/(Cr+Al+Fe^{3+})$ in spinel with Al_2O_3 in pyroxene.....24
5. Estimate of the geotherm beneath Summit Lake and depth of origin of the ultramafic xenoliths.....32
6. Compositions of pyroxenes from Seward Peninsula ultramafic xenoliths.....55
7. Equilibration temperatures of Seward Peninsula ultramafic xenoliths.....60
8. Locations of xenolith-bearing lavas and cinder cones in the Canadian Cordillera.....65
9. Equilibration temperatures of xenoliths from the Canadian Cordillera using Wells (1977) two-pyroxene geothermometer.....67
10. Schematic illustrating parameters involved in dissolution kinetics.....77
11. Liquidus phase equilibria of KR-13 alkali basalt.....85
12. Backscattered electron images of textures produced during dissolution experiments.....88
13. Change in radius of crystals versus time for

dissolution experiments at 5 kbar.....96
14. Change in radius of crystals versus time for dissolution experiments at 12 kbar.....97
15. Change in radius of crystals versus time for dissolution experiments at 30 kbar.....98
16. Dissolution rates versus reciprocal temperature for experiments at 5, 12 and 30 kbar.....100
17. Concentration profiles adjacent to a dissolving olivine crystal.....106
18. Concentration profiles adjacent to a dissolving clinopyroxene crystal.....107
19. Concentration profiles adjacent to a dissolving spinel crystal.....108
20. Dissolution rates versus reciprocal temperature for data at 1 bar and high pressure.....121
21. Diopside-anorthite binary join to illustrate driving forces for dissolution of diopside and anothite.....123
22. Model calculations for the dissolution of peridotite and pyroxenite xenoliths in an alkali basalt magma.....132
23. Temperature-depth profiles for non-adiabatic ascent of an alkali basalt magma in a conduit.....134
24. Dissolution behaviour of xenoliths in an alkali basalt magma during non-adiabatic ascent.....135

List of Tables

1. Chemical composition of the Summit Lake host basalt.....9
2. Mineral chemistry of the Summit Lake ultramafic xenoliths.....16
3. Mineral chemistry of the Lightning Peak ultramafic xenoliths.....40
4. Mineral chemistry of the amphibole in the Lightning Peak ultramafic xenolith and other selected analyses of pargasitic amphibole from the literature.....42
5. Mineral chemistry of the Seward Peninsula ultramafic xenoliths.....52
6. Compositions of starting materials for the dissolution experiments.....81
7. Summary of the textures produced during dissolution experiments.....86
8. Results of the dissolution experiments.....92
9. Activation energies for dissolution at 5, 12 and 30 kbar.....103
10. Single component cation diffusivities in the melt adjacent to dissolving crystals, calculated by two different methods.....111

I. Introduction

A. Opening comments

There have been many studies of the petrology and geochemistry of ultramafic xenoliths found in alkali basalts in recent years (e.g., Kuno and Aoki, 1970; Frey and Prinz, 1978; Irving, 1980; Hawkesworth and Norry, 1983 and references therein). These investigations have been designed primarily to investigate the nature, composition and geothermal conditions existing in the upper mantle. Furthermore, it is important to have a knowledge of the composition of the upper mantle in order to model most magmatic processes, since many of the basaltic rocks we observe are directly related to melting processes in the upper mantle.

It has been assumed that the proportions of ultramafic xenoliths that are observed at the Earth's surface are representative of their proportions in the upper mantle. However, there have been few studies concerned with the survival and digestion of ultramafic xenoliths in magmas both in the upper mantle and during their transport to the surface (e.g., Kutolin and Agafonov, 1978; Scarfe et al., 1980). Therefore, it is essential to determine the stability of an upper mantle

mineralogy in alkali basalt magmas, because assumed upper mantle compositions have been used extensively in melting studies and phase relations to determine the compositions of magmas and their modifications in the upper mantle.

B. Background

Previous work on the petrology and geochemistry of ultramafic xenoliths found in alkali basalts and kimberlites is extensive (e.g., Dawson, 1980; Hawkesworth and Norry, 1983) and only the pertinent literature will be reviewed in this section. There have been a number of studies concerned with the mineralogy, mineral chemistry and geochemistry of ultramafic xenoliths found in alkali basalts in western North America (e.g., Best, 1974; Littlejohn and Greenwood, 1974; Wilshire and Shervais, 1975; Francis, 1976a; Frey and Prinz, 1978; Smith and Roden, 1981; Fujii and Scarfe, 1982; Roden et al., 1984). In these cases, Tertiary and Recent extensional tectonism has resulted in the production of alkali basalts that host a wide variety of ultramafic xenoliths. The major conclusions of this work are that the upper mantle is dominated by spinel lherzolite at depths less than approximately 60 km, and that the upper mantle at present is largely anhydrous and of a relatively uniform composition,

characteristically depleted in basaltic components (e.g., Littlejohn and Greenwood, 1974; Fujii and Scarfe, 1982). However, it has been shown by detailed study that the upper mantle is mineralogically and chemically heterogeneous (e.g., Wilshire and Shervais, 1975; Frey and Prinz, 1978; Fujii and Scarfe, 1982) and in some cases, where hydrous minerals have been documented, mantle metasomatic processes have been shown to be important in the modification of the upper mantle composition and in the generation of alkali basaltic magmas (e.g., Francis, 1976a; Roden et al., 1984).

In the Canadian Cordillera, studies of ultramafic xenoliths have not revealed the presence of any hydrous minerals. In fact, although both chrome diopside-bearing xenoliths and aluminous augite-bearing xenoliths are present (Littlejohn and Greenwood, 1974; Fujii and Scarfe, 1982; Wilshire and Shervais, 1975), the mineralogy and mineral chemistry of the upper mantle is remarkably constant.

Because peridotite xenoliths are much more abundant than any other ultramafic xenolith rock type, it has been suggested that pyroxene-rich xenoliths may preferentially dissolve in alkali basalt magmas and that pyroxenite is a more important constituent of the upper mantle than is commonly believed (Kutolin and Agafonov, 1978). In order to investigate this

possibility, Kutolin and Agafonov (1978) conducted experiments at 1 bar to determine the dissolution rates of the major upper mantle minerals in an alkalic melt. This study was subsequently followed by a similar series of experiments at high pressure by Scarfe et al. (1980). The results of both investigations were that olivine dissolves much slower than pyroxene and therefore that pyroxene-rich xenoliths may preferentially dissolve in alkali basalt magmas. However, Scarfe et al. (1980) argued that the rapid ascent rates of alkali basalts would prevent dissolution to a large extent. Related studies on the dissolution kinetics of minerals in silicate melts have shown that it is possible to determine dissolution mechanisms (e.g., Cooper and Kingery, 1964; Kuo and Kirkpatrick, 1985), dissolution rates (e.g., Scarfe et al., 1980; Thornber and Huebner, 1985; Donaldson, 1984a; Kuo and Kirkpatrick, 1985), crystal/melt textural relationships (Tsuchiyama, 1985a; b; Donaldson, 1984b) and cation diffusion rates in melts (e.g., Harrison and Watson, 1983; 1984) from petrologically important dissolution experiments.

C. Objectives

This thesis was initiated in attempt to evaluate two distinct, but related, aspects of the petrology of

ultramafic xenoliths in alkali basalts. Each chapter is written in the form of a paper and therefore has its own introduction and conclusions. Firstly, the mineralogy and mineral chemistry of three suites of previously undocumented ultramafic xenoliths from British Columbia and western Alaska are presented in chapters 2 to 4. In chapter 5, the data of chapters 2 and 3 are summarized along with other data from the literature to obtain a picture of the nature of the upper mantle beneath the Canadian Cordillera. In chapter 6, an experimental study of the dissolution of the upper mantle minerals in an alkali basalt melt to pressures of 30 kilobars is presented. In addition, a simple model is developed to predict the dissolution behaviour of ultramafic xenoliths in alkali basalt magmas as a function of xenolith radius, magma ascent time and superheating. Chapter 7 summarizes the results of chapters 2 to 6 and relates the two aspects of the petrology of ultramafic xenoliths.

II. The petrology of ultramafic xenoliths from Summit Lake, near Prince George, British Columbia

A. Introduction

Ultramafic xenoliths in alkali basaltic flows of Late Tertiary to Recent age from British Columbia have been documented in several recent publications (e.g., Littlejohn and Greenwood, 1974; Fiesinger and Nicholls, 1977; Hamilton, 1981; Brearley et al., 1982; Fujii and Scarfe, 1982; Nicholls et al., 1982; Scarfe et al., 1982; Ross, 1983). Most of these papers have focussed on the mineralogy and mineral chemistry of chrome diopside-bearing ultramafic xenoliths and their petrological significance. The chemistry and equilibration temperatures of the xenoliths have been used to discuss the geothermal conditions, composition and properties of the source region in the upper mantle beneath several areas in British Columbia.

In this chapter the petrography, mineralogy and mineral chemistry of a suite of approximately 200 ultramafic xenoliths in an alkali basalt flow is described from a locality at Summit Lake, 40 km north of Prince George, British Columbia (Grid Ref. 122° 45' W. 54° 25' N). Both chrome diopside-bearing and aluminous augite-bearing xenoliths are described and the dominant rock type is spinel lherzolite. Using element partition geothermometers, the temperatures of

equilibration of the xenoliths in the upper mantle are discussed. Some non-equilibrium features are briefly discussed and it is concluded that the upper mantle beneath north-central British Columbia is heterogeneous and banded on a scale of centimeters to meters.

B. Geological Setting

According to map sheet NTS 93J (GSC map 1204A), the host alkali basalt belongs to the Miocene Endako Group of volcanic rocks within the Omenica Belt in Central British Columbia (Souther, 1977). However, it is possible that the flow is much younger because the relationship between the flow and glacial activity is uncertain. The basalt, which is well exposed in a quarry, forms a columnar jointed flow of at least 25m in thickness and contains both upper mantle and crustal xenoliths. No contact relationships with the adjoining rocks are exposed, thus it is difficult to estimate the exact thickness of the flow.

C. Analytical methods

Microprobe analyses of the nodule minerals, host basalt phases and whole rock host basalt were carried out on ARL EMX and ARL SEMQ electron microprobes using ORTEC energy dispersive spectrometers in the Department of Geology, University of Alberta. Line scans by wavelength dispersive analysis were used to investigate

heterogeneities within minerals. Operating conditions for EDA were 15 kV voltage. The probe current and counting times varied according to which microprobe was utilised (see Table 1, Table 2). A rastered beam area (15 μm x 15 μm) was used for both samples and standards during routine analysis. A point beam was used in the analysis of exsolution lamellae. All microprobe spectra were processed with full ZAF corrections using EDATA2 (Smith and Gold, 1979). The detection limit using the above operating conditions for EDA is approximately 500 ppm, and accuracies for major and minor elements are comparable to WDA (Smith, 1976). The excellent agreement between results for EDA and WDA analysis have been demonstrated by Reed and Ware (1973) and Mori and Kanehira (1984).

Electron microprobe analyses on the whole rock basalt were carried out on glass beads, fused in air at 1300°C for two hours. Ferrous iron in the whole rock basalt was determined on powders by wet chemistry after the method of Wilson (1960).

D. Host basalt

The Summit Lake host basalt contains 5% microphenocrysts of olivine (Fo_{85-74}) in a groundmass of unzoned plagioclase (An_{85-74}), titanaugite and titanomagnetite. The groundmass also contains Ti-rich biotite, always accompanied by leucite. Leucite, almost

SiO_2	46.2
TiO_2	1.80
Al_2O_3	15.9
Fe_2O_3	2.94
FeO	5.80
MnO	0.14
MgO	9.32
CaO	10.0
Na_2O	2.96
K_2O	2.83
P_2O_5	0.49
TOTAL	98.38

CIPW NORM

Or	17.01
Ab	8.75
An	22.15
Ne	9.05
Di	16.59
Hd	3.44
Fo	11.14
Fa	2.91
Mt	4.33
Il	3.48
Ap	1.16

Table 1. Chemistry and CIPW norm of the Summit Lake basalt. Analysis done with ARL SEMQ microprobe: probe current 4 nA, counting time 240 seconds (based on count rate of 5000 cps).

pure $KAlSi_2O_6$, occurs in interstitial patches suggesting that it was one of the last phases to crystallize. Xenocrysts of olivine, plagioclase, spinel and clinopyroxene are also present in the basalt. All xenocrysts are resorbed, suggesting crystal-melt disequilibrium. Mineral phases were verified by microprobe analysis.

The chemical analysis and CIPW norm for the basalt are shown in Table 1. The rock contains 9% normative nepheline but there is no modal nepheline, therefore the rock is a basanitoid according to the classification of MacDonald and Katsura (1964) or a potassic series alkali basalt (Irvine and Baragar, 1971). The rock is enriched in K_2O relative to Na_2O when compared to other alkalic basalts of this type in British Columbia (Fiesinger and Nicholls, 1977; Nicholls et al., 1982). This K_2O enrichment is reflected in the high normative orthoclase content and in the appearance of potassium-bearing phases, biotite and leucite, in the modal mineralogy.

E. Ultramafic xenoliths

The ultramafic xenoliths, trapped within the alkali basalt flow, are subangular to subrounded, with diameters ranging in size from 1-15cm (average size 5cm). Xenoliths commonly have sharp contacts with the host basalt, but occasionally show thin reaction rinds,

especially where pyroxene is at the periphery of the xenolith. Over 300 xenoliths, of which 79% are ultramafic, have been collected to date. The ultramafic xenolith population (Fig. 1, columns 2 and 3) is dominated by spinel lherzolite with lesser amounts of wehrlite, clinopyroxenite, olivine websterite, websterite and dunite. One hundred of these rocks are plotted in terms of their modal proportions of olivine, orthopyroxene and clinopyroxene in Fig. 2. Olivine, orthopyroxene and clinopyroxene usually constitute greater than 90% of each xenolith. Spinel is present in most of the xenoliths and no hydrous minerals have been observed.

The ultramafic xenoliths may be further categorised according to the presence of either green or black clinopyroxene (Wilshire and Shervais, 1975). All spinel lherzolites and olivine websterites contain a green chromian diopside. Conversely, all clinopyroxenites and wehrlites contain black aluminous augites. There are also occasional banded nodules that incorporate thin (<1 cm.) bands of interlayered green-pyroxene spinel lherzolite and black-pyroxene wehrlite or clinopyroxenite.

Petrography

Textures within the nodules are commonly metamorphic or, very rarely, relic magmatic and all are

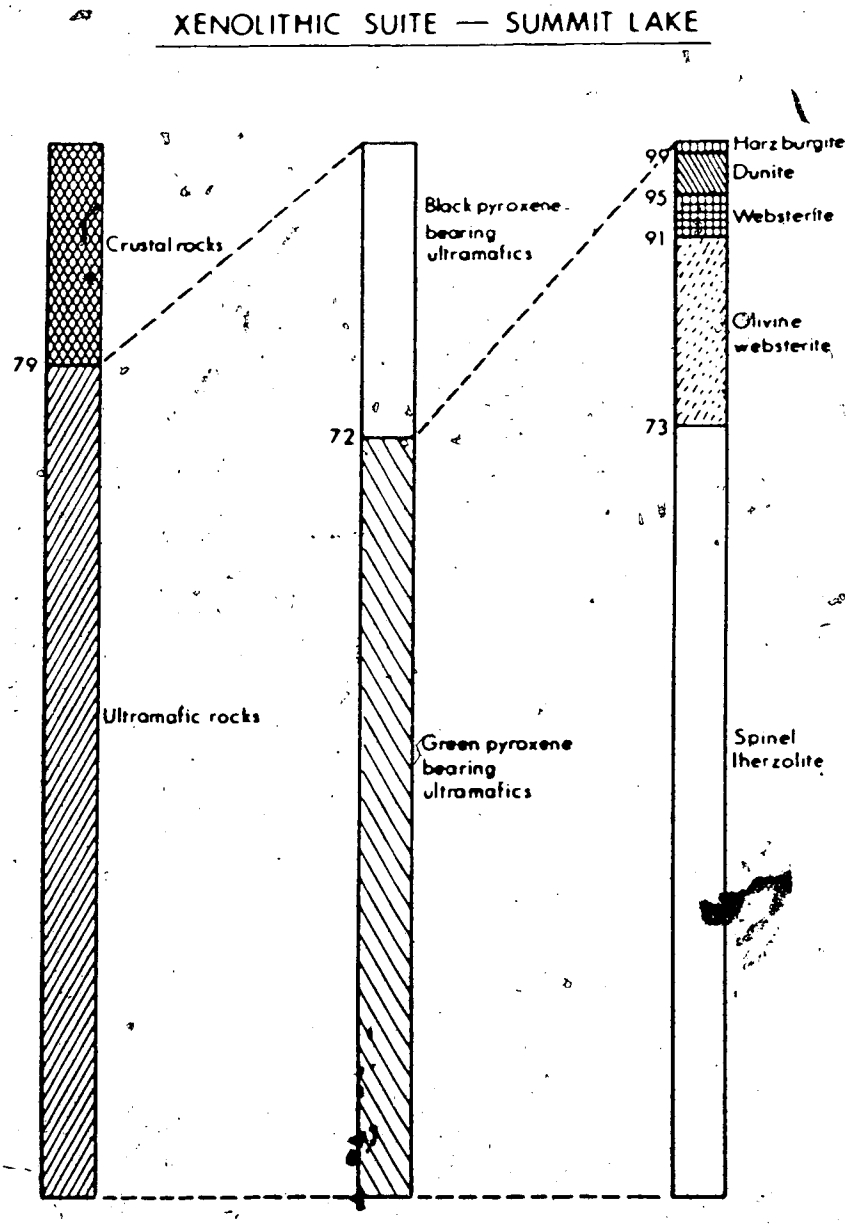

Figure 1. Distribution of xenolith types in volume % at Summit Lake. Represents data from field and laboratory estimates.

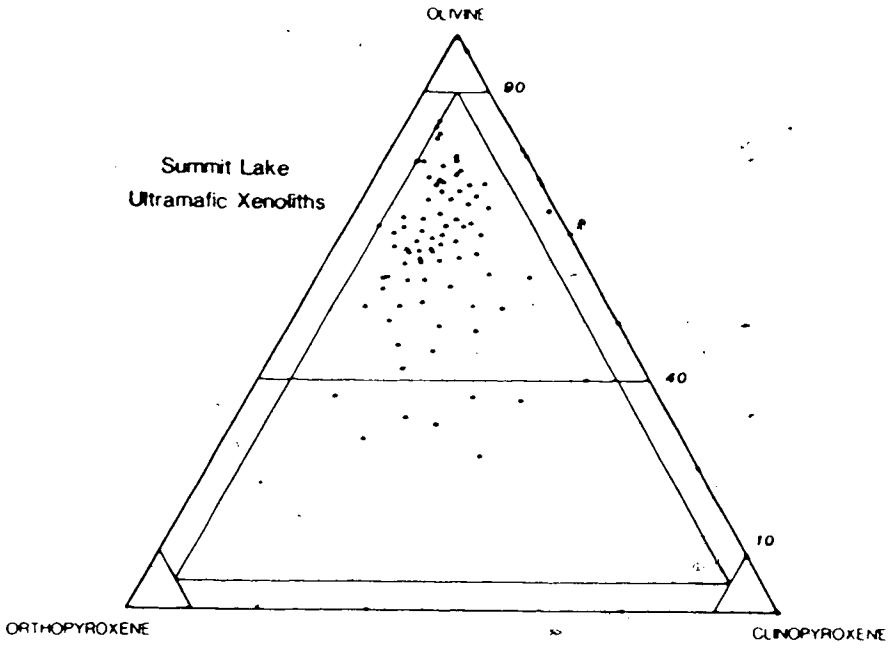

Figure 2. Laboratory estimates of ultramafic xenolith mineralogy in terms of the modal proportions of olivine, orthopyroxene and clinopyroxene. Modal mineralogy estimated by point counting 100 randomly chosen thin sections.

protogranular according to the terminology of Mercier and Nicolas (1975). Triple points between minerals, especially olivines, are very common, although occasional embayments suggest a relict magmatic history (Irving, 1980). Other textural details have been described by Ross (1983).

Olivine is usually the predominant mineral ranging to >5mm. in diameter, with an average size of 2mm. The only indication of deformation in olivine is the occasional presence of kink banding.

Orthopyroxene is normally elongate and approximately 1-2mm. in length. It commonly shows ragged edges and pockets of glass within grains, presumably due to reaction after entrapment within the host lava (e.g., Kuno and Aoki, 1970). Exsolution lamellae in orthopyroxene, parallel to (010), were only observed in one sample (SL-99).

In five of the xenoliths, the clinopyroxene appears to have been partially melted, as shown by vermicular pockets of glass within grains and around their edges. This may also have occurred during transport by the host magma.

Exsolution phenomena were only found in one xenolith. Xenolith SL-222 is a spinel lherzolite containing a chrome diopside-rich band, the clinopyroxenes of which have exsolved enstatite and spinel. The exsolution lamellae, parallel to (010) and

(001) are 150 and 30 microns in width, respectively. The compositions of the exsolution lamellae are shown in Table 2.

Spinels are commonly interstitial, but occasionally they occur as inclusions in olivine. The colour of the spinel varies with composition. Chrome-rich spinels are blood-red while aluminous spinels are pale green. Aluminous spinels are always associated with aluminous clinopyroxenes, regardless of whether the clinopyroxenes are aluminous augite or chrome diopside. In xenolith SL-141, there are three texturally discrete spinel phases (Table 2). Spinel SPN 6-1 occurs within olivine grains, SPN 1-1 is interstitial and contains small rounded melt inclusions, and SPN 3-1 occurs within the xenolith and is concentrated along the contact with the host basalt.

Mineral Chemistry

A total of thirty xenoliths were investigated by electron microprobe. Representative chemical analyses of the phases in the nodules are given in Table 2.

Olivine

In all but one of the xenoliths, olivine has a range of forsterite content from Fo_{89}-Fo_{91}, the average being Fo_{90}. The concentration of NiO is between 0.3-0.6 wt% in all xenoliths and there is a positive

(a)	SL-33	SL-49	SL-53	SL-99	SL-141	SL-151	SL-153	SL-154
(b)	OLV 1-1	OLV 2-1	OLV 1-1	OLV 2-1	OLV 1-1	OLV 2-1	OLV 2-1	OLV 2-1
SiO_2	40.2	40.4	40.2	40.3	38.7	39.5	40.0	40.0
TiO_2	n.d.	n.d.	n.d.	n.d.	n.d.	n.d.	n.d.	n.d.
Al_2O_3	0.14	n.d.	0.14	0.21	n.d.	0.19	0.16	0.24
Cr_2O_3	n.d.	n.d.	n.d.	n.d.	n.d.	n.d.	n.d.	0.10
Fe_2O_3	n.a.	n.a.	n.a.	n.a.	n.a.	n.a.	n.a.	n.a.
FeO	10.6	8.52	10.0	9.60	14.3	11.4	11.6	9.71
MnO	0.14	0.13	0.16	0.13	0.25	0.19	0.20	0.18
MgO	48.2	50.3	48.8	49.7	46.2	48.1	48.8	49.9
CaO	0.11	0.14	0.14	0.12	0.09	0.13	0.12	0.15
Na_2O	n.d.	n.d.	n.d.	n.d.	n.d.	n.d.	n.d.	n.d.
K_2O	n.d.	n.d.	n.d.	n.d.	n.d.	n.d.	n.d.	n.d.
NiO	0.46	0.52	0.49	0.53	0.42	0.34	0.38	0.50
TOTAL	99.85	100.01	99.93	100.59	99.96	99.85	101.26	100.78
O	4.000	4.000	4.000	4.000	4.000	4.000	4.000	4.000
Si	0.993	0.987	0.990	0.984	0.974	0.981	0.980	0.977
Al	0.004	n.d.	0.004	0.006	n.d.	0.006	0.005	0.007
Ti	n.d.	n.d.	n.d.	n.d.	n.d.	n.d.	n.d.	n.d.
Cr_{3+}	n.d.	n.d.	n.d.	n.d.	n.d.	n.d.	n.d.	0.002
Fe_{3+}	n.a.	n.a.	n.a.	n.a.	n.a.	n.a.	n.a.	n.a.
Fe_{2+}	0.219	0.174	0.206	0.196	0.301	0.237	0.238	0.198
Mn	0.003	0.003	0.003	0.003	0.005	0.004	0.004	0.004
Mg	1.774	1.832	1.791	1.809	1.734	1.780	1.781	1.816
Ca	0.003	0.004	0.004	0.003	0.002	0.003	0.003	0.004
Na	n.d.	n.d.	n.d.	n.d.	n.d.	n.d.	n.d.	n.d.
K	n.d.	n.d.	n.d.	n.d.	n.d.	n.d.	n.d.	n.d.
Ni	0.009	0.010	0.010	0.010	0.009	0.007	0.007	0.010
SUM	3.005	3.010	3.008	3.011	3.025	3.018	3.018	3.018
Mg/(Mg+Fe)	0.89	0.91	0.90	0.90	0.85	0.88	0.88	0.90
Ca *	0.1	0.2	0.2	0.2	0.1	0.2	0.2	0.2
Mg *	88.9	91.2	89.5	90.1	85.1	88.1	88.1	90.0
Fe *	11.0	8.6	10.3	9.7	14.8	11.7	11.7	9.8
(c)	Sp-L	Sp-L	Sp-L	Sp-L	Sp-L	Sp-Wh	Sp-Wh	Sp-L

n.d. - not detected, n.a. - not analyzed. All Fe in silicates expressed as FeO. Fe_2O_3 in spinel by stoichiometry. (a) sample number, (b) analysis number, (c) rock types (spinel lherzolite = Sp-L, spinel wehrlite = Sp-Wh, clinopyroxenite = Cpt)
Xenolith SL-53 is spinel lherzolite with a cross-cutting clinopyroxenite vein
* Ca, Mg and Fe are recalculated to 100% for olivine, orthopyroxene and clinopyroxene.
Average uncertainties in microprobe analyses of olivines (wt%): SiO_2, 0.2%; Al_2O_3, 0.02%; Cr_2O_3, 0.03%; FeO, 0.15%; MnO 0.05%; MgO, 0.2%; CaO, 0.02%; NiO, 0.08%.

Table 2. Mineral chemistry of Summit Lake ultramafic xenoliths. Analyses done on an ARL SEMQ microprobe (operating conditions as in Table 1) and an ARL EMX microprobe: probe current 20 nA, counting time 400 seconds (based on count rate of 3000 cps). Uncertainties in microprobe analyses calculated at the 95% confidence level (±2 sigma). Errors calculated from the square root of the sums of squares of the errors associated with random x-ray generation of sample peak and background and standard peak for each element.

	SL-33 OPX 2-1	SL-49 OPX 1-1	SL-53 OPX 1-1	SL-99 OPX 2-1	SL-141 OPX 1-1	SL-154 OPX 1-1	SL-222[1] OPX 1-1
SiO_2	54.4	55.3	53.8	53.9	53.7	54.3	55.7
TiO_2	0.17	n.d.	0.12	0.15	n.d.	0.17	n.d.
Al_2O_3	5.62	2.68	5.57	4.90	3.36	4.94	3.55
Cr_2O_3	0.50	0.77	0.40	0.66	0.60	0.53	0.62
Fe_2O_3	n.a.	n.a.	n.a.	n.a.	n.a.	n.a.	n.a.
FeO	6.76	5.44	6.49	6.16	9.14	6.00	6.84
MnO	0.14	0.13	0.11	0.13	0.19	0.13	0.12
MgO	32.0	33.8	32.2	32.7	31.8	32.5	31.9
CaO	1.20	1.25	1.14	1.12	1.09	1.12	1.15
Na_2O	n.d.	n.d.	0.43	n.d.	n.d.	n.d.	n.d.
K_2O	n.d.	n.d.	n.d.	n.d.	n.d.	n.d.	n.d.
NiO	0.13	0.18	0.09	0.17	0.14	0.14	0.15
TOTAL	100.92	99.55	100.35	99.89	100.02	99.83	100.03
O	6.000	6.000	6.000	6.000	6.000	6.000	6.000
Si	1.871	1.920	1.862	1.871	1.889	1.882	1.930
Al	0.228	0.110	0.227	0.200	0.139	0.202	0.145
Ti	0.004	n.d.	0.003	0.004	n.d.	0.004	n.d.
Cr_{3+}	0.014	0.021	0.011	0.018	0.017	0.015	0.017
Fe_{3+}	n.a.	n.a.	n.a.	n.a.	n.a.	n.a.	n.a.
Fe_{2+}	0.194	0.158	0.188	0.179	0.269	0.174	0.198
Mn	0.004	0.004	0.003	0.004	0.006	0.004	0.004
Mg	1.640	1.750	1.661	1.692	1.668	1.679	1.648
Ca	0.044	0.047	0.042	0.042	0.041	0.042	0.043
Na	n.d.	n.d.	0.029	n.d.	n.d.	n.d.	n.d.
K	n.d.	n.d.	n.d.	n.d.	n.d.	n.d.	n.d.
Ni	0.004	0.005	0.003	0.005	0.004	0.004	0.004
SUM	4.003	4.015	4.029	4.015	4.033	4.006	3.989
Mg/(Mg+Fe)	0.89	0.92	0.90	0.90	0.86	0.91	0.89
Ca	2.4	2.4	2.3	2.2	2.1	2.2	2.3
Mg	87.3	89.5	87.8	88.5	84.3	88.6	87.2
Fe	10.3	8.1	9.9	9.3	13.6	9.2	10.5
	Sp-L	Sp-L	Sp-L	Sp-L	Sp-L	Sp-L	

1 - SL-222 OPX 1-1 - exsolution lamella (see text)
Average uncertainties in microprobe analyses of orthopyroxenes (wt%): SiO_2, 0.2%; TiO_2, 0.04%; Al_2O_3, 0.05%; Cr_2O_3, 0.05%; FeO, 0.10%; MnO, 0.04%; MgO, 0.2%; CaO, 0.04%; Na_2O, 0.04%; NiO, 0.06%.

Table 2. Mineral chemistry of Summit Lake ultramafic xenoliths.

	SL-33 CPX 1-1	SL-49 CPX 1-1	SL-53 CPX 1-1	SL-53[2] CPX 2-1	SL-53[2] CPX 3-1	SL-53[2] CPX 4-1	SL-99 CPX 1-1
SiO_2	51.3	53.3	50.4	47.2	46.6	46.5	51.8
TiO_2	0.51	n.d.	0.44	1.18	1.27	1.33	0.36
Al_2O_3	6.92	3.02	6.98	10.9	11.4	11.4	6.60
Cr_2O_3	0.86	1.32	0.92	n.d.	0.09	0.11	1.22
Fe_2O_3	n.a.	n.a.	n.a.	n.a.	n.a.	n.a.	n.a.
FeO	3.62	2.66	3.51	7.17	7.21	7.17	3.14
MnO	0.14	0.08	0.11	0.14	0.15	0.13	0.09
MgO	16.5	18.3	16.1	11.7	11.8	11.8	16.4
CaO	19.5	20.8	19.1	21.7	21.5	21.5	19.1
Na_2O	1.20	0.85	1.39	n.d.	n.d.	n.d.	1.47
K_2O	n.d.	n.d.	n.d.	n.d.	n.d.	n.d.	n.d.
NiO	0.17	0.11	0.12	n.d.	n.d.	n.d.	n.d.
TOTAL	100.72	100.44	99.07	99.99	100.02	99.94	100.18
O	6.000	6.000	6.000	6.000	6.000	6.000	6.000
Si	1.847	1.923	1.846	1.746	1.724	1.721	1.868
Al	0.294	0.128	0.301	0.475	0.497	0.497	0.281
Ti	0.014	n.d.	0.012	0.033	0.035	0.037	0.010
Cr_{3+}	0.024	0.038	0.027	n.d.	0.003	0.003	0.035
Fe_{3+}	n.a.	n.a.	n.a.	n.a.	n.a.	n.a.	n.a.
Fe_{2+}	0.109	0.080	0.107	0.222	0.223	0.222	0.095
Mn	0.004	0.002	0.003	0.004	0.005	0.004	0.003
Mg	0.885	0.984	0.879	0.645	0.651	0.651	0.882
Ca	0.752	0.804	0.749	0.860	0.852	0.852	0.738
Na	0.084	0.059	0.099	n.d.	n.d.	n.d.	0.103
K	n.d.	n.d.	n.d.	n.d.	n.d.	n.d.	n.d.
Ni	0.005	0.003	0.004	n.d.	n.d.	n.d.	n.d.
SUM	4.018	4.021	4.027	3.985	3.990	3.987	4.015
Mg/(Mg+Fe)	0.89	0.93	0.89	0.74	0.75	0.75	0.90
Ca	43.1	43.0	43.2	49.8	49.4	49.4	43.1
Mg	50.7	52.7	50.6	37.4	37.7	37.7	51.4
Fe	6.2	4.3	6.2	12.8	12.9	12.9	5.5
	Sp-L	Sp-L	Sp-L	Cpt	Cpt	Cpt	Sp-L

2 - SL-53 CPX 2-1, CPX 3-1, CPX 4-1 - Al-augites

Average uncertainties in microprobe analyses of chrome diopside clinopyroxenes (wt%): SiO_2, 0.2%; TiO_2, 0.08%; Al_2O_3, 0.07%; Cr_2O_3, 0.06%; FeO, 0.07%; MnO, 0.03%; MgO, 0.1%; CaO, 0.1%; Na_2O, 0.09%; NiO, 0.05%. Average uncertainties in microprobe analyses of aluminous augite clinopyroxenes (wt%): SiO_2, 0.2%; TiO_2, 0.04%; Al_2O_3, 0.1%; Cr_2O_3, 0.03%; FeO, 0.11%; MnO, 0.04%; MgO, 0.1%; CaO, 0.1%.

Table 2. Mineral chemistry of Summit Lake ultramafic xenoliths.

	SL-141[3] CPX 1-1	SL-141 CPX 4-1	SL-151 CPX 1-1	SL-151 CPX 2-1	SL-153 CPX 1-1	SL-154 CPX 1-1	SL-222[4] CPX 1-1
SiO_2	49.1	52.2	49.3	50.3	50.9	51.5	53.1
TiO_2	1.34	0.42	1.20	1.14	0.56	0.49	0.20
Al_2O_3	7.73	5.06	8.48	8.94	6.46	6.44	4.66
Cr_2O_3	0.42	0.92	0.12	n.d.	1.06	1.16	1.38
Fe_2O_3	n.a.	n.a.	n.a.	n.a.	n.a.	n.a.	n.a.
FeO	4.85	4.90	4.30	4.22	3.63	3.19	3.65
MnO	0.08	0.09	0.08	n.d.	0.07	n.d.	n.d.
MgO	14.7	16.7	14.8	15.1	15.8	16.5	17.2
CaO	21.4	19.4	19.9	20.3	19.8	19.5	20.6
Na_2O	0.64	0.92	1.22	n.d.	1.26	1.34	0.41
K_2O	n.d.	n.d.	n.d.	n.d.	n.d.	n.d.	n.d.
NiO	n.d.	n.d.	0.09	n.d.	0.07	0.06	0.06
TOTAL	100.26	100.61	99.49	100.00	99.61	100.18	101.26
O	6.000	6.000	6.000	6.000	6.000	6.000	6.000
Si	1.797	1.882	1.804	1.819	1.857	1.862	1.901
Al	0.333	0.215	0.366	0.381	0.278	0.274	0.197
Ti	0.037	0.011	0.033	0.031	0.015	0.013	0.005
Cr^{3+}	0.012	0.026	0.003	n.d.	0.031	0.033	0.039
Fe^{3+}	n.a.	n.a.	n.a.	n.a.	n.a.	n.a.	n.a.
Fe^{2+}	0.148	0.148	0.132	0.128	0.111	0.096	0.109
Mn	0.002	0.003	0.002	n.d.	0.002	n.d.	n.d.
Mg	0.802	0.919	0.807	0.814	0.859	0.889	0.918
Ca	0.839	0.749	0.780	0.787	0.774	0.755	0.790
Na	0.045	0.064	0.087	n.d.	0.089	0.094	0.028
K	n.d.	n.d.	n.d.	n.d.	n.d.	n.d.	n.d.
Ni	n.d.	n.d.	0.003	n.d.	0.002	0.002	0.003
SUM	4.015	4.017	4.017	3.960	4.018	4.018	3.990
Mg/(Mg+Fe)	0.84	0.86	0.86	0.86	0.89	0.90	0.89
Ca	46.9	41.3	45.4	45.5	44.4	43.4	43.5
Mg	44.8	50.6	47.0	47.1	49.3	51.1	50.5
Fe	8.3	8.1	7.6	7.4	6.3	5.5	6.0
	Sp-L	Sp-L	Sp-Wh	Sp-Wh	Sp-Wh	Sp-L	

3 - SL-141 CPX 1-1 - clinopyroxene next to spinel at basalt/xenolith contact
4 - SL-222 CPX 1-1 - host clinopyroxene with exsolution of orthopyroxene and spinel lamellae

Table 2. Mineral chemistry of Summit Lake ultramafic xenoliths.

	SL-33 SPN 2-1	SL-49 SPN 1-1	SL-99 SPN 2-1	SL-141[5] SPN 1-1	SL-141[6] SPN 3-1	SL-141[7] SPN 6-1
SiO_2	0.13	n.d.	0.14	0.20	0.27	0.17
TiO_2	0.19	n.d.	0.19	0.47	0.32	0.34
Al_2O_3	56.1	27.7	50.5	34.4	56.7	32.4
Cr_2O_3	10.4	40.7	15.9	27.1	5.40	29.1
Fe_2O_3	3.81	4.77	4.25	9.30	8.41	9.35
FeO	8.37	10.7	7.98	14.5	10.2	14.9
MnO	n.d.	n.d.	n.d.	0.29	0.17	0.30
MgO	21.1	16.8	20.6	15.1	20.2	14.5
CaO	n.d.	n.d.	n.d.	n.d.	n.d.	n.d.
Na_2O	n.d.	n.d.	n.d.	n.d.	n.d.	n.d.
K_2O	n.d.	n.d.	n.d.	n.d.	n.d.	n.d.
NiO	0.43	0.22	0.52	0.35	0.47	0.38
TOTAL	100.53	100.89	100.08	101.71	102.14	101.44
O	4.000	4.000	4.000	4.000	4.000	4.000
Si	0.003	n.d.	0.004	0.006	0.007	0.005
Al	1.699	0.950	1.570	1.161	1.710	1.108
Ti	0.004	n.d.	0.004	0.010	0.006	0.007
Cr	0.211	0.936	0.332	0.613	0.109	0.668
Fe^{3+}	0.074	0.104	0.084	0.200	0.162	0.204
Fe^{2+}	0.180	0.261	0.176	0.348	0.219	0.361
Mn	n.d.	n.d.	n.d.	0.007	0.004	0.007
Mg	0.808	0.729	0.810	0.644	0.770	0.627
Ca	n.d.	n.d.	n.d.	n.d.	n.d.	n.d.
Na	n.d.	n.d.	n.d.	n.d.	n.d.	n.d.
K	n.d.	n.d.	n.d.	n.d.	n.d.	n.d.
Ni	0.010	0.005	0.011	0.008	0.010	0.009
SUM	2.989	2.985	2.991	2.997	2.997	2.996
Mg/(Mg+Fe)	0.82	0.74	0.82	0.65	0.78	0.63
Al *	85.6	47.7	79.1	58.8	86.3	56.0
Cr^{3+} *	10.7	47.0	16.7	31.1	5.5	33.7
Fe^{3+} *	3.7	5.3	4.2	10.1	8.2	10.3
	Sp-L	Sp-L	Sp-L	Sp-L	Sp-L	Sp-L

5 - SL-141 SPN 1-1 - interstitial spinel with inclusions
6 - SL-141 SPN 3-1 - spinel next to clinopyroxene at basalt/xenolith contact
7 - SL-141 SPN 6-1 - spinel included in olivine
* Al, Cr and Fe^{3+} recalculated to 100% for spinel.
Uncertainties in microprobe analyses of spinels varies greatly with composition; For SL-49: Al_2O_3, 0.2%; Cr_2O_3, 0.3%; MgO, 0.1%; NiO, 0.07%; For SL-151: TiO_2, 0.04%; Al_2O_3, 0.3%; Cr_2O_3, 0.05%; MgO, 0.1%; NiO, 0.10%.

Table 2. Mineral chemistry of Summit Lake ultramafic xenoliths.

	SL-151 SPN 5-1	SL-153 SPN 1-1	SL-154 SPN 1-1	SL-222[8] SPN 1-1
SiO_2	n.d.	0.19	n.d.	0.36
TiO_2	0.23	0.32	0.21	0.20
Al_2O_3	63.0	51.5	51.3	37.0
Cr_2O_3	2.10	14.1	15.8	27.1
Fe_2O_3	4.69	4.65	3.63	7.35
FeO	6.98	9.41	8.43	10.1
MnO	n.d.	n.d.	n.d.	0.28
MgO	22.7	20.1	20.6	17.7
CaO	n.d.	n.d.	n.d.	n.d.
Na_2O	n.d.	n.d.	n.d.	n.d.
K_2O	n.d.	n.d.	n.d.	n.d.
NiO	0.42	0.38	0.40	0.37
TOTAL	100.12	100.66	100.37	100.46
O	4.000	4.000	4.000	4.000
Si	n.d.	0.005	n.d.	0.010
Al	1.859	1.590	1.587	1.223
Ti	0.004	0.006	0.004	0.004
Cr^{3+}	0.042	0.292	0.328	0.601
Fe^{3+}	0.088	0.092	0.072	0.155
Fe^{2+}	0.146	0.206	0.185	0.237
Mn	n.d.	n.d.	n.d.	0.007
Mg	0.847	0.785	0.806	0.740
Ca	n.d.	n.d.	n.d.	n.d.
Na	n.d.	n.d.	n.d.	n.d.
K	n.d.	n.d.	n.d.	n.d.
Ni	0.008	0.009	0.008	0.008
SUM	2.994	2.985	2.991	2.985
Mg/(Mg+Fe)	0.85	0.79	0.81	0.76
Al	93.5	80.6	79.9	61.8
Cr_{3+}	2.1	14.8	16.5	30.4
Fe^{3+}	4.4	4.6	3.6	7.8
	Sp-Wh	Sp-Wh	Sp-L	

8 - SL-222 SPN 1-1 - spinel exsolution lamella (see text)

Table 2. Mineral chemistry of Summit Lake ultramafic xenoliths.

correlation between NiO and forsterite content of the olivine. Olivine shows no intragrain heterogeneity except in one xenolith (SL-151), in which there is enrichment of CaO at the rim of the olivine where it is adjoined by clinopyroxene. Therefore, it is possible that there has been post-equilibration diffusion of cations as a result of heating during the transport of the xenolith within the host magma (Takahashi, 1980a; Ozawa, 1983).

Orthopyroxene

Orthopyroxene compositions vary from $Wo_2En_{90}Fs_8$ to $Wo_2En_{78}Fs_{20}$ (Fig. 3). The average enstatite content is En_{90}. Al_2O_3 varies from 2-6 wt% and Cr_2O_3 from 0.4-0.8 wt%. In a general way, as the En content increases, Cr_2O_3 increases and Al_2O_3 decreases and a good inverse correlation exists between Al_2O_3 in orthopyroxene and $Cr/(Cr+Al+Fe^{3+})$ in spinel (Fig. 4). Orthopyroxenes show no evidence of intragrain chemical heterogeneity.

Clinopyroxene

The compositions of both green and black clinopyroxenes are given in Table 2, and plotted in terms of Ca, Mg and Fe in Fig. 3. Chrome diopsides vary in composition from $Wo_{48}En_{53}Fs_4$ to $Wo_{48}En_{48}Fs_4$. Al_2O_3 in chrome diopsides varies from 2.5-7.0 wt% and Cr_2O_3

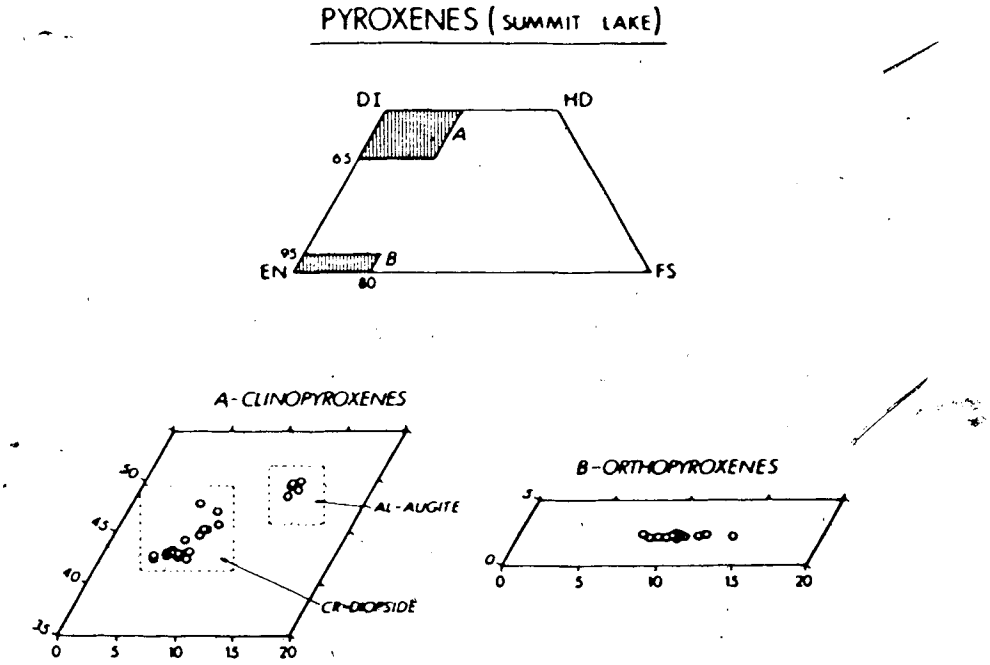

Figure 3. Compositions of pyroxenes in ultramafic xenoliths.

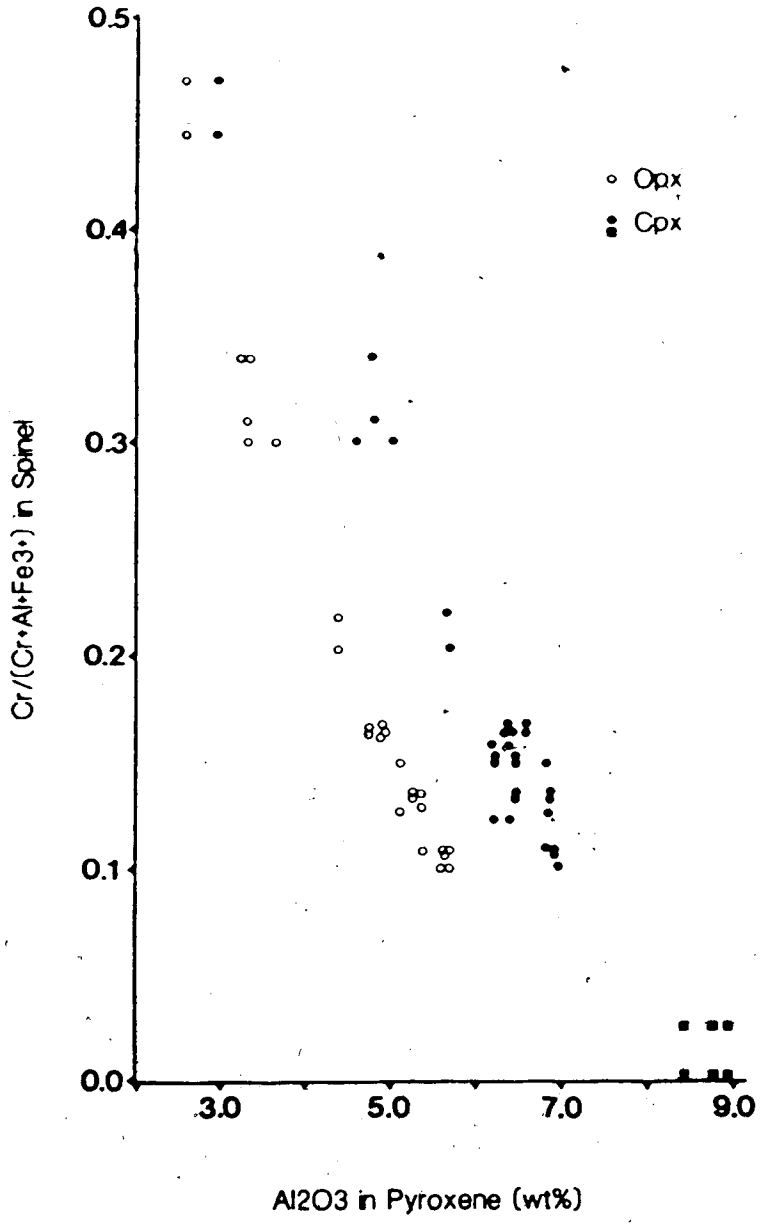

Figure 4. Variation of $Cr/(Cr+Al+Fe^{3+})$ in spinel with Al_2O_3 in pyroxene. Open circles - orthopyroxenes, closed circles - chrome diopside, squares - aluminous chrome diopside (see text for discussion).

varies from 0-1.4 wt% from nodule to nodule, depending on the composition of the coexisting spinel. There is a good correlation between Al_2O_3 in diopside and $Cr/(Cr+Al+Fe^{3+})$ in spinel (Fig. 4). As anticipated, there is a strong negative correlation between Al_2O_3 and Cr_2O_3 in diopside. The clinopyroxenes in SL-151 are unusual in that they have higher Al_2O_3 (8.0-9.0 wt%) and TiO_2, but lower Cr_2O_3 than all other chrome diopsides in the xenoliths (Fig. 4). Chemically, these clinopyroxenes are transitional towards black clinopyroxene in that CaO, FeO, Al_2O_3, and MgO are intermediate between chrome diopside and aluminous augite. Black clinopyroxenes have high CaO, FeO, Al_2O_3, and TiO_2, but low MgO, Cr_2O_3, and Na_2O compared to chrome diopsides (SL-53 CPX 2-1,3-1,4-1, Table 2). Al_2O_3 is always greater than 10.5 wt%.

No heterogeneities in Ca, Mg and Fe were detected in grains of unaltered and unreacted clinopyroxenes. Exsolution textures in clinopyroxene were found in one of the thirty xenoliths. The host clinopyroxene is a chrome diopside that has exsolved both enstatite and aluminous spinel (Table 2).

Spinel

Spinels vary widely in Cr_2O_3 and Al_2O_3 content throughout the suite of xenoliths. Cr_2O_3 varies from 2.1-40.7 wt% and Al_2O_3 varies from 27.7-63.0 wt%.

Except in unusual circumstances where it is clear that several spinel phases coexist (e.g., SL-141), there appears to be no significant variation in spinel composition within individual nodules. $Mg/(Mg+Fe^{2+})$ varies from 0.65 to 0.85 and there are good correlations between Cr_2O_3 and Al_2O_3 content in spinel and $Cr/(Cr+Al+Fe^{3+})$ in spinel versus Al_2O_3 in pyroxene (Fig. 4). No zoning was detected in spinels by microprobe.

F. Discussion

Xenoliths with chrome diopside

Microprobe analyses of xenoliths that contain chrome diopside indicate nothing unusual about the mineral chemistry of these xenoliths, except for SL-141 which will be discussed later. The compositions of the mineral phases fall within the accepted limits for xenoliths of this type (e.g., Kuno and Aoki, 1970; Littlejohn and Greenwood, 1974). Olivine averages Fo_{90}, orthopyroxene averages En_{90}, and Al_2O_3 in pyroxene shows a good negative correlation with $Cr/(Cr+Al+Fe^{3+})$ in spinel as discussed previously in the literature (e.g., Fujii and Scarfe, 1982). Thus, the relatively refractory compositions of the Summit Lake chrome diopside xenoliths may represent a residuum remaining after at least one phase of partial melting. A similar

conclusion has been reported in numerous other publications (e.g., Kuno and Aoki, 1970; Littlejohn and Greenwood, 1974; Fujii and Scarfe, 1982).

Exsolution textures are rare in pyroxenes from ultramafic xenoliths; however, at Summit Lake, lamellar exsolution of spinel and orthopyroxene has been noted in a chrome diopside band approximately 1cm wide. The host clinopyroxene is low in aluminum and high in Cr_2O_3 and Na_2O, similar in composition to chrome diopsides that do not show exsolution. The $Wo_2En_{9.7}Fs_{1.1}$ composition of the orthopyroxene lamellae is identical to orthopyroxene grains in the xenoliths. However, the spinel contains more Cr_2O_3 and total iron than is commonly present in spinels from Summit Lake. Clinopyroxene seems to have first exsolved orthopyroxene, depleting the host in Mg and Fe and enriching it in Cr and Al. Continued subsolidus cooling caused the clinopyroxene to exsolve spinel lamellae that transgress the earlier orthopyroxene lamellae.

Further evidence of the complex history of some of the Summit Lake ultramafic xenoliths is indicated by the presence of glass, commonly observed in pyroxenes (Maaløe and Printzlau, 1979) and by reaction rims around spinels. Clinopyroxenes in several of the xenoliths exhibit ragged edges that contain small vermicular pockets of glass. In some cases, the glass is more pervasive and it is present throughout the

grain. More rarely, orthopyroxenes show similar features. The presence of glass or quenched melt in the pyroxenes may be caused by either instability due to decompression as the xenolith is transported to the surface, or to heating of the xenolith by the host basalt.

Reaction rims, 0.01-0.02mm in width, are common around spinels which have a high Cr_2O_3 content, which suggests that the Cr-rich spinel may become unstable as the xenolith is brought to shallower depths.

Xenolith SL-141 is unusual in that there are three discrete spinel phases (Table 2) all with markedly different modes of occurrence, as noted previously. Spinel SPN 3-1 always adjoins clinopyroxene and it is possible that this spinel has resulted either from exsolution of clinopyroxene or that it formed by reaction, triggered by temperature differences during incorporation of the xenolith in the host basalt.

The silicate minerals in SL-141 are more iron-rich than in any other Summit Lake xenolith (Table 2). Olivine is $Fo_{8.5}$, orthopyroxene $Wo_2En_{84}Fs_{14}$ and chrome diopside $Wo_{44}En_{51}Fs_5$. It is possible that the xenolith represents a cumulate, which has been texturally re-equilibrated within the upper mantle. Similar iron-rich xenoliths have been reported in the literature (e.g., Wilkinson and Binns, 1977).

Xenoliths with aluminous augite

Black clinopyroxene-bearing xenoliths are less common than those containing chrome diopside (Fig. 1). All aluminous augite occurs in thin dyke-like bodies of clinopyroxenite up to 2cm in width and as discrete phases in wehrlite xenoliths. The black aluminous augites observed at Summit Lake are compositionally similar to those described previously in the literature (e.g., Aoki and Kushiro, 1968; Wilshire and Shervais, 1975; Frey and Prinz, 1978). According to the terminology of Frey and Prinz (1978), the Summit Lake aluminous augite xenoliths would belong to their Group II xenoliths; however, the aluminous augites presented in this paper are more aluminous (Al_2O_3 usually >11.0 wt%) and have no Na_2O. They have higher TiO_2, FeO and CaO, but less Cr_2O_3, MgO and SiO_2 than chrome diopside (Table 2). It is possible that some clinopyroxenes from Summit Lake are intermediate between the two clinopyroxene types. For example, clinopyroxene in SL-151 contains values of Al_2O_3, CaO, FeO and MgO that lie between chrome diopside and aluminous augite (Table 2). These clinopyroxenes contain between 8 and 9 wt% Al_2O_3 and coexist with highly aluminous spinels. Although the clinopyroxenes in SL-151 are chrome diopsides and agree with the trend observed in Fig. 4, they do form a distinct group.

Because of the high concentrations of non-quadrilateral components, aluminous augite clinopyroxenes plot closer to the diopside-hedenbergite join when projected into the pyroxene quadrilateral (Fig. 3). The proposal that the aluminous augites are precipitates from an alkalic liquid at high pressure along narrow conduits within spinel lherzolite (Irving, 1980) readily explains their occurrence in thin bands that cross-cut spinel lherzolite xenoliths.

Estimation of Equilibration Temperatures and Pressures

The compositions of the coexisting minerals in chrome diopside xenoliths were used to estimate the equilibration temperature of the ultramafic xenoliths. Several geothermometers are applicable, but the two-pyroxene thermometer of Wells (1977) was chosen for this study because it has been commonly used in similar work (Fujii and Scarfe, 1982) and comparison of data is therefore facilitated. The equilibration temperatures of the Summit Lake chrome diopside-bearing xenoliths range between 1050-1150°C, but cluster tightly around 1080-1100°C. These are subsolidus temperatures and the errors are ±50°C for the geothermometer and ±10°C for the microprobe analyses.

The limitations of geothermometry have been discussed extensively in the literature (e.g., Henry and Medaris, 1980; Lindsley et al., 1981; Fujii and

Scarfe, 1982) and further detailed discussion is not warranted here. However, it is worth noting that the geothermometer recently devised by Lindsley and Andersen (1983) and discussed by Lindsley (1983) has not been used. Unfortunately the geothermometer is not applicable to pyroxenes from ultramafic xenoliths because of the presence of an excess of additional components such as Al_2O_3, which do not permit accurate projection into the pyroxene quadrilateral (Lindsley and Andersen, 1983). Similar problems arise for aluminous augites and the chemistry of aluminous augite renders it unsuitable for geothermometry.

In the absence of suitable geobarometers, Fig. 5a shows the geotherm beneath Summit Lake that was constructed using the calculated equilibration temperatures and the published stability field of spinel lherzolite. Using these constraints, the geotherm beneath this locality appears to be steeper than other localities in British Columbia (Fujii and Scarfe, 1982; Scarfe et al., 1982). Alternatively, assuming that the xenoliths were equilibrated on the Cordilleran geotherm (Ranalli, 1980), one can estimate the depth of origin of the xenoliths more precisely (Fig. 5b). In this case the depth of origin can be bracketed between 55-65 km (18-20 kbar). Ross (1983) published a geotherm for Summit Lake xenoliths using the methods of pyroxene thermobarometry (Mercier, 1976;

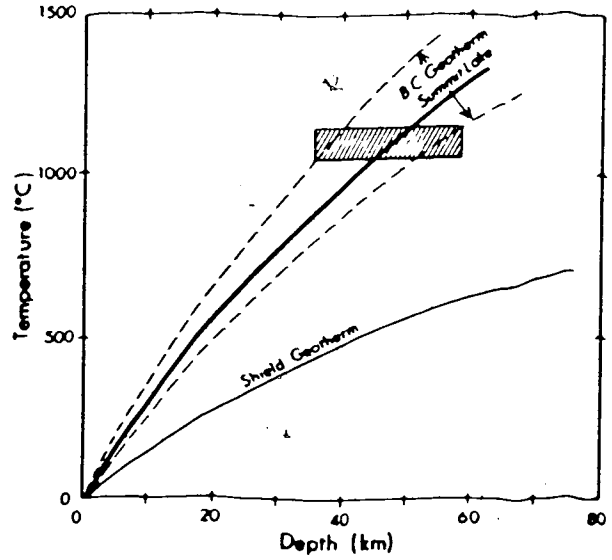

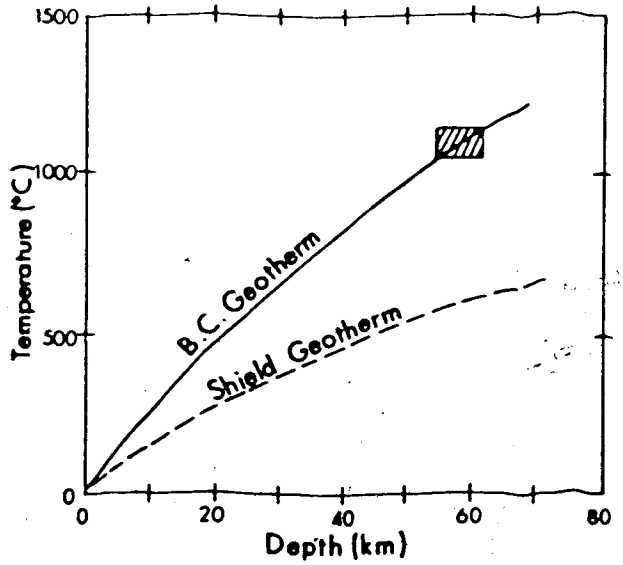

Figure 5a. Estimate of the geotherm beneath Summit Lake using the temperatures of equilibration and the pressures estimated from published phase equilibrium studies. Dashed lines indicate possible errors in the geotherm. 5b. Estimate of the depth of origin of chrome diopside xenoliths using a Cordilleran geotherm (Ranalli, 1980). The depth is constrained by the temperatures of equilibration projected onto the geotherm.

1980). This geotherm has not been included in Fig. 5 because the methods of Mercier (1980) are believed to be controversial and require experimental data on the effect of Cr_2O_3 on the solubility of Al_2O_3 in orthopyroxene coexisting with spinel.

In addition to the above considerations, we must be certain that ultramafic xenoliths were equilibrated in the upper mantle and have suffered no subsequent modifications of their mineral chemistry. Recently, evidence has been presented for solid-state diffusion of cations between the mineral phases in some ultramafic xenoliths (e.g., Takahashi, 1980a; Smith and Roden, 1981; Ozawa, 1983). It is not clear, however, whether the zoning observed in these cases is produced by heating by the host magma (minimum 7 hrs. duration, Fujii and Scarfe, 1982) or by a longer duration event within the upper mantle. The effect is usually of the order of tens of microns (e.g., Ozawa, 1983) and is restricted to the edges of grains. In the case of the Summit Lake xenoliths, the analytical strategy was carefully designed to avoid the edges of grains, except where tests for homogeneity were concerned. Thus, the chemical analyses presented are of the cores of grains, and any grains showing reaction or melting were avoided. Therefore, the temperatures derived from the Summit Lake xenoliths represent subsolidus equilibration temperatures within the upper mantle.

G. Summary

A study of approximately 200 upper mantle xenoliths from Summit Lake, north-central British Columbia indicates that the upper mantle beneath Summit Lake is heterogeneous and banded on a scale of centimeters to meters. The xenoliths are granular and the dominant mineralogy is spinel lherzolite. Both chrome diopside and aluminous augite clinopyroxene series xenoliths are present.

Equilibration temperatures of xenoliths with chrome diopside are between 1080-1100°C using the Wells (1977) geothermometer. Assuming that the xenoliths were equilibrated on the Cordilleran geotherm of Ranalli (1980), the depth of origin is calculated to be between 55-65 km. These temperatures are somewhat higher than those derived from similar suites of the same age in southern British Columbia, suggesting that either the xenoliths were derived from a deeper source region or that the geotherm varies between north-central and southern British Columbia.

III. Amphibole in a spinel lherzolite xenolith: evidence for volatiles and partial melting in the upper mantle beneath southern British Columbia

A. Introduction

Ultramafic mantle xenoliths in alkali basalts have been documented from several localities in British Columbia (e.g., Littlejohn and Greenwood, 1974; Fiesinger and Nicholls, 1977; Hamilton 1981; Brearley et al., 1982; Fujii and Scarfe, 1982; Scarfe et al., 1982; Nicholls et al., 1982). The xenoliths always occur in alkalic volcanics found mainly within the Intermontane Belt of British Columbia (Souther, 1977; Nicholls et al., 1982). The mineralogical composition of the ultramafic xenoliths varies from pyroxenite to dunite, but the predominant type is chrome diopside-bearing spinel lherzolite (Fujii and Scarfe, 1982). On the other hand, the mineral chemistry of the silicate minerals within the xenoliths is relatively constant (Littlejohn and Greenwood, 1974; Fujii and Scarfe, 1982). Element partitioning geothermometers have shown that the equilibration temperatures of the xenoliths are in the subsolidus region of spinel lherzolite, varying from 950°C in southern British Columbia to 1100°C in north central British Columbia (Littlejohn and Greenwood, 1974; Brearley et al. 1982; Fujii and Scarfe, 1982; Nicholls et al., 1982).

No hydrous minerals have been previously observed within any of the xenoliths from British Columbia, although amphiboles and micas have been described in both garnet- and spinel-bearing ultramafic xenoliths from elsewhere in the world (e.g., Dawson and Smith, 1982). In spinel-bearing xenoliths, the most common hydrous mineral is amphibole. Pargasitic amphibole commonly occurs in chrome diopside-bearing spinel lherzolites and kaersutite occurs in aluminous augite-bearing xenoliths (Wilshire and Shervais, 1975; Frey and Prinz, 1978; Wilshire et al., 1980; Dawson and Smith, 1982). The presence of hydrous minerals in ultramafic xenoliths is important in mantle petrology. Their stability in spinel- and garnet lherzolites is central to current ideas on volatile storage (Boettcher et al., 1979; Delaney et al., 1980; Smith et al., 1981; Ito et al., 1983), metasomatism and magmatic processes in the upper mantle (e.g., Boettcher and O'Neil, 1980; Irving, 1980).

This chapter describes the first reported occurrence of amphibole in an ultramafic xenolith from Lightning Peak, near Vernon, British Columbia. The mineralogy and mineral chemistry of the ultramafic xenolith is presented. The occurrence and mineral chemistry of the amphibole is then described and the implications for the generation of basaltic magmas and the composition of the upper mantle beneath that part

of southern British Columbia are briefly discussed.

B. Field setting and petrography

The ultramafic xenoliths at Lightning Peak (49° 52.7'N, 118° 31.7'W) occur in an alkali basaltic lava flow. The host basalt contains phenocrysts of olivine (10-15%) and titanaugite (2-5%) in a fine grained groundmass of granular clinopyroxene, magnetite and plagioclase microlites. The phenocrysts range up to 2mm in size. The groundmass also contains irregular patches of K-feldspar (microcline) which poikilitically enclose other groundmass phases. This is especially evident around xenocrysts and at the contact between the basalt and the xenolith. Xenocrysts of olivine, orthopyroxene and spinel are abundant (15-20%). Olivine and orthopyroxene xenocrysts have 1-2mm reaction coronas suggesting crystal-melt disequilibrium. The contact between the host basalt and the xenolith is sharp. The host basalt has been dated at 2.5 ±0.1 Ma by the K-Ar method (B.N. Church pers. comm.).

The xenolith that contains the amphibole is a subrounded, chrome diopside-bearing, spinel lherzolite, approximately 10cm in diameter. The estimated mode of the xenolith is olivine (60%), orthopyroxene (20%), clinopyroxene (10%), spinel (5%) and amphibole (<5%). Grain sizes within the xenolith vary from <1mm (amphibole) to 4mm (olivine) and textures are

predominantly protogranular metamorphic (Mercier and Nicolas, 1975). Amphibole occurs as anhedral interstitial grains up to 2mm in size. It is typically red-brown in colour, shows weak pleochroism and inclined extinction (5-15°). The most notable feature of the amphibole in thin section is evidence of melting, shown by small, dark areas around the edges of grains. Some grains have suffered more pervasive melting, in which the melted regions occur throughout the mineral grain. These grains were avoided during electron microprobe analysis.

C. Analytical methods

The mineral phases in the Lightning Peak xenolith were analysed at the University of Alberta using an ARL SEMQ electron microprobe fitted with an ORTEC energy dispersive spectrometer. All analyses were performed by energy dispersive analysis with operating conditions of 15 kV accelerating potential, 4 nA probe current and a counting time of 240 seconds. A rastered beam of approximately 15 μm x 15 μm was used in the analysis of the anhydrous minerals. A point beam was used in the analysis of the amphibole grains, in order to avoid the melted regions within the grains. Because the amphibole is likely to degrade under the beam, the sample was moved continuously under a point beam during each analysis. Only the core portions of amphiboles which

showed the least amount of melting were analysed and, because of the widespread melting, no attempt was made to investigate intragrain heterogeneity in the amphibole. Microprobe spectra were processed with full ZAF corrections by EDATA2 (Smith and Gold, 1979). All iron in the analyses is reported as FeO. The amphibole structural formulae were calculated water free on the basis of 23 oxygens as recommended by Leake (1978).

D. Ultramafic xenoliths

The compositions of the mineral phases in the xenolith, except amphibole, are given in Table 3. The assemblage and mineral chemistry is typical of an upper mantle which is inferred to have undergone some previous partial melting (e.g., Kuno and Aoki, 1970; Fujii and Scarfe, 1982). Olivine is Fo_{90}, orthopyroxene $Wo_1En_{90}Fs_9$, and clinopyroxene is chrome diopside ($Wo_{47}En_{47}Fs_6$). Spinel is aluminous (Al_2O_3=58.9 wt%) and $Mg/(Mg+Fe^{2+})$ in spinel is 0.83. No intragrain or intergrain heterogeneities were detected in any of the anhydrous mineral phases.

The equilibration temperatures of the Lightning Peak ultramafic xenoliths may be estimated with the two-pyroxene geothermometer of Wells (1977). The temperatures are calculated to be between 960-970°C, which is well below the solidus of spinel lherzolite (e.g., Carmichael et al., 1974; Takahashi and Kushiro,

	OLV 2-1	OPX 1-1	CPX 1-1	SPN 1-1
SiO_2	40.8 (0.2)	55.9 (0.3)	52.9 (0.2)	0.20 (0.03)
TiO_2	n.d.	n.d.	0.57 (0.04)	n.d.
Al_2O_3	n.d.	4.43 (0.06)	7.07 (0.07)	58.9 (0.3)
Cr_2O_3	n.d.	0.32 (0.06)	0.86 (0.05)	9.43 (0.11)
Fe_2O_3	n.a.	n.a.	n.a.	2.57
FeO	9.82 (0.13)	6.36 (0.11)	2.66 (0.07)	7.99
MnO	0.17 (0.04)	0.14 (0.03)	0.08 (0.02)	0.16 (0.02)
MgO	48.7 (0.2)	34.0 (0.2)	15.5 (0.1)	21.6 (0.2)
CaO	n.d.	0.59 (0.03)	20.8 (0.1)	n.d.
Na_2O	n.d.	n.d.	1.37 (0.11)	n.d.
K_2O	n.d.	n.d.	n.d.	n.d.
NiO	0.52 (0.07)	0.15 (0.04)	n.d.	0.49 (0.07)
TOTAL	100.01	101.89	101.81	101.34
O	4.000	6.000	6.000	4.000
Si	1.001	1.896	1.874	0.005
Al	n.d.	0.177	0.295	1.757
Ti	n.d.	n.d.	0.015	n.d.
Cr_{3+}	n.d.	0.009	0.024	0.189
Fe_{2+}	n.a.	n.a.	n.a.	0.049
Fe	0.202	0.180	0.079	0.169
Mn	0.004	0.004	0.002	0.003
Mg	1.782	1.719	0.818	0.815
Ca	n.d.	0.021	0.789	n.d.
Na	n.d.	n.d.	0.094	n.d.
K	n.d.	n.d.	n.d.	n.d.
Ni	0.010	0.004	n.d.	0.010
SUM	2.999	4.011	3.990	2.997
Mg/(Mg+Fe)	0.90	0.91	0.91	0.83
* Ca(Al)	0.0	1.1	46.8	88.1
* Mg(Cr)	89.8	89.5	48.5	9.5
* Fe(Fe^{3+})	10.2	9.4	4.7	2.4

n.d. - not detected, n.a. - not analyzed
All Fe in silicates expressed as FeO
Fe_2O_3 in spinel by stoichiometry
Average analyses of at least 4 analyses per mineral - 2 standard deviation uncertainties in parentheses
* Ca, Mg and Fe recalculated to 100% for silicate minerals; Al, Cr and Fe^{3+} recalculated to 100% for spinel.

Table 3. Mineral chemistry of the Lightning Peak ultramafic xenolith. See Table 2 for evaluation of uncertainties in microprobe analyses.

1983). Using the same geothermometer, Fujii and Scarfe (1982) obtained similar temperatures for ultramafic xenoliths from nearby West Kettle River in southern British Columbia. It appears, therefore, that the Late Cenozoic alkali basalt host magmas are sampling the same level of the upper mantle at both localities.

Amphibole mineral chemistry

Representative microprobe analyses of the amphibole are given in Table 4. The amphibole is extremely calcic (CaO = 10.4-10.7 wt%), magnesian ($Mg/(Mg+Fe^{2+}) = 0.89$) and low in K_2O. All grains are titaniferous (TiO_2 = 2.3 wt%) and Cr_2O_3 is 1.0 wt%. The amphiboles show no intergrain heterogeneities (Table 4).

According to the classification scheme of Leaké (1978), the Lightning Peak amphibole is a pargasite. Pargasite and Ti-pargasite have been observed in ultramafic xenoliths from other localities in the world (e.g., Frey and Prinz, 1978; Dawson and Smith, 1982). Comparative analyses of pargasitic amphiboles from other chrome diopside-bearing xenoliths are also given in Table 4. Except for minor variations in TiO_2, FeO and MgO, the Lightning Peak pargasite compares closely with these analyses.

Evans (1982) has recently defined compositional fields for pargasite stably coexisting with a spinel

	1	2	3	4	5	6	7	8
SiO_2	43.3	42.9	43.2	43.2	43.3	43.51	43.18	43.3
TiO_2	2.26	2.24	2.31	2.24	2.34	0.49	1.67	1.8
Al_2O_3	15.7	15.2	15.5	15.4	15.5	14.74	14.87	15.4
Cr_2O_3	1.08	1.04	1.06	1.00	1.10	1.07	1.18	1.13
FeO	3.77	3.89	3.96	3.81	4.03	4.00	4.40	4.7
MnO	0.15	n.d.	0.10	n.d.	n.d.	0.09	0.10	n.d.
MgO	17.1	17.6	17.5	17.1	17.7	19.18	18.0	17.3
CaO	10.7	10.4	10.5	10.5	10.6	10.70	10.57	10.8
Na_2O	3.46	3.71	3.74	3.59	3.54	3.93	3.09	3.5
K_2O	0.12	0.15	0.20	0.12	0.18	0.19	1.63	0.02
TOTAL	97.64	97.13	98.07	96.96	98.29	97.90	98.69	97.95
O	23.000	23.000	23.000	23.000	23.000	23.000	23.000	23.000
Si	6.121	6.106	6.095	6.146	6.092	6.159	6.111	6.126
Al	2.616	2.550	2.577	2.582	2.570	2.459	2.480	2.568
Ti	0.240	0.240	0.245	0.240	0.248	0.052	0.178	0.191
Cr	0.121	0.117	0.118	0.112	0.122	0.120	0.132	0.126
Fe^{2+}	0.446	0.463	0.467	0.453	0.474	0.473	0.521	0.556
Mn	0.018	n.d.	0.012	n.d.	n.d.	0.011	0.012	n.d.
Mg	3.603	3.734	3.680	3.626	3.712	4.047	3.797	3.648
Ca	1.621	1.586	1.587	1.600	1.598	1.623	1.603	1.637
Na	0.948	1.024	1.023	0.990	0.966	1.078	0.848	0.960
K	0.022	0.027	0.036	0.022	0.032	0.034	0.294	0.004
SUM	15.755	15.846	15.841	15.773	15.813	16.056	15.976	15.817
Mg/(Mg+Fe)	0.89	0.89	0.89	0.89	0.89	0.90	0.88	0.87

n.d. - not detected, FeO is total Fe. H_2O assumed to be difference from 100%. Analyses 1 to 5, this study. Analyses have the following 2 standard deviation uncertainties: SiO_2, 0.2; TiO_2, 0.06; Al_2O_3, 0.2; Cr_2O_3, 0.05; FeO, 0.10; MnO, 0.02; MgO, 0.2; CaO, 0.1; Na_2O, 0.23; K_2O, 0.02; Analysis 6 is analysis 3, 7 analysis 11, 8 analysis 14 from Dawson and Smith (1982)

Table 4. Lightning Peak amphiboles and other selected analyses of pargasite from ultramafic xenoliths. See Table 2 for evaluation of uncertainties in microprobe analyses.

lherzolite mineralogy. The Lightning Peak pargasite falls well within these fields and thus we infer that this pargasite is in equilibrium with an upper mantle of spinel lherzolite composition.

E. Discussion

The presence of amphibole in ultramafic xenoliths has been interpreted in different ways depending on its composition and mode of occurrence. Kaersutite is commonly found in pyroxene-bearing veins which transgress xenoliths of the chrome diopside xenolith suite (Wilshire and Shervais, 1975; Francis, 1976a; Irving, 1980; Wilshire et al., 1980). This type of occurrence has been ascribed to infiltration metasomatism by alkalic fluids along veins (Francis, 1976a; Irving, 1980; Wilshire et al., 1980). Other kaersutitic amphiboles are believed to result from crystallization of intercumulus liquid of nephelinite composition (Frey and Prinz, 1978).

Pargasitic amphiboles in chrome diopside-bearing xenoliths are believed to be either in textural equilibrium with the other mineral phases in the xenolith (Varne, 1970), or they are considered to be metasomatic replacements of spinel in spinel lherzolite (e.g., Francis, 1976a; Wilshire et al., 1980), or of garnet or clinopyroxene in garnet lherzolites (Nixon and Boyd, 1979). In the latter case, it is evident that

pargasite is stable at pressures within the garnet field of the upper mantle. However, Aoki and Kushiro (1968) argued that pargasite from Dreiser Weiher formed at 20-30 km depth within the lower crust. Therefore, pargasite appears to be stable through a wide pressure range, a fact recently confirmed by Gilbert et al. (1982) and Jenkins (1983).

The occurrence and texture of the pargasite at Lightning Peak suggests that the amphibole crystallized in the xenolith at a pressure within the spinel stability field of the upper mantle and it appears to be in textural and chemical equilibrium with the other xenolith mineral phases. There is no evidence that the amphibole is replacing any mineral and it does not occur in veins. It is suggested that the amphibole crystallized from a metasomatic fluid that percolated along grain boundaries of the lherzolite. This mechanism has been proposed previously to account for the metasomatic introduction of hydrous minerals in the upper mantle (Frey and Prinz, 1978; Boettcher et al., 1979; Boettcher and O'Neil, 1980; Bailey, 1982). The origin of the metasomatic fluids is the subject of considerable debate, but they may be related to the evolution of a volatile-rich fluid produced by the dehydration of subducted material (Boettcher and O'Neil 1980).

In southern British Columbia, subduction was active during the Late Cenozoic period when the calc-alkaline lavas of the Garibaldi region were produced (Fiesinger, 1975; Fiesinger and Nicholls, 1977; Nicholls et al., 1982). Therefore, it is possible that the amphibole in the Lightning Peak ultramafic xenolith has formed from metasomatic fluids, produced by dehydration of the slab which was subducted beneath southern British Columbia during the Late Cenozoic. The fluids have since modified the upper mantle beneath certain areas of southern British Columbia. Heterogeneities in the upper mantle beneath British Columbia have been discussed in the literature (Fujii and Scarfe, 1982; Nicholls et al., 1982). In these cases, anhydrous spinel lherzolite contains bands or veins rich in chrome diopside and aluminous augite (Fujii and Scarfe 1982). Therefore, the occurrence of amphibole in the ultramafic xenolith at Lightning Peak is further evidence that parts of the upper mantle beneath British Columbia are heterogeneous.

The melting observed in the pargasite can be interpreted in several ways. Melting could be produced as a result of the xenolith being incorporated in the magma. The increase in temperature of approximately 300°C (assuming an ambient temperature of 960-970°C in the upper mantle) would cause the amphibole to break down according to the reaction proposed by Holloway

(1973) and Jenkins (1983):

2Pargasite + Vapour --- 3Diopside + 2Forsterite + Spinel + Liquid (1)

This reaction proceeds in the presence of pure H_2O at approximately 1050°C at pressures within the spinel stability field. However, pargasite is stable above 1100°C if the vapour is an H_2O-CO_2 mixture (Holloway, 1973; Gilbert et al., 1982). Alternatively, the amphibole would begin to melt due to decompression as the host magma ascended to the surface. If adiabatic ascent is assumed, then reaction (1) will again be applicable (Jenkins, 1983). Unfortunately, it is not possible to ascertain whether this reaction is operative because the melting products can not be positively identified. The third alternative is that natural partial melting may have taken place in the upper mantle. In this case, the partial melt would be quenched as the xenolith was transported to the surface.

Melting of pargasite at high pressure in the presence of H_2O will produce a liquid close to nephelinite in composition (Varne, 1968; Holloway, 1973; Jenkins, 1983). Alkalic magmatism has been important in Late Cenozoic times in British Columbia (Nicholls et al., 1982) and the lavas erupted range in composition from nephelinite to alkali basalt

(Fiesinger, 1975; Fiesinger and Nicholls, 1977; Nicholls et al., 1982). However, the lavas can not be in equilibrium with spinel lherzolite containing olivine of Fo_{90} composition and as a result it has been proposed that either the upper mantle is more iron-rich than is observed in ultramafic xenoliths or that the lavas have been compositionally modified during ascent (Nicholls et al., 1982). Therefore, the melting of pargasite-bearing spinel lherzolite in the upper mantle to produce nephelinite may be one mechanism of generating the alkaline volcanic rocks observed in British Columbia.

F. Conclusions

The pargasitic amphibole that occurs in a spinel lherzolite xenolith from Lightning Peak is the first occurrence of amphibole from the upper mantle in British Columbia. The pargasite is in textural and chemical equilibrium with the lherzolite. Its presence is further evidence of the heterogeneous nature of the upper mantle beneath British Columbia and it may have formed as a result of metasomatism by fluids evolved from material subducted under southern British Columbia during the Cenozoic. Late Cenozoic alkaline volcanics of the Intermontane Belt of British Columbia may be the product of partial melting of an upper mantle of pargasite-bearing spinel lherzolite.

IV. The petrology of ultramafic xenoliths from the Seward Peninsula, western Alaska: a preliminary investigation

A. Introduction

Ultramafic xenoliths have been found in alkali basaltic rocks in several areas in western Alaska and the Aleutian island arc (Fig. 1 in Swanson et al., 1985). The Aleutian island arc has been formed by subduction of the Pacific Plate beneath the North American Plate, whereas the western Alaska area is dominated by extensional tectonism (Swanson et al., 1985). The entirely different tectonic settings of these two areas could provide an insight into the nature of the underlying upper mantle (Swanson et al., 1985). However, the petrology of ultramafic xenoliths from Alaska and the Aleutian Islands is poorly known, with the exception of Nunivak Island (e.g., Francis, 1976a; b; Roden et al., 1984). Extensive mantle metasomatism has been proposed as the mechanism which most adequately explains the mineralogy, geochemistry and textures present in the xenoliths found on Nunivak Island.

In this chapter, the results of a study of a suite of 25 ultramafic xenoliths from Virginia Butte on the Seward Peninsula of western Alaska are presented.

The petrography, mineralogy and mineral chemistry of selected xenoliths indicates that the upper mantle beneath this locality is dominantly composed of spinel lherzolite. However, the compositions of the silicate minerals varies from xenolith to xenolith, indicating that the upper mantle is chemically heterogeneous, possibly as a result of metasomatism. Comparative geothermometry suggests that the geotherm beneath this locality is similar to those proposed for localities in British Columbia.

B. Petrography

The ultramafic xenoliths vary in size from <1cm to 5cm in diameter and are relatively coarse grained with crystals of 1-4mm in size. Chrome diopside-bearing spinel lherzolite is the most abundant rock type (85%), with subordinate harzburgite (~10%) and wehrlite (5%). The host basalt enclosing the xenoliths is an olivine-phyric basalt (Table 5; Swanson et al., 1981), with olivine phenocrysts comprising 10-15% by volume. The groundmass of the basalt consists of granular clinopyroxene, magnetite and plagioclase laths, which occasionally exhibit a crudely developed trachytic texture. Thin sections of 10 of the ultramafic xenoliths were examined. Textures within the xenoliths are predominantly metamorphic and mostly equigranular,

although protogranular and relict magmatic textures are sometimes preserved (Mercier and Nicolas, 1975). The only evidence for deformation is the ubiquitous presence of kink banding in olivine. The contact between the host basalt and the xenoliths is usually sharp; however, olivine and orthopyroxene grains at the periphery of the xenolith occasionally have ragged edges, which may be evidence of partial dissolution of the xenolith by the basalt. Some xenoliths have been invaded by the host basalt along grain boundaries, resulting in partial or total replacement of some of the mineral phases by plagioclase.

In the spinel lherzolites, olivine is the dominant mineral comprising >50% by volume of all the xenoliths. Orthopyroxene (10-30%), clinopyroxene (5-20%) and spinel (0-10%) are the subordinate mineral phases. Pyroxenes rarely exhibit exsolution textures, and only orthopyroxene shows any evidence of unmixing. In this case, large grains of orthopyroxene have exsolved lamellae of clinopyroxene (<10μm in width) parallel to (001). Pyroxene grains often contain vermicular pockets of glass, suggesting that they have been partially melted. Other evidence of reaction textures is the occurrence of reaction rims of spinel + glass around spinel grains, due to decompression.

C. Mineral chemistry

Analytical methods

The compositions of the minerals in 8 of the ultramafic xenoliths were analyzed by electron microprobe. Both energy dispersive and wavelength dispersive techniques were used. Operating conditions for EDA were 15 kV accelerating potential, 4 nA probe current, 240 second counting times and a rastered beam area of 15 μm x 15 μm. For investigations into mineral heterogeneities WDA was used with a probe current of 24 nA, and 40 second counting times on both standards and samples. All microprobe analyses were processed with full ZAF corrections using EDATA2 (Smith and Gold, 1979). Errors in the analyses are quoted at the 2 standard deviation level of the amount present.

D. Results

Representative analyses of the constituent minerals in the ultramafic xenoliths are shown in Table 5. In general, the majority of the xenoliths contain olivine with a composition of around Fo_{90}, coexisting with chrome diopside, orthopyroxene and spinel all with high Mg/(Mg+Fe) ratios. However, the mineral phases in two of the eight xenoliths studied were more iron-rich. No intragrain heterogeneities were detected in any of

	1	2	3	4	5	6	7	8	9
(a)	BAS	AL-2	AL-1	AL-6	AL-15	AL-2	AL-1	AL-6	AL-15
SiO_2	43.31	52.7	52.5	51.6	51.6	54.2	54.7	54.5	54.0
TiO_2	3.18	0.14	0.47	0.46	0.50	n.d.	0.12	0.10	0.10
Al_2O_3	14.17	5.61	4.74	5.73	6.94	3.88	3.88	3.32	4.80
Cr_2O_3	n.a.	0.70	0.73	0.94	0.62	0.25	0.41	0.32	0.34
Fe_2O_3	4.14	n.a.	n.a.	n.a.	n.a.	n.a.	n.a.	n.a.	n.a.
FeO	7.89	3.75	2.41	2.42	3.41	9.67	6.47	6.37	7.56
MnO	0.17	n.d.	n.d.	n.d.	n.d.	0.17	0.16	0.17	0.14
MgO	9.95	15.7	16.6	16.0	15.9	31.8	34.0	33.8	32.9
CaO	9.15	19.8	21.6	21.4	19.6	0.51	0.53	0.51	0.70
Na_2O	3.55	1.26	1.37	1.51	1.23	n.d.	n.d.	n.d.	n.d.
NiO	n.a.	0.09	0.08	n.d.	0.09	n.d.	0.14	0.15	0.12
K_2O	1.43	n.d.	n.d.	n.d.	n.d.	n.d.	n.d.	n.d.	n.d.
TOTAL	96.94	99.75	100.50	100.06	99.89	100.48	100.41	99.24	100.66
				Structural Formulae					
O		6.000	6.000	6.000	6.000	6.000	6.000	6.000	6.000
Si		1.912	1.893	1.870	1.866	1.894	1.888	1.902	1.869
Ti		0.004	0.013	0.013	0.014	n.d.	0.003	0.003	0.003
Al		0.240	0.201	0.245	0.296	0.160	0.158	0.137	0.196
Cr_{3+}		0.020	0.021	0.027	0.018	0.007	0.011	0.009	0.009
Fe_{2+}		n.a.	n.a.	n.a.	n.a.	n.a.	n.a.	n.a.	n.a.
Fe^{2+}		0.114	0.073	0.073	0.103	0.283	0.187	0.186	0.219
Mn		n.d.	n.d.	n.d.	n.d.	0.005	0.005	0.005	0.004
Mg		0.849	0.892	0.864	0.857	1.656	1.749	1.758	1.697
Ca		0.769	0.834	0.831	0.759	0.019	0.020	0.019	0.026
Na		0.089	0.096	0.106	0.086	n.d.	n.d.	n.d.	n.d.
Ni		0.003	0.002	n.d.	0.003	n.d.	0.004	0.004	0.003
SUM		4.000	4.025	4.029	4.002	4.024	4.025	4.023	4.026
Mg/(Mg+Fe)		0.88	0.93	0.92	0.89	0.85	0.90	0.90	0.89
Ca *		44.4	46.4	47.0	44.2	1.0	1.0	1.0	1.3
Mg *		49.0	49.6	48.9	49.8	84.6	89.4	89.6	87.4
Fe *		6.6	4.0	4.1	6.0	14.4	9.6	9.4	11.3

Analysis 1 - host basalt, analyses 2-17 from spinel lherzolites, 2-5 clinopyroxenes, 6-9 orthopyroxenes. Average 2 sigma errors (wt%): Clinopyroxene - Na_2O, 0.11%; MgO, 0.1%; Al_2O_3, 0.07%; SiO_2, 0.2%; CaO, 0.1%; TiO_2, 0.06%; Cr_2O_3, 0.05%; FeO, 0.09%; NiO, 0.06%; Orthopyroxene - MgO, 0.2%; Al_2O_3, 0.06%; SiO_2, 0.2%; CaO, 0.02%; TiO_2, 0.03%; Cr_2O_3, 0.06%; MnO, 0.04%; FeO, 0.11%; NiO, 0.05%.

* Ca, Mg and Fe recalculated to 100% for pyroxenes

Table 5. Host rock and mineral compositions: Seward Peninsula. See Table 2 for evaluation of uncertainties in microprobe analyses.

(a)	10	11	12	13	14	15	16	17
	AL-2	AL-1	AL-6	AL-15	AL-2	AL-1	AL-6	AL-15
SiO_2	39.10	40.00	40.0	39.3	n.d.	0.24	0.21	0.20
TiO_2	n.d.	n.d.	n.d.	n.d.	n.d.	0.12	0.12	0.17
Al_2O_3	n.d.	n.d.	n.d.	n.d.	55.5	54.6	53.9	58.5
Cr_2O_3	n.d.	n.d.	n.d.	n.d.	9.48	12.4	12.8	7.45
Fe_2O_3	n.a.	n.a.	n.a.	n.a.	4.32	2.36	2.88	2.90
FeO	15.3	9.96	9.95	13.4	10.3	8.38	8.21	9.39
MnO	0.20	0.10	0.11	0.17	0.24	0.18	0.19	0.14
MgO	44.4	48.8	48.7	45.8	19.4	20.6	20.7	20.4
CaO	n.d.	n.d.	n.d.	0.08	n.d.	n.d.	n.d.	n.d.
Na_2O	n.d.	n.d.	n.d.	n.d.	n.d.	n.d.	n.d.	n.d.
NiO	0.37	0.37	0.39	0.39	0.41	0.35	0.32	0.48
TOTAL	99.27	99.23	99.15	99.14	99.65	99.23	99.33	99.63
				Structural formulae				
O	4.000	4.000	4.000	4.000	4.000	4.000	4.000	4.000
Si	0.990	0.991	0.992	0.991	n.d.	0.006	0.006	0.005
Ti	n.d.	n.d.	n.d.	n.d.	n.d.	0.002	0.002	0.003
Al	n.d.	n.d.	n.d.	n.d.	1.718	1.686	1.665	1.780
Cr_{3+}	n.d.	n.d.	n.d.	n.d.	0.197	0.257	0.265	0.152
Fe^{3+}	n.a.	n.a.	n.a.	n.a.	0.085	0.046	0.057	0.056
Fe^{2+}	0.321	0.206	0.206	0.283	0.227	0.184	0.180	0.203
Mn	0.004	0.002	0.002	0.004	0.005	0.004	0.004	0.003
Mg	1.688	1.802	1.800	1.722	0.759	0.804	0.809	0.785
Ca	n.d.	n.d.	n.d.	0.002	n.d.	n.d.	n.d.	n.d.
Na	n.d.	n.d.	n.d.	n.d.	n.d.	n.d.	n.d.	n.d.
Ni	0.007	0.007	0.008	0.008	0.009	0.007	0.007	0.010
SUM	3.010	3.008	3.008	3.009	3.000	2.996	2.995	2.997
Mg/(Mg+Fe)	0.84	0.90	0.90	0.86	0.77	0.81	0.82	0.80
Al *					85.9	84.8	83.8	89.5
Cr^*					9.8	12.9	13.4	7.7
Fe^{3+} *					4.3	2.3	2.8	2.8

(a) sample number, analyses 10-13 olivine, 14-17 spinel.
n.d. - not detected, n.a. - not analyzed. Fe_2O_3 in spinel by stoichiometry.
Average 2 sigma errors (wt%): Olivine - MgO, 0.2%; SiO_2, 0.2%; CaO, 0.03%; MnO, 0.03%; FeO, 0.15%; NiO, 0.08%; Spinel - MgO, 0.2%; Al_2O_3, 0.3%; SiO_2, 0.04%; TiO_2, 0.04%; Cr_2O_3, 0.15%; MnO, 0.02%; FeO, 0.10%; NiO, 0.06%
* Al, Cr and Fe^{3+} recalculated to 100% for spinel.

Table 5. Host rock and mineral compositions: Seward Peninsula.

the mineral phases, although minor intergrain chemical differences occur within some xenoliths, especially in the case of spinel.

Olivine

The compositions of the olivines from the Seward Peninsula xenoliths most commonly cluster around Fo_{9_0} and range from Fo_{8_8} to Fo_{9_2}. In contrast, the olivines in two other xenoliths studied are Fo_{8_4} and Fo_{8_8}, respectively. In both cases, these olivines coexist with other phases that have accordingly low Mg/(Mg+Fe) ratios. The Ni content of all the olivines is relatively constant. Calcium in olivine is below the detection limit (approximately 0.05 wt%) for energy dispersive analysis in most cases.

Orthopyroxene

The compositions of orthopyroxene analyses are plotted in Figure 6 in terms of their Wo, En and Fs components. Orthopyroxene is magnesian, usually of $Wo_1En_{9_0}Fs_{1_0}$ composition, but has compositions of $Wo_1En_{8_8}Fs_{1_1}$ and $Wo_1En_{8_7}Fs_{1_2}$ in the xenoliths which contain olivine of Fo_{8_4} and Fo_{8_8}, respectively. Al_2O_3 in orthopyroxene is also variable (3.30-4.98 wt%) and bears no relationship to the Mg/(Mg+Fe) ratio. However, the Al_2O_3 content of orthopyroxene (and

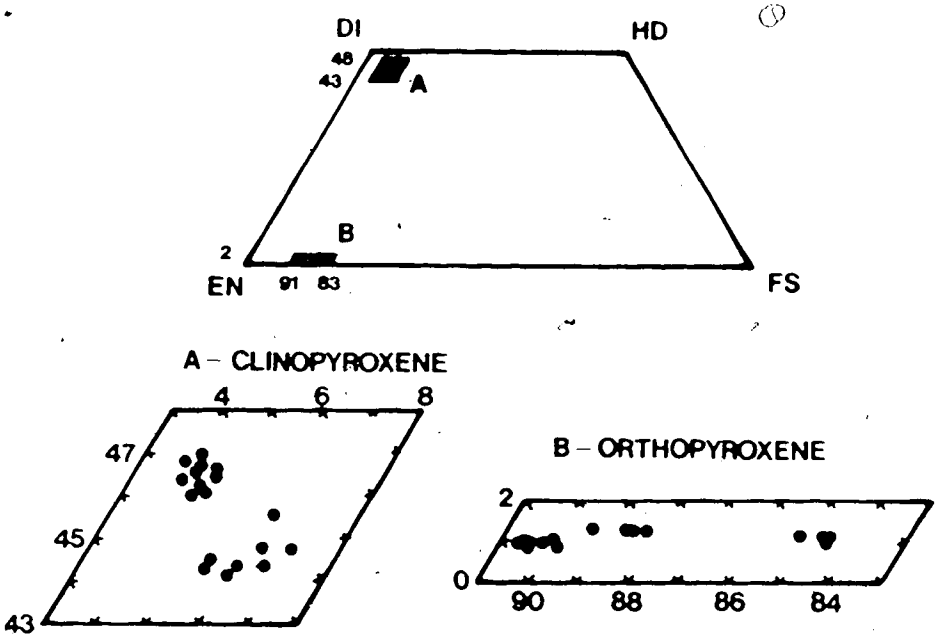

Figure 6. Compositions of pyroxenes from Seward Peninsula ultramafic xenoliths.

clinopyroxene) shows a systematic inverse correlation with $Cr/(Cr+Al+Fe^{3+})$ in coexisting spinel as noted previously in the literature (e.g., Fujii and Scarfe, 1982).

Clinopyroxene

Clinopyroxenes in the xenoliths studied are all chrome diopside; no aluminous augite-bearing xenoliths were found. The compositions of the chrome diopsides are plotted in Figure 6. The common chemistry of chrome diopside in these xenoliths is $Wo_{47}En_{47}Fs_{6}$ with variations to $Wo_{45}En_{48}Fs_{7}$ coexisting with Fo_{88} olivine and $Wo_{44}En_{50}Fs_{6}$ coexisting with Fo_{88} olivine. The distinction between the three chemically distinct xenolith types is not so clear in clinopyroxene as it is in olivine and orthopyroxene. Al_2O_3 in clinopyroxene (4.74-7.08 wt%) bears a similar relationship to $Cr/(Cr+Al+Fe^{3+})$ in spinel as that of orthopyroxene. Na_2O ranges from 1.23-1.51 wt% and Cr_2O_3 ranges from 0.62-0.92 wt%. TiO_2 has a low concentration (<0.60 wt%), and is highest in the most magnesian clinopyroxenes. The Mg/(Mg+Fe) ratios in both orthopyroxene and clinopyroxene vary sympathetically with Fo content of olivine (see Table 5).

Spinel

Spinel also shows distinct compositional

variation in conjunction with the other mineral phases and is best exemplified by the Mg/(Mg+Fe) ratio, which is 0.81-0.82 in xenoliths with Mg-rich phases, but ranges to 0.75-0.77 and 0.79-0.80 in the more iron-rich xenoliths. In all the xenoliths analyzed, spinel shows minor intergrain chemical variations within a particular xenolith and varies greatly from xenolith to xenolith. Spinel is always aluminous (Al_2O_3>50 wt%), and Cr_2O_3 varies from 7.15-12.8 wt%. Ferric iron, calculated by stoichiometry, occupies the remainder of the M3 cation site.

E. Discussion

The majority of the ultramafic xenoliths from the Seward Peninsula have textures and mineral compositions indicating that they were equilibrated on the geotherm and that they are residual after at least one partial melting event (e.g., Kuno and Aoki, 1970; Frey and Prinz, 1978; Fujii and Scarfe, 1982). These xenoliths contain olivine of Fo_{90} composition which coexists with lesser proportions of orthopyroxene, clinopyroxene and spinel with high Mg/(Mg+Fe) ratios (Table 5). However, two xenoliths, which have approximately identical modal proportions of minerals, have more iron-rich mineral compositions. These xenoliths contain olivines of Fo_{84} and Fo_{80} composition, which coexist with minerals having a lower

Mg/(Mg+Fe) ratio (Table 5, Fig. 6). The more iron-rich xenoliths have equigranular and protogranular textures (Mercier and Nicolas, 1975) similar to "normal" xenoliths. Therefore, we infer that these xenoliths simply represent volumetrically small portions of the upper mantle beneath the Seward Peninsula, which are more iron-rich than the depleted xenoliths. It is possible that the iron-rich xenoliths are high pressure cumulates, which have texturally re-equilibrated in the upper mantle over a period of time. However, the only possible evidence of a cumulate origin is the limited exsolution shown by large grains of orthopyroxene, although this is not diagnostic for rocks formed in this manner.

Other iron-rich lherzolite xenoliths which have been described previously are attributed to different origins. Wilkinson and Binns (1977) concluded that the xenolith from Spring Mountain, Australia was not cognate with the host basalt and that it represented a part of the upper mantle which could produce iron-rich tholeiitic magmas. Kuno and Aoki (1970) ascribed the variation in lherzolite composition at Itinome-gata to varying degrees of partial melting and extraction of basaltic magmas from primordial material. Frey and Prinz (1978), on the basis of trace element data, stated that the iron-rich lherzolites from San Carlos were of metasomatic origin and that the metasomatic

event had been erased by subsequent recrystallization. In the case of the xenoliths from the Seward Peninsula, there is no direct evidence to support any of these hypotheses. However, the pervasive metasomatism present at Nunivak Island (Francis, 1976a; b; Roden et al., 1984) suggests that the chemical variation in the upper mantle beneath the Seward Peninsula may also be due to a similar metasomatic event. A more detailed search for hydrous minerals in the xenoliths and isotopic and trace element constraints are required to substantiate this possibility.

Geothermometry

The compositions of the coexisting mineral phases in each of the xenoliths analyzed were used to calculate temperatures of equilibration in the upper mantle. Several published geothermometers are applicable and the results of the temperatures obtained from four different geothermometers are shown in Fig. 7. It should be stressed that these thermometers were selected for comparative purposes and that only the two-pyroxene thermometer of Wells (1977) will be used to discuss absolute temperatures. The xenoliths containing olivine of composition Fo_{90} are most abundant and using the geothermometer of Wells (1977), the temperatures of equilibration of these xenoliths range from 910-950°C; therefore, the geotherm beneath

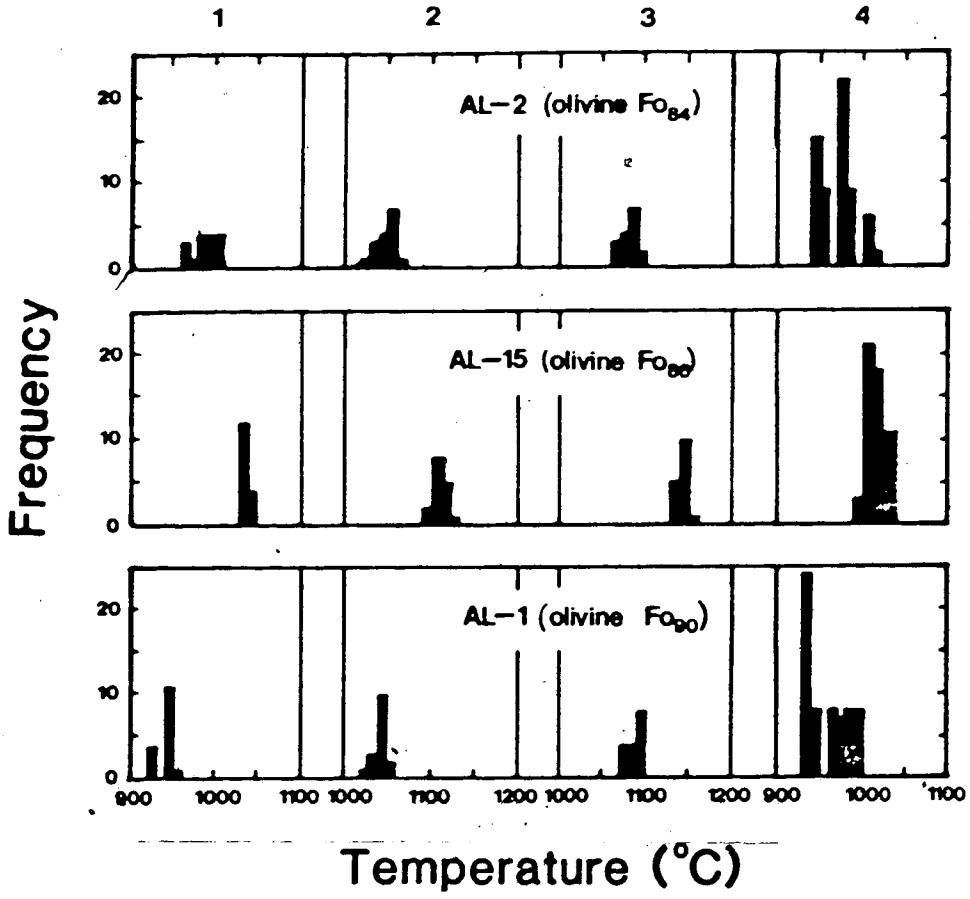

Figure 7. Comparative plot of equilibration temperatures of three Seward Peninsula xenoliths using four different geothermometers. 1-Wells (1977) opx-cpx; 2-Wood and Banno (1973) opx-cpx; 3-Fujii (1977) opx-cpx; 4-Fujii (1976) ol-opx-sp.

Material adapted from above sources.

the Seward Peninsula may be similar to that proposed by Fujii and Scarfe (1982) for West Kettle River, British Columbia. Equilibration temperatures of the xenolith containing olivine of $Fo_{..}$ composition are identical within error to those discussed above for all five geothermometers presented. However, temperature estimates for the xenolith containing olivine of $Fo_{..}$ composition, taking into account the error in temperature of a particular geothermometer, are systematically approximately 50°C higher. The discrepancy between the temperatures may reflect small local perturbations in the geotherm. Equilibration temperatures calculated for xenoliths with similar relatively iron-rich compositions taken from the literature span the range exhibited by the iron-rich xenoliths at this locality for all the relevant geothermometers.

F. Comparison with other ultramafic xenoliths from western Alaska

The mineralogy and mineral chemistry of ultramafic xenoliths from western Alaska have been summarized by Swanson et al., (1985). The xenolithic suite at the Seward Peninsula is different from other localities in that there is no amphibole (primary or secondary) present nor are there any xenoliths

containing aluminous augite (Group II xenoliths of Frey and Prinz, 1978). However, the mineral chemistry of the silicate phases is very similar to and overlaps with that at other localities. Relatively iron-rich xenoliths are found at other localities indicating that there may have been a regional event (e.g., metasomatism) which affected the upper mantle beneath western Alaska. It is concluded, therefore, that the lack of amphibole in the xenoliths found at the Seward Peninsula may simply be due to sampling.

G. Conclusions

A preliminary study of a suite of ultramafic xenoliths from the Seward Peninsula, western Alaska indicates that the upper mantle beneath this region is chemically heterogeneous. The majority of the xenoliths contain mineral phases with compositions that indicate that they were well equilibrated on the geotherm. Equilibration temperatures in the upper mantle calculated from a two-pyroxene geothermometer range from 910-950°C for these xenoliths. Two xenoliths, however, contain mineral phases which are systematically more iron-rich, suggesting that portions of the upper mantle may have equilibrated with an Fe-rich metasomatic fluid. A similar origin has been proposed to expain the mineralogy, mineral chemistry

and textures present in xenoliths from nearby Nunivak Island.

V. The nature of the upper mantle beneath the Canadian Cordillera: an overview

A. Introduction

Numerous studies dealing with the petrological aspects of ultramafic xenoliths from the Canadian Cordillera have been conducted (e.g., Littlejohn and Greenwood, 1974; Fiesinger and Nicholls, 1977; Sinclair et al., 1978; Nicholls et al., 1982; Fujii and Scarfe, 1982; Ross, 1983). However, only Nicholls et al. (1982) and Ross (1983) have attempted to model the geothermal conditions existing in the entire Cordilleran upper mantle. Nicholls et al., (1982) used both petrological evidence from lavas and ultramafic xenoliths and seismic evidence to derive a model for the upper mantle. On the other hand Ross (1983) used geothermometry and rheological evidence to construct temperature-depth profiles for eight ultramafic xenolith localities in the Cordillera.

In this chapter, the volume of petrological data accumulated on ultramafic xenoliths will be used to discuss the nature of the upper mantle beneath the Canadian Cordillera. Chemical analyses from twelve localities (Fig. 8) taken from previous chapters, the literature and unpublished data are used to calculate equilibrium temperatures in the upper mantle using

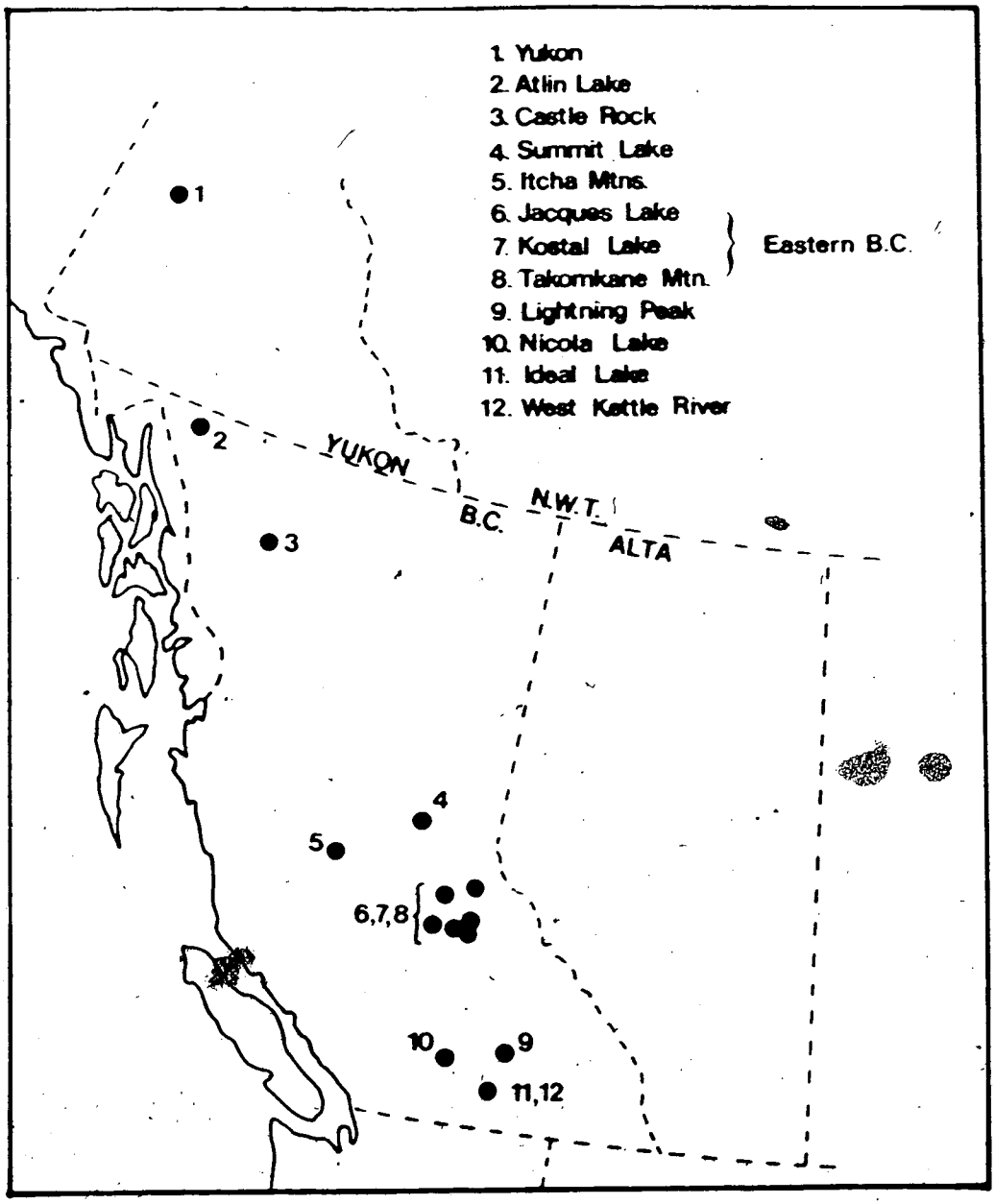

Figure 8. Location of xenolith-bearing lavas and cinder cones in the Canadian Cordillera.

two-pyroxene geothermometry. The results are discussed in terms of the spatial temperature distribution in the upper mantle and the depth of origin of ultramafic xenoliths in this region.

B. Geothermometry and Discussion

It has recently been shown that the semi-empirical, two-pyroxene geothermometer of Wells (1977), which has been consistently used throughout this thesis, closely approximates conditions achieved in experiments of garnet peridotite equilibria (Nickel and Green, 1985; Nickel et al., 1985). Consequently, this geothermometer is used to determine the equilibrium temperatures of the ultramafic xenoliths from the Canadian Cordillera. The results of the geothermometry are shown in Fig. 9, which is a plot of temperature against number of samples for the twelve xenolith localities in Fig. 8 from North (top) to South (bottom). It is clear from Fig. 9 that there is no obvious systematic temperature increase or decrease from North to South along the Cordillera. The highest temperatures are recorded at Summit Lake and Takomkane Mountain (>1100°C), the lowest temperatures at Jacques Lake (<900°C).

The temperatures obtained by Ross (1983) using the method of Mercier (1980) are systematically higher for each locality, although there is some overlap in

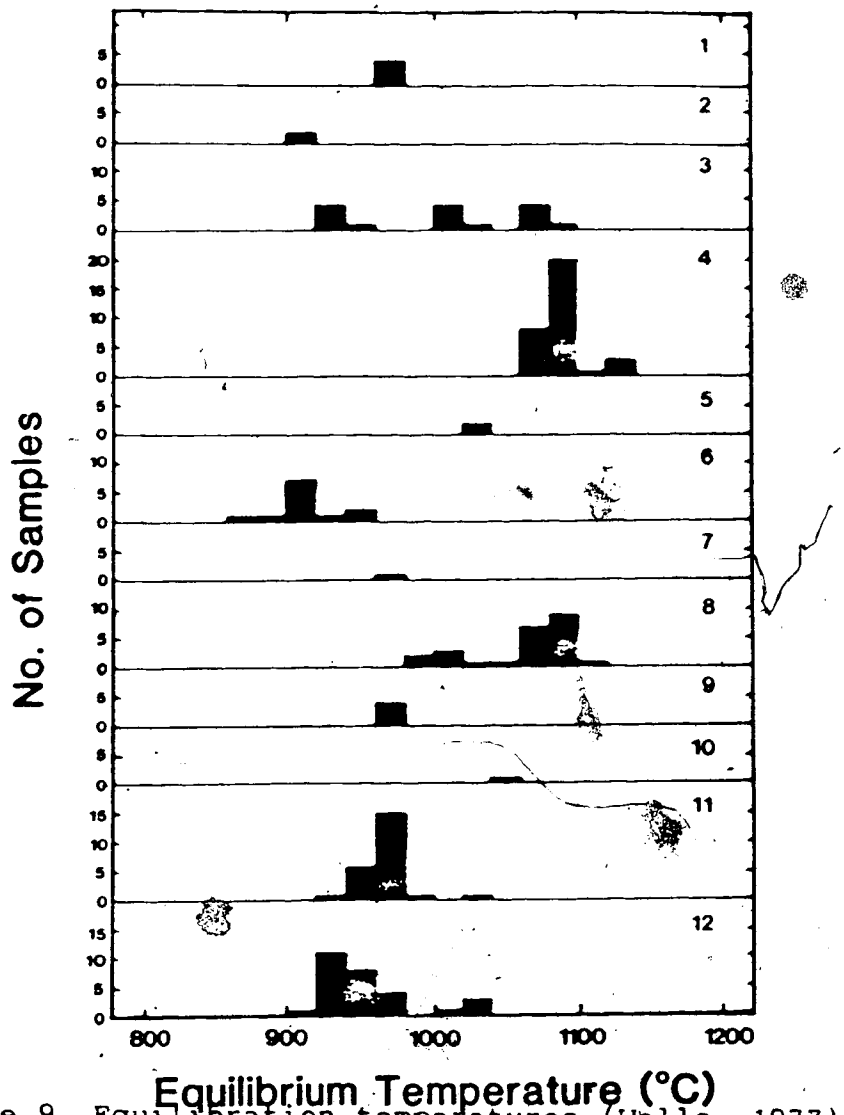

Figure 9. Equilibration temperatures (Wells, 1977) of twelve localities in the Canadian Cordillera. 1-Yukon (Sinclair et al., 1978), 2-Atlin Lake (Nicholls et al., 1982), 3-Castle Rock (Littlejohn and Greenwood, 1974; Scarfe and Fujii, unpubl. data), 4-Summit Lake (this study), 5-Itcha Mtns. (Nicholls et al., 1982), 6-Jacques Lake (Littlejohn and Greenwood, 1974; Scarfe and Fujii, unpubl. data), 7-Kostal Lake (Fiesinger and Nicholls, 1977), 8-Takomkane Mtn. (Fiesinger and Nicholls, 1977; Scarfe and Fujii, unpubl. data), 9-Lightning Peak (this study), 10- Nicola Lake (Littlejohn and Greenwood, 1974), 11-Ideal Lake (Scarfe and Fujii, unpubl. data), 12-West Kettle River (Fujii and Scarfe, 1982).

Material adapted from above sources.

the temperature distribution in most cases. However, the relative differences in temperatures obtained using either geothermometer are still evident. Ross (1983) also used the method of Mercier (1980) to estimate the depth of origin of the ultramafic xenoliths. While this is an internally consistent method for estimating the relative differences in the geotherm, it is not acceptable for evaluating absolute pressures due to the absence of experimental calibration of the geobarometer.

The isotopic ages on the ultramafic xenoliths from several localities within the Canadian Cordillera have been demonstrated to be generally older than 200Ma (Min, 1985). The obvious interpretation of these ages is that the upper mantle has not been subjected to any thermal resetting since that time, and that the ultramafic xenoliths record evidence of a thermal event in the Paleozoic. Sneeringer et al. (1984) have recently determined the diffusivity of Sr in diopside, which is the major host for Sr in an anhydrous upper mantle. They showed that Sr diffusivity in diopside is sufficiently slow to be compatible with the existence of large scale heterogeneities in the upper mantle. Moreover, assuming that convective upwelling velocities are 1-5cm/yr and that the geothermal gradient beneath British Columbia is 10-20°C/km, the resulting cooling rate for the upper mantle is of the order of

100-1000°C/Ma, corresponding to a closure temperature (Dodson, 1973) for Sr of between 900-1000°C (see model of Sneeringer et al., 1984). Above this temperature, Sr will re-equilibrate with respect to the upper mantle mineral phases. However, below 900°C, Sr isotopic determinations may record past equilibration events. In the case of the xenoliths from British Columbia, it is possible that the xenoliths, which have been dated isotopically, do record temperatures related to a Paleozoic event such as the collision of the suspect terranes. These xenoliths all give equilibration temperatures between 900-1000°C. It would be interesting to ascertain an isotopic date of xenoliths at other localities (e.g., Summit Lake) where the xenoliths appear to record a temperature above the closure temperature of Sr.

The other constraint on the interpretation of equilibration temperatures in the upper mantle is the ages of the host basalts, which are all younger than 5Ma with the possible exception of Summit Lake (Littlejohn and Greenwood, 1974; Nicholls et al., 1982; Ross, 1983). The equilibration temperatures of the ultramafic xenoliths are, therefore, representative of conditions existing in the upper mantle prior to the age of their respective host basalts.

In accord with previous discussions in Chapter 2 and Fujii and Scarfe (1982) and the lack of a reliable

geobarometer for spinel-bearing xenoliths, it is possible to interpret the temperatures presented in Fig. 9 in two ways. Firstly, assuming that all the xenoliths were derived from the same depth, the temperature differences may indicate that the geotherm varies slightly beneath each locality. In this case, the geotherm is most variable in central British Columbia (Summit Lake to Takomkane Mountain), with northern and southern British Columbia and the Yukon having a relatively constant geothermal gradient. This conclusion is not inconsistent with the fact that central British Columbia has recently been an area of volcanic activity (e.g., Fiesinger and Nicholls, 1977; Nicholls et al., 1982).

The second interpretation of the temperatures in Fig. 9 relies on the assumption of a constant geotherm throughout the Cordilleran region (e.g., Ranalli, 1980). This assumption necessarily produces a range in the depth of origin for the xenoliths at each locality. For the temperature range shown in Fig. 9, the range in the depth corresponds to 40-60 km, which is not unreasonable for spinel-bearing xenoliths.

In reality, it is probable that the temperature distribution preserved by the ultramafic xenoliths represents a combination of a different depth of origin and a locally perturbed geotherm beneath certain areas of the Cordillera. To assume that either the xenoliths

are all incorporated in the host magmas at the same depth or that the geotherm is constant over an area of upper mantle 2000 km in extent, is highly unlikely.

C. Conclusions

The nature of the upper mantle beneath the Canadian Cordillera has been summarized. By using two-pyroxene geothermometry of chemical analyses of ultramafic xenoliths from twelve localities along the Cordillera, it has been shown that there is a temperature range of 850-1150°C for the xenoliths. There appears to be no systematic temperature variation along the Cordillera. The Yukon, northern and southern British Columbia record similar equilibrium temperatures; however, central British Columbia has a wide variation in temperatures between different localities. This temperature distribution may be explained by a local perturbation of the geotherm in this region coupled with the host magmas sampling the xenoliths from different depths.

VI. Dissolution rates of upper mantle minerals in an alkali basalt melt at high pressure: an experimental study and implications for ultramafic xenolith survival

A. Introduction

The predominance of peridotite xenoliths found in alkali basalts and kimberlites is evidence for an upper mantle composed of olivine-rich peridotite (e.g., Yoder, 1976). Nevertheless, pyroxene-rich xenoliths are well represented at a few localities. The eclogites at the Roberts Victor Mine, South Africa (Carswell and Dawson, 1970; Dawson 1980; 1981) and the abundant garnet pyroxenites on Hawaii (Jackson and Wright, 1970) are two examples. The general paucity of pyroxenites and eclogites relative to peridotite xenoliths has lead to the suggestion that either (1) pyroxenites are only locally important constituents of the upper mantle (Yoder, 1976), or (2) they preferentially dissolve in alkalic magmas while in the upper mantle or during transport to the surface (Kutolin and Agafonov, 1978).

The dissolution of crystals in silicate melts has been studied by a number of workers (e.g., Cooper and Kingery, 1964; Cooper and Schut, 1980; Scarfe et al., 1980; Thornber and Huebner, 1985; Harrison and Watson, 1983; 1984; Donaldson, 1984a; Chekhmir and Epel'baum, 1985; Kuo and Kirkpatrick, 1985; Tsuchiyama 1985a; b). However, few studies have dealt with the dissolution of

mafic minerals in mafic melts (Kutolin and Agafonov, 1978; Scarfe et al., 1980; Thornber and Huebner, 1985; Donaldson, 1984a). Kutolin and Agafonov (1978) performed experiments at 1 bar to determine the relative dissolution rates of the major upper mantle minerals in an alkalic melt. They concluded that pyroxene dissolves more rapidly than olivine. This behavior was also observed by Scarfe et al. (1980) at high pressure (12.5-20 kbar).

Because of the absence of systematic data on the dissolution rates of ultramafic xenoliths in alkali basalt melts at high pressure, the dissolution rates of the major upper mantle minerals olivine, orthopyroxene, clinopyroxene, garnet and spinel have been investigated in an alkali basalt melt to pressures of 30 kbar. It is shown that the relative rates of dissolution of these minerals at each pressure is strongly related to the liquidus phase relationships of the melt. It is concluded that dissolution is a steady-state process brought about by the diffusion of mineral constituents away from the crystal/melt interface. By utilizing these data, a simple model that predicts the dissolution of ultramafic xenoliths in alkali basalt magmas is presented and the petrological significance of the conclusions is briefly discussed.

For the purposes of this chapter, dissolution is defined as:

$$S_1 + L_1 \longrightarrow L_2 \ (\pm S_{2\ldots}) \qquad (2)$$

where S_1 is a solid, L_1 is a melt, L_2 is a melt of different composition to L_1, and $S_{2\ldots}$ are solids crystallized as a result of the dissolution of S_1.

B. Theory of dissolution kinetics

The theoretical aspects of the kinetics of crystal dissolution in melts have been discussed in some detail by Cooper (1962), Cooper and Kingery (1964), Kuo and Kirkpatrick (1985) and Tsuchiyama (1985c). Dissolution may be regarded as a process involving four steps: (1) transport of the reactants to the crystal/melt interface (2) reaction at the interface (3) transport of the products away from the crystal/melt interface (4) removal of the latent heat of dissolution (Kuo and Kirkpatrick, 1985). Step (4) involves thermal diffusion and is not likely to be the rate-limiting process of dissolution due to the large thermal diffusivities in silicate melts ($\sim 10^{-2}$-10^{-3} cm^2/sec; Kuo and Kirkpatrick, 1985). Steps (1) and (3) involve mass transport (diffusion) in the melt and therefore the rate-limiting step for dissolution in this case is the diffusivity of melt components. Step (2) is the rate-limiting step in interface-controlled dissolution (Kuo and Kirkpatrick, 1985). Because

interface-controlled kinetics have been shown to be important only in dissolution processes where the crystal and melt have the same composition (Kuo and Kirkpatrick, 1985), they will not be discussed further here. If the crystal and melt have different compositions, diffusion-controlled dissolution is the governing process. Three different processes involving diffusion-controlled dissolution are: (1) molecular diffusion, (2) diffusion under conditions of natural convection, (3) diffusion under conditions of forced convection (Cooper and Kingery, 1964; Kuo and Kirkpatrick, 1985). Because the experiments conducted in this study are of the "static" type, diffusion under conditions of forced convection is not likely to be an important process, and is therefore not considered further. Cooper and Kingery (1964) and Kuo and Kirkpatrick (1985) showed that dissolution by diffusion under conditions of forced convection are only applicable in rotating crystal experiments.

Molecular diffusion

In the case of dissolution controlled by molecular diffusion, diffusion takes place across a boundary layer of thickness δ in the melt, where the concentration of a particular species in the melt varies from an original bulk value (C_i) to a value at

the interface (C_s) which is assumed to be the equilibrium saturation composition (Fig. 10; Cooper and Schut, 1980; Harrison and Watson, 1984; Kuo and Kirkpatrick, 1985). An effective boundary layer thickness (δ') may also be defined:

$$\delta' = \frac{C_s - C_i}{(dC/dx)_s} \qquad (3)$$

where $(dC/dx)_s$ is the concentration gradient at the interface. The relationship between the rate of dissolution (u) and diffusion in the melt (D) can be described by the Noyes-Nernst equation:

$$u = \frac{D(C_s - C_i)}{\delta'} \qquad (4)$$

This equation suggests that if the diffusivity, dissolution rate and boundary layer concentrations are fixed, then the processes involved in diffusion-controlled dissolution may be found from the thickness (or growth) of the effective boundary layer. In the case where the effective boundary layer grows with increasing time then the process is called molecular diffusion (Cooper, 1962; Cooper and Kingery, 1964) and the appropriate equation for a binary system is:

$$\pi^{1/2} \alpha \, \mathrm{erfc}\, \alpha \exp \alpha^2 = \frac{-(w_s - w_i)}{(1 - w_s)} \qquad (5)$$

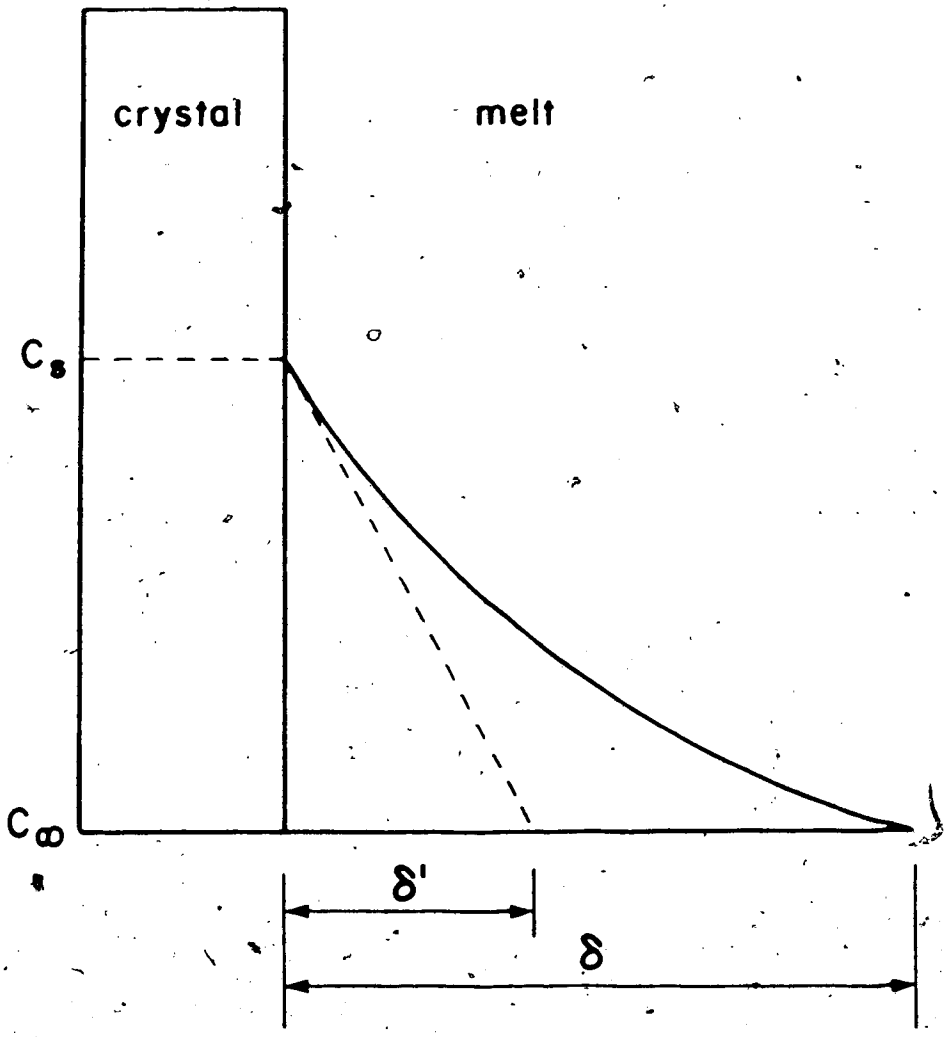

Figure 10. Schematic diagram illustrating the concentration profile of a species in the melt adjacent to a dissolving crystal. C_s is the equilibrium saturation composition, C_∞ is the bulk melt composition, δ is the boundary layer thickness and δ' is the effective boundary layer thickness. Dashed line is the concentration gradient at the crystal/melt interface $(dC/dx)_s$.

(Cooper, 1962). In this equation, $\alpha = \Delta r/2(Dt)^{1/2}$, D is the effective binary diffusion coefficient (EBDC), Δr is the change in thickness of the effective boundary layer, w_s and w_i are the weight fractions of components at the interface and in the bulk melt, respectively, and erfc is the complementary error function. Because α is a constant in this equation, the rate of dissolution decreases with $t^{1/2}$ and therefore dissolution governed by molecular diffusion alone will produce a straight line on a plot of Δr versus $t^{1/2}$. Also, the dissolution rate varies as a function of the square root of the diffusion coefficient (D) in this process.

Natural convection

Diffusion-controlled dissolution under conditions of natural convection have been reported in several studies (e.g., Cooper and Kingery, 1964; Kuo and Kirkpatrick, 1985). The convection process is initiated by density or surface energy differences between the melt at the crystal/melt interface and the bulk melt (Cooper and Kingery, 1964). This results in a virtually time-independent or steady state dissolution process where the effective boundary layer thickness does not change and a plot of Δr versus t produces a straight line. In practice, some time-lag is experienced in the early stages of dissolution where

molecular diffusion is the rate-controlling process, after which dissolution involves mass transport by both diffusion and convection (Cooper and Kingery, 1964; Kuo and Kirkpatrick, 1985). The relevant mathematical equation to describe this latter process is:

$$u = 0.505 \left[\frac{g\Delta\rho}{\eta_s z}\right]^{1/4} D_s^{3/4} \frac{(C_s - C_i)}{(1 - C_s V_i)} \qquad (6)$$

(Cooper and Kingery, 1964; Kuo and Kirkpatrick, 1985). In this equation, g is the gravitational constant, $\Delta\rho = (\rho_s - \rho_i)/\rho_i$, ρ_s is the melt density at the interface, ρ_i is the bulk melt density, η_s is the kinematic viscosity at the interface, z is the distance from the leading edge of the crystal, D_s is the EBDC at the interface and V_i is the partial molar volume of the dissolving species. The time independence of dissolution and the dependence of the dissolution rate on $D^{3/4}$ are evident from this equation.

C. Experimental procedure

Dissolution experiments

Starting materials for the dissolution experiments were an alkali basalt rock powder and spheres of olivine, orthopyroxene, chrome diopside, spinel and garnet, separated from ultramafic xenoliths

or megacrysts (Table 6). The crystals were ground into spheres using a method described by Bond (1951). Each sphere was cleaned ultrasonically in dilute HCl, washed in distilled water, dried and then measured at least six times with a micrometer. The basalt was initially dried at 900°C for 24 hours at the QFM oxygen buffer, and stored at 110°C between experiments. The spheres were placed on a thin bed of alkali basalt powder in a graphite capsule, which was then packed tightly with more powder. The graphite capsule was fired at 800°C for approximately three minutes both before and after the capsule was loaded to drive off any water adsorbed on the surface. The capsule was then inserted into a talc-pyrex piston-cylinder assembly and dried for eight hours at 110°C. Graphite capsules were used in all experiments in order to maintain the oxygen fugacity in the wustite stability field (Thompson and Kushiro, 1972).

Experiments were performed in a solid-media piston cylinder apparatus (Boyd and England, 1960). Temperatures were monitored by a Pt/Pt13%Rh thermocouple without any correction for pressure and are accurate to $\pm$10°C. Pressures were monitored continuously during each run with a Bourdon-Tube Heise gauge and are accurate to $\pm$0.5 kbar. For further details of the calibration and experimental procedures see Fujii and Scarfe (1985). Time series experiments

	1	2	3	4	5	6
SiO_2	40.0	n.d.	42.31	54.7	52.3	48.6
TiO_2	n.d.	0.24	0.81	n.d.	0.41	2.20
Al_2O_3	n.d.	64.7	21.68	4.54	6.47	15.6
Fe_2O_3	n.a.	4.30	n.a.	n.a.	n.a.	3.13
FeO	10.0	7.73	10.44	5.97	2.67	8.53
MnO	0.15	0.12	0.38	0.15	n.d.	0.16
MgO	48.2	22.2	19.40	34.3	16.2	6.30
CaO	0.18	n.d.	4.75	0.72	19.7	9.85
Na_2O	n.d.	n.d.	0.12	n.d.	1.45	3.50
K_2O	n.d.	n.d.	n.d.	n.d.	n.d.	1.21
NiO	0.48	0.56	n.d.	0.15	0.05	n.d.
Cr_2O_3	n.d.	n.d.	0.46	0.49	1.19	n.d.
P_2O_5	n.d.	n.d.	n.d.	n.d.	n.d.	0.51
H_2O	n.a.	n.a.	n.a.	n.a.	n.a.	0.02
Total	99.01	99.85	100.35	101.02	100.44	99.61

n.d.- not detected, n.a.- not analyzed, 1. olivine, 2. spinel, 3. garnet, 4. orthopyroxene, 5. clinopyroxene, 6. KR-13 alkali basalt. FeO in alkali basalt by wet chemistry, Fe_2O_3 in spinel by stoichiometry.

Table 6. Starting compositions for the dissolution experiments.

were done for each mineral in order to evaluate the time-dependence of dissolution. All runs were quenched at a rate of approximately 125°C/sec by switching off the power to the graphite furnace. At the termination of each experiment, the graphite capsule was sectioned and ground until the maximum diameter of the partially dissolved spheres was exposed.

In order to detect water possibly incorporated in the melt during the experiment, wafers of glass from a one hour experiment were analyzed for H_2O by a micromanometric technique (Harris, 1981). The concentration of water was <0.1 wt%, which is not considered sufficient to affect the rate of dissolution (e.g., Harrison and Watson, 1983).

Phase equilibrium experiments

The liquidus phases of KR-13 alkali basalt were determined from 5 kbar to 30 kbar pressure in the piston-cylinder apparatus. Graphite capsules were loaded with alkali basalt powder in the same manner as described in the previous section. Experiments were run up to the desired temperature and were held at that temperature for a duration of 1 day, before quenching. Run products were identified optically and the crystalline phases were examined with an electron microprobe for major elements. The principal objective of the liquidus phase equilibrium experiments was to

determine the liquidus phase and the approximate temperature of the liquidus at each pressure. Therefore, no reversal experiments were attempted.

D. Analytical method

Concentration profiles in the glass next to the mineral spheres in the dissolution experiments and analyses of the crystalline phases in the liquidus phase equilibrium experiments were obtained by both energy and wavelength dispersive microprobe methods. Excellent agreement was found between the EDA and WDA analyses when both methods were used on the same glass. The agreement between EDA and WDA analyses has been previously noted by Reed and Ware (1973) and Fujii and Scarfe (1985). During EDA, a 15 kV accelerating potential, 4 nA probe current and 240 second counting time were employed. For WDA, a 10nA probe current and 40 second counting times were used on peak and background positions. A point beam was used in both EDA and WDA analysis. All microprobe data were processed with full ZAF corrections using EDATA2 (Smith and Gold, 1979).

E. Results of experiments

Liquidus phase equilibria

The results of the liquidus phase equilibria experiments are shown in Fig. 11. The liquidus phase at 5 kbar is olivine of Fo_{75} composition. From approximately 7.5 to at least 30 kbar, clinopyroxene (augite) is the liquidus phase. In accord with previous studies, the Na_2O and Al_2O_3 contents of the clinopyroxene increase with increasing pressure (e.g., Green and Ringwood, 1968; Bultitude and Green, 1971). At 30 kbar, the Al_2O_3 content is 14.5 wt%. The liquidus temperatures, bracketed to $\pm 10^{\circ}C$, were used to determine the temperatures at which the dissolution experiments were conducted.

Dissolution experiments

Crystal/melt textural relationships

The textures produced during the dissolution experiments are summarized in Table 7.

Textures at 5 kbar

In all experiments at 5 kbar, olivine crystals have no reaction textures. The dissolution of orthopyroxene

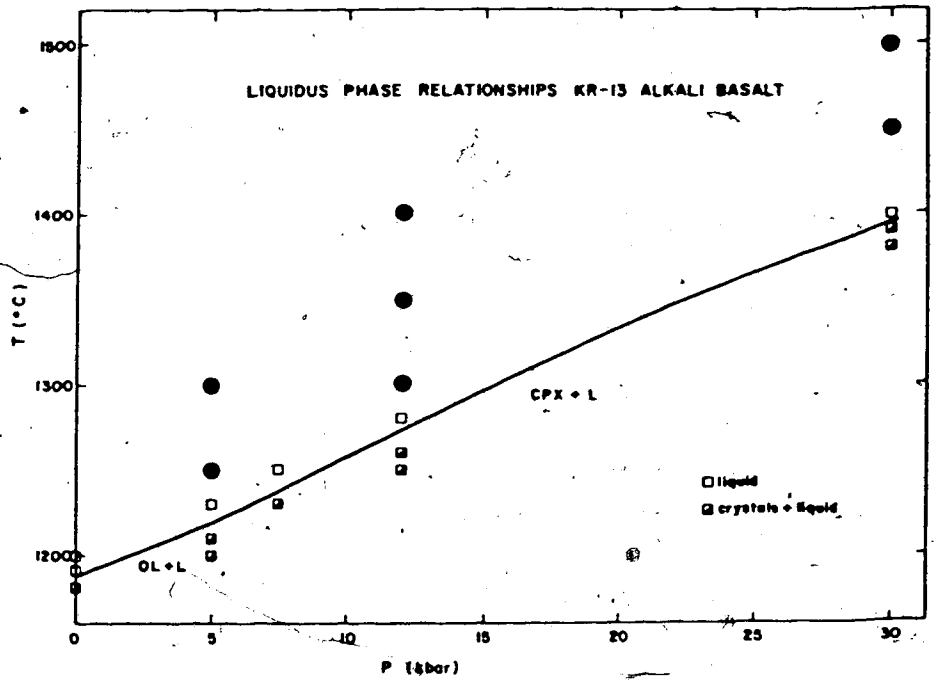

Figure 11. Liquidus phase equilibria of KR-13 alkali basalt. OL - olivine, CPX - clinopyroxene, L - liquid (glass). Filled circles represent the pressure and temperature of the dissolution experiments.

	5 kbar	12 kbar	30 kbar
Olivine	x	x	spin. cpx + gl
Orthopyroxene	ol (Fo_{90}) + chr + gl	x	spin. cpx + gl
Clinopyroxene	chr + gl	x	spin. cpx + gl
Spinel	v. sp + gl	v. sp + gl	spin. + gl
Garnet	-	ol (Fo_{90}) + opx + sp + gl	x

x = no reaction texture, - = no experiment conducted. ol = olivine, chr = chromite, sp = spinel, v. sp = vermicular spinel, gl = glass, opx = orthopyroxene, cpx = clinopyroxene, spin. = spinifex texture.

Table 7. Summary of textures produced during the dissolution experiments.

produces a thin band of equant chromite crystals at the original crystal/melt interface and further dissolution causes olivine crystals of $Fo_{..}$ composition to crystallize (Fig. 12a). Melt (glass) forms intersertal patches between the olivine crystals. Clinopyroxene also reacts to form a thin layer of chromite crystals at the original interface (Fig. 12b). Thereafter, dissolution of clinopyroxene produces glass only. Spinel dissolution forms a vermicular rim of spinels more Cr- and Fe-rich and less Mg- and Al-rich than the original spinel composition. Irregular patches of glass are trapped between the vermicular crystals (Fig. 12c).

Textures at 12 kbar

Olivine, orthopyroxene and clinopyroxene exhibit no reaction textures and appear to dissolve by simple dissolution (Tsuchiyama, 1985a; b). Spinel has a similar vermicular texture to that at 5 kbar. Garnet has a complex reaction relationship. Initially, dissolution of garnet produces olivine crystals of $Fo_{..}$ composition. Further dissolution results in the formation of an aggregate of aluminous orthopyroxene and spinel (Fig. 12d). The spinel exhibits a quench texture around the edge of the aggregate.

Figure 12. Back scattered electron images of textures produced during dissolution experiments. a. (top) Orthopyroxene dissolution to olivine + chromite + glass (5 kbar, 1300°C, 30 minutes). b. (bottom) Clinopyroxene dissolution to chromite + glass (5 kbar, 1300°C, 30 minutes).

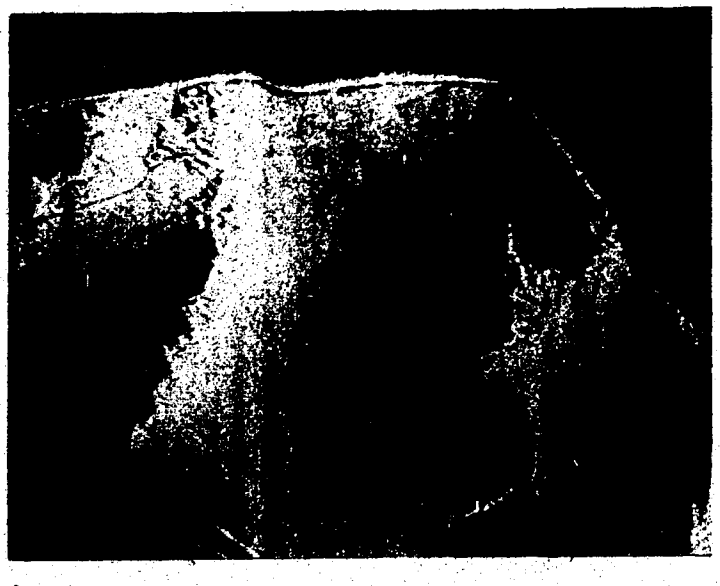

Figure 12c. (top) Spinel dissolution to spinel + glass (5 kbar, 1250°C, 30 minutes). d. (bottom) Garnet dissolution to olivine + orthopyroxene + spinel + glass (12 kbar, 1300°C, 10 minutes).

Figure 12e. Olivine with quench crystals of clinopyroxene and interstitial glass (30 kbar, 1450°C, 10 minutes).

Textures at 30 kbar

At 30 kbar, garnet has no reaction texture. All the other four phases exhibit spinifex textures, characteristic of rapidly quenched glass. Olivine has quench crystals of clinopyroxene with intersertal glass (Fig. 12e). In each case, the width of the zone of quench crystals represents the difference between the original and final crystal/melt interface.

Dissolution rates

The results of the dissolution experiments are given in Table 8 and shown in Figs. 13, 14, 15. It is evident from Figs. 13, 14, 15 that the rate of dissolution is independent of time, indicating that dissolution in these experiments is a steady-state process (Cooper and Kingery, 1964; Kuo and Kirkpatrick, 1985) and that a steady-state has been reached in the duration of the shortest experiment (10 minutes). Kuo and Kirkpatrick (1985) reached a similar conclusion from their experiments at 1 bar. In rare cases, such as the dissolution of clinopyroxene at 12 kbar and 1400°C, dissolution appears to be dependent on time. However, in order to investigate this possibility, the concentration profiles for each experiment were obtained. Each profile is identical within analytical error, thus indicating that steady-state has been achieved in this case also (Kuo and Kirkpatrick, 1985).

Table 8. Results of the dissolution experiments.

Run #	P (kbar)	T (°C)	r_i (cm)	r_f (cm)	Δr (cm)	t (sec)
02SP	30	1500	0.033	0.022±0.002	0.011±0.002	1800
03OL	30	1500	0.058	0.039	0.019	600
04SP	30	1500	0.037	0.035	0.002	600
04GT			0.048	0.025	0.023	
04EN			0.045±0.002	0.037	0.008±0.002	
05DI	30	1500	0.041±0.002	0.026±0.002	0.015±0.002	600
07OL	30	1450	0.054±0.002	0.054±0.002	0.000±0.002	600
07SP			0.037	0.037	0.000	
07GT			0.040	0.035	0.005	
08OL	30	1450	0.068	0.058±0.002	0.010±0.002	1800
08GT			0.042	0.029±0.003	0.013±0.003	
08SP			0.037	0.036	0.001	
09OL(1)	30	1450	0.069±0.002	0.058±0.002	0.011±0.002	1800
09OL(2)			0.058	0.048	0.010	
10EN	30	1450	0.036	0.031±0.002	0.005±0.002	600
10DI			0.036±0.002	0.033±0.002	0.003±0.002	
11EN	30	1450	0.050	0.043	0.007	1800
12OL	30	1450	0.073	0.054±0.002	0.019±0.002	3600
12GT			0.049±0.002	0.027±0.002	0.022±0.002	
12SP			0.037	0.034±0.002	0.003±0.002	
13OL	30	1450	0.084±0.002	0.046±0.002	0.038±0.002	7200
14GT	30	1450	0.053±0.002	0.018	0.035±0.002	7200
14SP			0.052	0.048	0.004	
19GT	30	1500	0.072±0.002	D	>0.072±0.002	1800
21DI	30	1450	0.039±0.002	0.038	0.001±0.002	1800
22OL	30	1450	0.053	0.043±0.002	0.010±0.002	1500
23OL	30	1450	0.048±0.002	0.038±0.002	0.010±0.002	1500
25DI	30	1450	0.034±0.002	0.029	0.005±0.002	3600
27SP	30	1500	0.054	0.014	0.040	7200
28EN	30	1450	0.050	0.034±0.002	0.016±0.002	3600

OL - olivine, SP - spinel, DI - chrome diopside, EN - orthopyroxene, GT - garnet, r_i - initial radius of sphere, r_f - final radius of sphere, Δr - change in sphere radius.

D - sphere completely dissolved. Errors are ±0.001 cm unless otherwise stated.

Table 8. Results of the dissolution experiments.

Run #	P (kbar)	T (°C)	r_i (cm)	r_f (cm)	Δr (cm)	t (sec)
30DI	30	1450	0.036±0.002	0.030±0.002	0.006±0.002	7200
31OL	30	1500	0.086	0.081±0.002	0.005±0.002	300
32EN	30	1500	0.050±0.002	0.030	0.020±0.002	1800
32DI			0.034±0.002	D	>0.034±0.002	
35OL	12	1300	0.045	0.043	0.002	1800
35SP			0.031	0.030	0.001	
35GT			0.042	D	>0.042	
37OL	12	1300	0.047	0.044	0.003	3600
38SP	12	1300	0.037	0.037	0.000	3600
40SP	12	1300	0.039	0.038	0.001	7200
43OL	12	1350	0.049	0.048	0.001	1200
44SP	12	1350	0.030	0.030	0.000	1800
47SP	12	1400	0.038	0.037	0.001	1800
48GT	12	1300	0.054±0.002	D	>0.054±0.002	1200
49GT	12	1300	0.057	0.047	0.010	600
50GT	12	1400	0.079±0.002	D	>0.079±0.002	600
52EN	12	1300	0.043	0.041	0.002	1800
52DI			0.039±0.002	0.039±0.002	0.000±0.002	
53EN	12	1400	0.065	0.060	0.005	1800
53DI			0.043	0.028	0.015	
54EN	12	1350	0.044	0.039	0.005	1800
54DI			0.029	0.026	0.003	
55OL	12	1400	0.059±0.002	0.049	0.010±0.002	3600
55SP			0.041	0.041	0.000	
56EN	12	1300	0.035	0.031	0.004	7200
56DI			0.030	0.029	0.001	
57OL	12	1350	0.048	0.044	0.004	3600
57SP			0.029	0.029	0.000	
59OL	12	1400	0.052	0.043	0.009	1800
60SP	12	1400	0.038	0.036	0.002	3600
61EN	12	1300	0.034	0.032	0.002	3600
61DI			0.029	0.028	0.001	

Table 8. Results of the dissolution experiments.

Run #	P (kbar)	T (°C)	r_i (cm)	r_f (cm)	Δr (cm)	t (sec)
62EN	12	1350	0.048±0.002	0.041	0.007±0.002	3600
62DI			0.031	0.026	0.005	
63EN	12	1400	0.061	0,051	0.010	3600
63DI			0.843	0.024	0.019	
64OL	12	1300	0.045	0.041	0.004	7200
64SP			0.026	0.026	0.000	
65OL	12	1350	0.052	0.044	0.008	7200
65SP			0.031	0.030	0.001	
66OL	12	1400	0.054±0.002	0.032	0.022±0.002	7200
66SP			0.042±0.002	0.040	0.002±0.002	
67OL	12	1400	0.051±0.002	0.039	0.012±0.002	3600
68OL(1)	12	1400	0.044	0.036	0.008	3600
68OL(2)			0.031	0.019	0.012	
69OL(1)	12	1400	0.041±0.002	0.027	0.014±0.002	3600
69OL(2)			0.036	0.022	0.014	
70OL(1)	12	1400	0.061	0.050±0.002	0.011±0.002	3600
70OL(2)			0.024	0.008	0.016	
71OL(1)	12	1400	0.042	0.035	0.007	3600
71OL(2)			0.028	0.012	0.016	
72OL(1)	12	1400	0.037	0.024	0.013	3600
72OL(2)			0.032	0.017	0.015	
73OL	5	1250	0.033	0.032	0.001	1800
73SP			0.030	0.030	0.000	
74EN	5	1250	0.037±0.002	0.035	0.002±0.002	1800
74DI			0.040±0.002	0.036	0.004±0.002	
75OL	5	1300	0.030	0.029	0.001	1800
75SP			0.029	0.029	0.000	
76EN	5	1300	0.034	0.030	0.004	1800
76DI			0.031	0.024	0.007	
77OL	5	1250	0.031	0.030	0.001	3600
77SP			0.023	0.023	0.000	
78EN	5	1250	0.035	0.029	0.006	3600

Run #	P (kbar)	T (°C)	r_i (cm)	r_f (cm)	Δr (cm)	t (sec)
78DI	5	1250	0.028	0.024	0.004	3600
79OL	5	1300	0.029	0.027	0.002	3600
79SP			0.025	0.023	0.002	
80EN	5	1300	0.034	0.027	0.007	3600
80DI			0.028	0.008	0.020	
81OL	5	1250	0.022	0.021	0.001	7200
81SP			0.022	0.021	0.001	
82EN	5	1250	0.036	0.029	0.007	7200
82DI			0.032	0.020	0.012	
83OL	5	1300	0.026	0.019	0.007	7500
83SP			0.026	0.023	0.003	
84EN	5	1300	0.046	0.029	0.017	7200
84DI			0.043	0.009	0.034	
85OL	12	1400	0.026	0.023	0.003	600
85DI			0.027	0.021	0.006	
86OL	12	1400	0.041	0.035	0.006	1200
86DI			0.032	0.020	0.012	

Table 8. Results of the dissolution experiments.

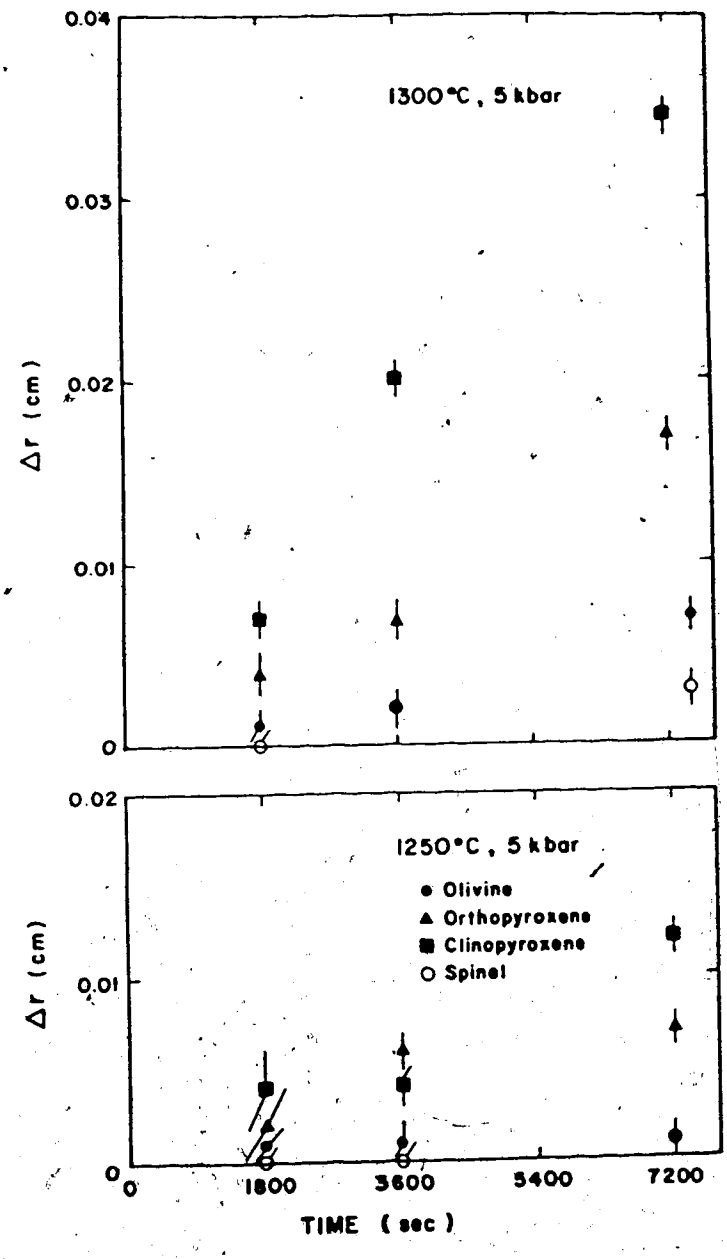

Figure 13. Change in radius (in cm) of crystals against time for experiments at 5 kbar and the temperatures indicated. Error bars on the individual points represent estimated errors during measurement of spheres before and after the experiments. The dissolution rate is calculated by a least-squares regression fit through the data points with a weighted value assigned to the origin.

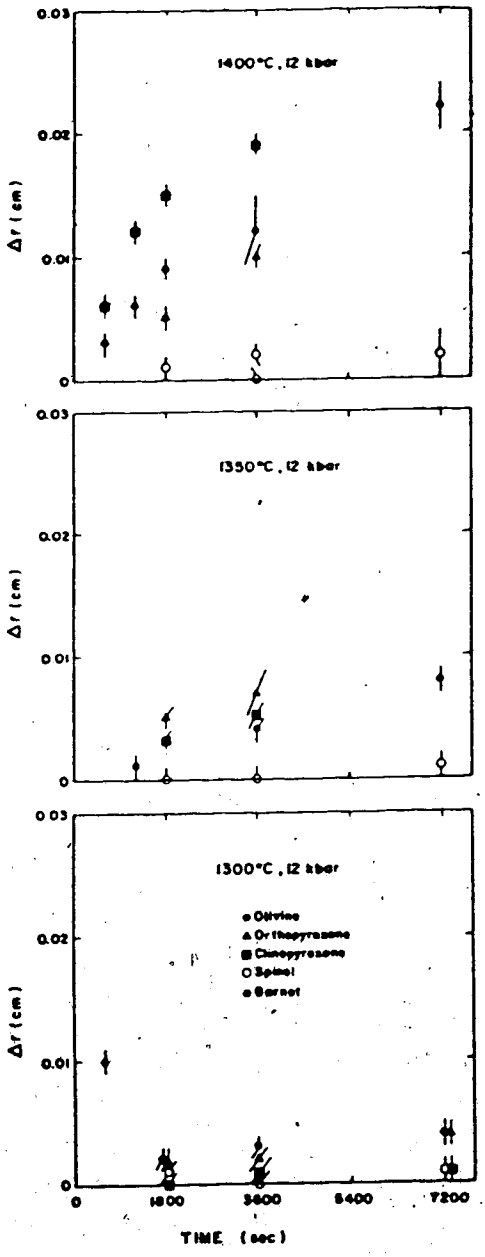

Figure 14. Change in radius (in cm) of crystals against time for experiments at 12 kbar and the temperatures indicated. See Fig. 13. for details of error bars and the calculation of dissolution rates.

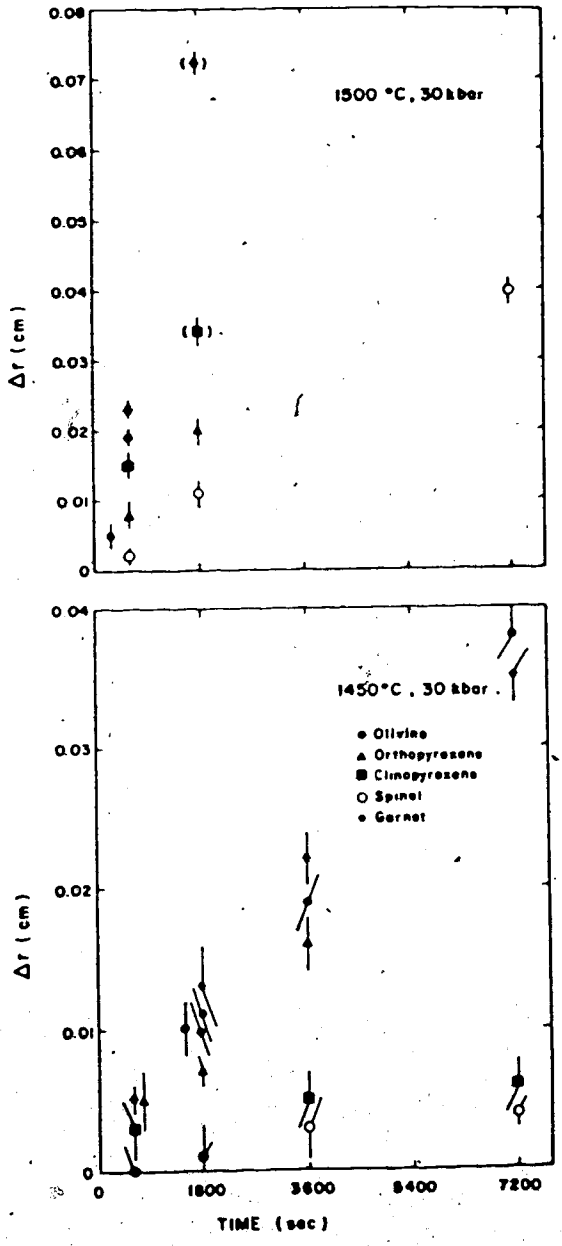

Figure 15. Change in radius (in cm) of crystal against time for experiments at 30 kbar and the temperatures indicated. Points with parentheses represent experiments where the sphere completely dissolved.

Therefore, the apparent time-dependence is probably a function of error in the measurement of the sphere size either before and/or after the experiment. Finally, in order to determine the effect of the run-up on the dissolution rate, several experiments were performed in the partial melt region. No dissolution was observed.

The dissolution rates were calculated by a least-squares regression fit through the data points with a weighted value assigned to the origin, because there is clearly no dissolution possible at zero time. The results are shown in Fig. 16. In cases where the rate of dissolution is slow (e.g., spinel at 1300°C and 12 kbar), the dissolution rate was calculated according to the following equation derived for bubble dissolution in liquid-gas systems (Epstein and Plesset, 1955):

$$\left[\frac{r}{r_i}\right] = 1 - \left[\frac{2Dt(C_s - C_i)}{\rho r_i^2}\right] \qquad (7)$$

The use and applicability of this equation has been discussed by Harrison and Watson (1984), who used the equation to calculate the dissolution rate of apatite in granitic melts. They noted that the equation gave very similar results to, and is easier to use than, the more commonly employed equation developed for heat transfer (Carslaw and Jaeger, 1959). In equation (7), r_i is the initial radius of the sphere, r is the final

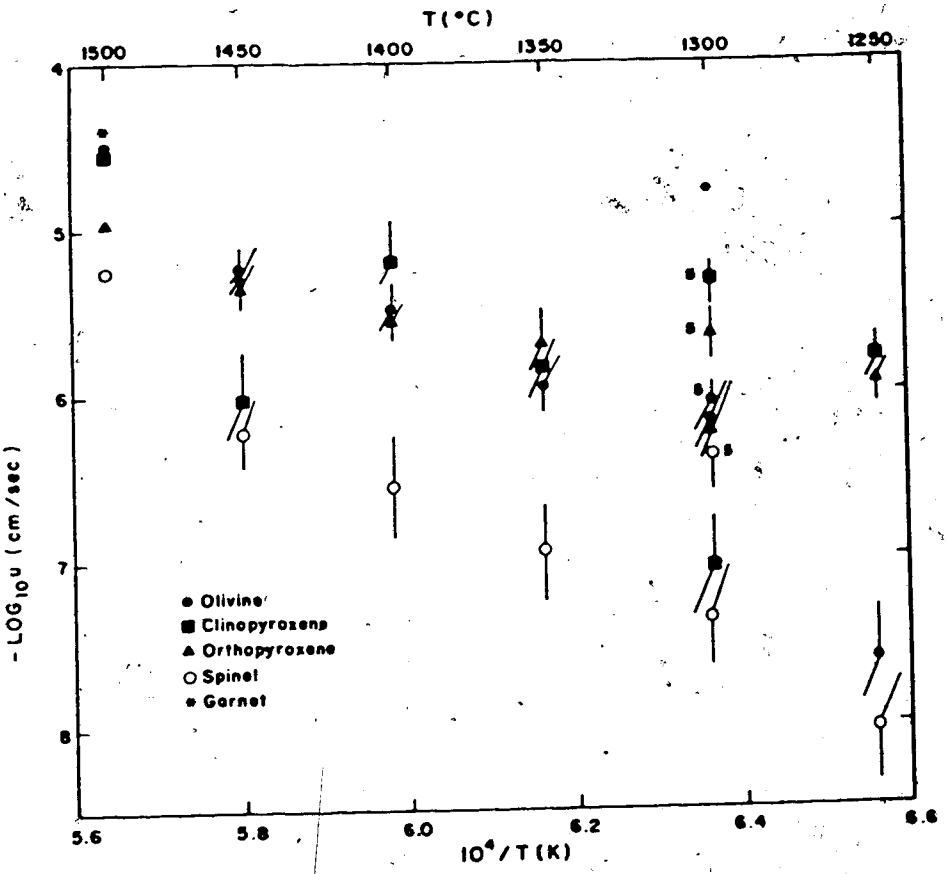

Figure 16. Logarithm of the dissolution rate taken from Figs. 13, 14, 15 versus reciprocal temperature. Error bars represent estimated errors in the best-fit lines from Figs. 13, 14, 15 propogated through the calculations.

radius, t is time, c_s is the equilibrium saturation composition at the crystal/melt interface, c_i is the initial concentration of the relevant species, ρ is the density of the bubble forming species (taken as the weight fraction of the species in the crystal multiplied by the density of the crystal) and D is the diffusion coefficient of the relevant species calculated from the following solution to the diffusion equation:

$$\frac{c_x - c_i}{c_s - c_i} = \text{erfc} \quad \frac{x}{2\sqrt{Dt}} \tag{8}$$

(Crank, 1975). Here, c_x is the concentration at distance x from the interface and erfc is the complementary error function. In order to calculate the dissolution rate, the diffusivity of the least mobile species in the melt (i.e. Al_2O_3 in the case of spinel dissolution) was utilized in each case. However, it should be noted that the error function approximation is a less than satisfactory fit to the concentration profile because of the presence of a moving interface. The effect of a moving interface in calculating diffusion coefficients is considered later, but generally results in an overestimation of D and hence the dissolution rate. The results of the calculations are also plotted in Fig. 16.

Dissolution at 5 kbar

At 5 kbar, the rates of dissolution of olivine, orthopyroxene, clinopyroxene and spinel were determined at 1250° and 1300°C (equivalent to superheatings of 25° and 75°C, respectively). The dissolution rates at both temperatures decrease in the order clinopyroxene > orthopyroxene > olivine > spinel. The temperature dependence of dissolution of each mineral may be fitted to an Arrhenius equation of the form:

$$u = u_o \exp \frac{-E_u}{RT} \qquad (9)$$

where u is the dissolution rate, u_o is a constant, E_u is the activation energy of dissolution, R is the gas constant and T is absolute temperature. Because only two temperatures were investigated at 5 kbar, the calculated activation energies are subject to large errors. However, it is probable that olivine and spinel have significantly larger activation energies than either orthopyroxene or clinopyroxene (Table 9).

Dissolution at 12 kbar

At 12 kbar, the dissolution rates of olivine, orthopyroxene, clinopyroxene and spinel were determined at 1300°, 1350° and 1400°C (25°, 75° and 125°C superheating, respectively). The dissolution rate of garnet is very rapid at this pressure such that only

	5 kbar	12 kbar	30 kbar
Olivine	335±16/28	84±6	210±14/42
Orthopyroxene	66±5	85±6/24	112±42
Clinopyroxene	111±12	223±40/35	420±55/43
Spinel	357±16/55	96±5	280±41/56
Garnet			252±28/56

Calculations at 5 and 30 kbar based on two temperatures. ±28/56 refers to the error (+28,-56 kcal/mole) calculated by fitting a line through the error bars on the individual dissolution rates.

Table 9. Activation energies (kcal/mole) of crystal dissolution at each pressure.

one experiment of 10 minutes duration was successful at 1300°C. All other experiments resulted in the complete dissolution of garnet (Table 8). The dissolution rate of spinel is slowest at each temperature. At 1300°C, the order of dissolution is olivine + orthopyroxene > clinopyroxene > spinel; whereas at 1400°C, the order of dissolution is clinopyroxene > olivine + orthopyroxene > spinel (Fig. 16). These dissolution rates were fit to the Arrhenius equation (9) by least-squares regression. Activation energies for dissolution were calculated as 84±6, 85±6, 223±40 and 96±5 kcal/mole for olivine, orthopyroxene, clinopyroxene and spinel, respectively.

Dissolution at 30 kbar

The dissolution rates of olivine, orthopyroxene, clinopyroxene, spinel and garnet were determined at 30 kbar and 1450°C (60° superheating). Several experiments were also conducted at 1500°C, but the dissolution rates are so fast at this temperature that detailed time-series experiments were not possible, and use of larger spheres resulted in the possible saturation of the melt with respect to dissolving mineral. However, the dissolution rates were calculated from Fig. 15 and are also plotted in Fig. 16. At 30 kbar and 1450°C, the order of dissolution is olivine + garnet + orthopyroxene > clinopyroxene > spinel and at 1500°C, the order is olivine + garnet + clinopyroxene >

orthopyroxene > spinel. Thus, the estimated activation energy of dissolution of clinopyroxene is significantly greater than the other minerals (Table 9).

Cation diffusivities

Selected concentration profiles in the glass adjacent to dissolving crystals are shown in Figs. 17, 18, 19. In order to determine whether steady-state had been reached in the experiments, the concentration profiles adjacent to olivine and clinopyroxene crystals at 1400°C and 12 kbar and several experimental durations were investigated. The concentration profiles in each case are identical both in the interface concentrations of each of the cations and the length of the profile for each element. This is an indication that dissolution is proceeding by diffusion across a boundary layer under conditions of natural convection (i.e. a steady-state process).

If dissolution is controlled by mass transport away from the crystal/melt interface, then it is possible to determine cation diffusivities in the melt adjacent to the dissolving crystal. This approach has been successfully carried out by Cooper and Schut (1980), Harrison and Watson (1983; 1984), Chekhmir and Epel'baum (1985) and Kuo and Kirkpatrick (1985). In this study, because the dissolving crystals are solid

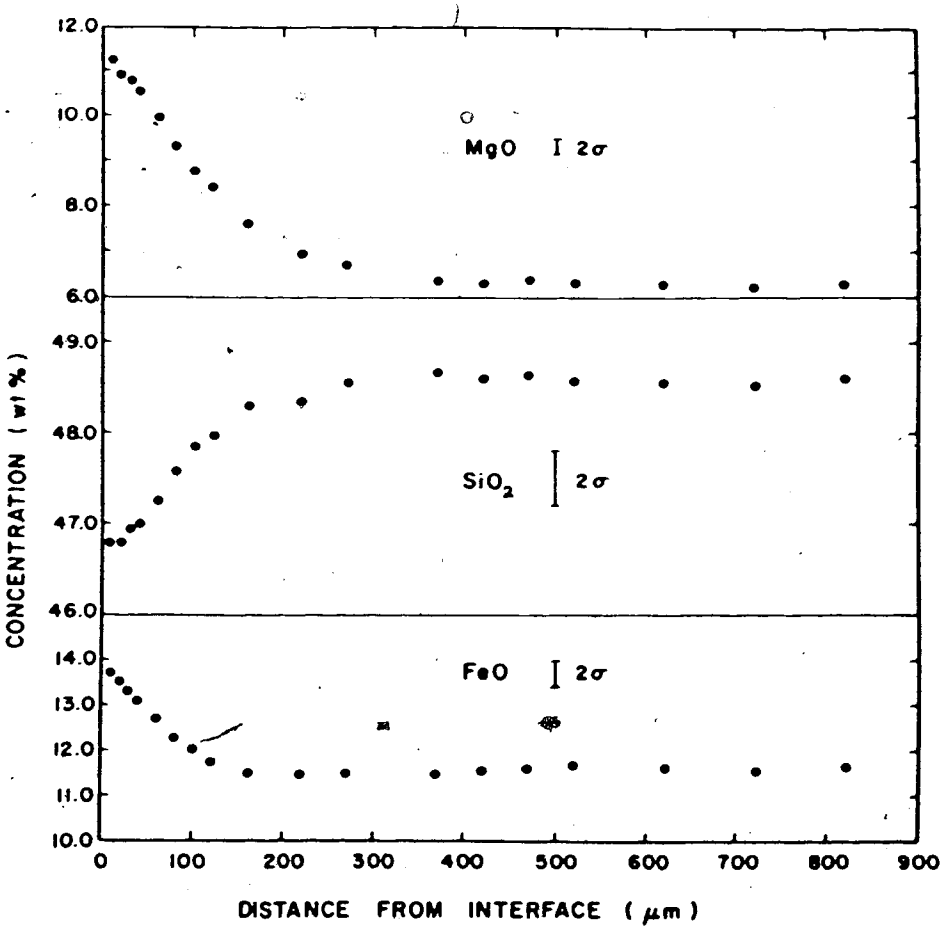

Figure 17. Concentration profiles of the major elements in the glass adjacent to a dissolving olivine crystal. Experiment made at 12 kbar, 1400°C for 60 minutes duration. Error bars are estimated ±2 sigma for each point (see Table 2).

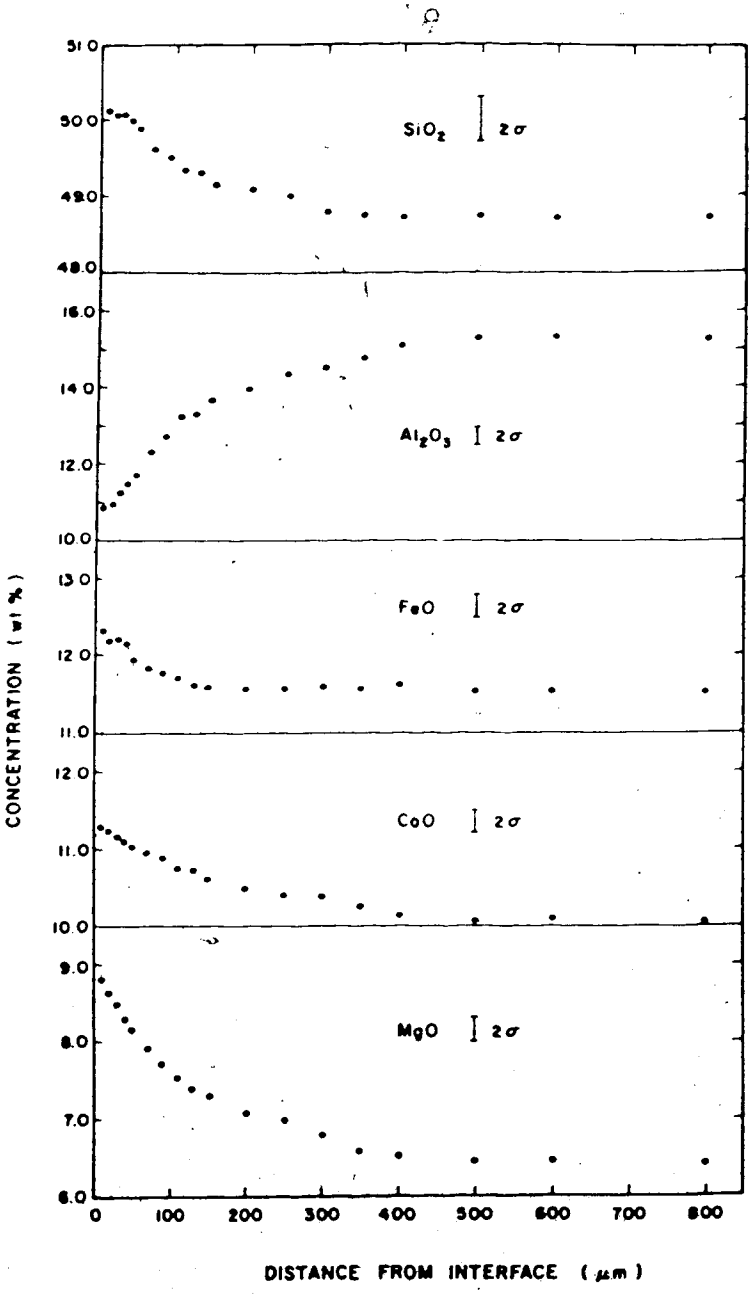

Figure 18. Concentration profiles of the major elements in the glass adjacent to a dissolving clinopyroxene crystal. Experiment made at 5 kbar, 1250°C for 30 minutes duration.

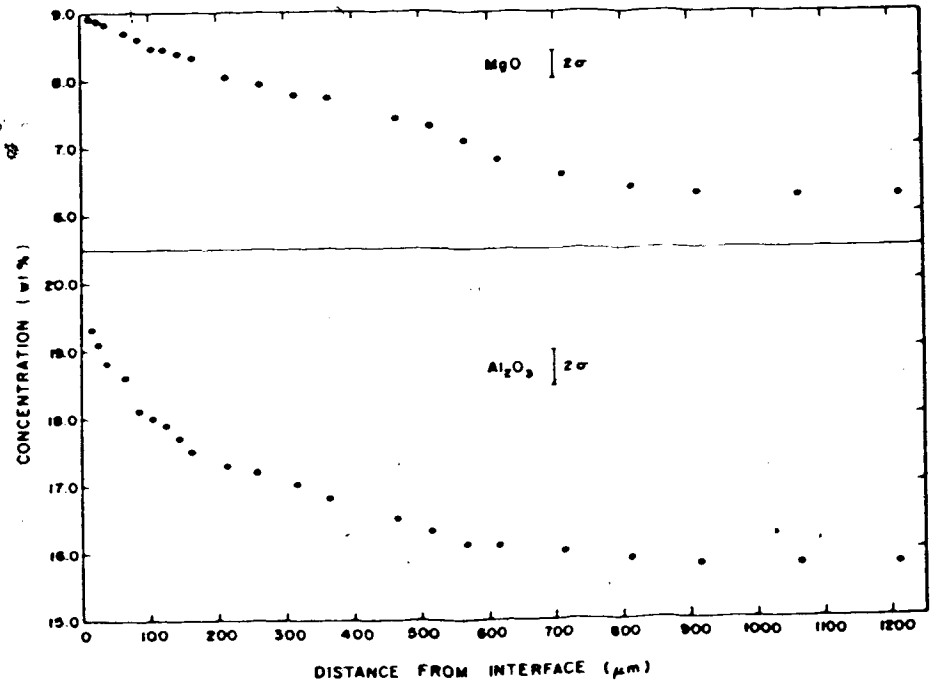

Figure 19. Concentration profiles of the major elements in the glass adjacent to a dissolving spinel crystal. Experiment made at 30 kbar, 1450°C for 30 minutes duration.

solutions of several components, it is possible to measure multicomponent chemical diffusivities. However, only the study by Cooper and Schut (1980) in the synthetic $CaO-Al_2O_3-SiO_2$ system has dealt with the effects of multicomponent diffusion during dissolution. Because of the complexity of the system in this study, the effect of multicomponent diffusion has been neglected.

Because of the effect of a moving interface during dissolution of a crystal, the diffusion equation for the steady-state case is:

$$D \frac{d^2c}{dx^2} + u \frac{dc}{dx} = 0 \qquad (10)$$

subject to the boundary conditions $c_L = c_i$ at $x=\infty$ and $c_L = c_i / k$ at $x=0$ (Kuo and Kirkpatrick, 1985). The solution to this equation has been derived by Smith et al. (1955):

$$\frac{c_L}{c_i} = 1 + \frac{1-k}{k} \exp\left(\frac{-ux}{D}\right) \qquad (11)$$

where c_L is the concentration of a particular species in the melt at distance x, c_i is the initial concentration of the species in the melt, k is the distribution coefficient, u is the dissolution rate and D is the diffusion coefficient.

The results of the calculation of single component

diffusivities for olivine, spinel and clinopyroxene dissolution are shown in Table 10. The most important point to note here is that the calculated diffusivities appear to depend strongly on the dissolution rate of the mineral, which should not be the case if diffusion is the only rate-controlling process. For example, at 1400°C and 12 kbar, the diffusion coefficient calculated for MgO is 2.85×10^{-9} for spinel dissolution, 5.18×10^{-8} for olivine dissolution and 1.02×10^{-7} for clinopyroxene dissolution. The dissolution rates of the three minerals decrease in the order clinopyroxene > olivine > spinel at this temperature and pressure. Therefore, it is possible that dissolution is controlled by a mixed process involving both diffusion and interface reaction. It may also be an indication that multicomponent effects and the speciation of diffusing components in the melt play an important role. Similar conclusions can be drawn for cation diffusivities at any temperature and pressure (c.f Table 10, Fig. 16).

In order to investigate this further, another method of calculation of cation diffusivities from dissolution experiments has been used (Cooper and Kingery, 1964). This method involves the use of the difference in density between the bulk melt and that close to the crystal/melt interface as the driving force for diffusion under conditions of natural or free

		5 kbar			12 kbar		30 kbar	
		1250°C	1300°C	1300°C	1350°C	1400°C	1450°C	1500°C
Olivine	MgO	1.91×10^{-9}	1.21×10^{-8}	7.79×10^{-9}	1.38×10^{-8}	5.18×10^{-8}	1.78×10^{-7}	1.45×10^{-6}
	FeO	1.25×10^{-9}	6.25×10^{-9}	3.95×10^{-9}	1.18×10^{-8}	2.34×10^{-8}	4.62×10^{-8}	2.75×10^{-7}
	SiO_2	1.79×10^{-9}	8.01×10^{-9}	3.79×10^{-9}	6.88×10^{-9}	3.13×10^{-8}	4.47×10^{-8}	1.78×10^{-7}
Clinopyroxene	MgO	1.51×10^{-8}			1.98×10^{-8}	1.02×10^{-7}		
	CaO	2.78×10^{-8}			2.72×10^{-8}	1.32×10^{-7}		
	Al_2O_3	1.25×10^{-8}			1.54×10^{-8}	6.98×10^{-8}		
	SiO_2	1.01×10^{-8}			1.64×10^{-8}	3.02×10^{-8}		
Spinel	MgO		3.82×10^{-9}	9.50×10^{-10}	1.63×10^{-9}	2.83×10^{-9}	3.02×10^{-8}	1.56×10^{-7}
	Al_2O_3		4.60×10^{-9}	3.50×10^{-10}	1.69×10^{-9}	3.62×10^{-9}	1.07×10^{-8}	8.50×10^{-8}

Table 10a. Single component diffusivities calculated by the method of Smith et al. (1955).

		5 kbar			12 kbar		30 kbar	
		1250°C	1300°C	1300°C	1350°C	1400°C	1450°C	1500°C
Olivine	MgO	6.98×10^{-9}	7.70×10^{-8}	1.74×10^{-8}	2.21×10^{-8}	6.87×10^{-8}	9.50×10^{-8}	5.20×10^{-7}
	FeO	1.41×10^{-8}	8.87×10^{-8}	4.15×10^{-8}	1.18×10^{-7}	2.38×10^{-7}	6.16×10^{-7}	
	SiO_2	2.87×10^{-9}	1.82×10^{-8}	9.85×10^{-9}	1.43×10^{-8}	5.40×10^{-8}	9.55×10^{-8}	
Clinopyroxene	MgO	9.06×10^{-8}			1.18×10^{-7}	2.98×10^{-7}		
	CaO	1.63×10^{-7}			1.74×10^{-7}	3.49×10^{-7}		
	Al_2O_3	4.71×10^{-8}			5.57×10^{-8}	2.03×10^{-7}		
	SiO_2	1.05×10^{-8}			1.18×10^{-8}	4.73×10^{-8}		
Spinel	MgO		2.92×10^{-7}	6.80×10^{-9}	1.41×10^{-8}	9.00×10^{-8}	3.85×10^{-8}	6.21×10^{-7}
	Al_2O_3		1.90×10^{-8}	1.18×10^{-9}	2.00×10^{-9}	4.13×10^{-9}	9.89×10^{-9}	4.41×10^{-8}

Table 10b. Single component diffusivities calculated by the method of Cooper and Kingery (1964).

convection. Equation (12) has been derived for a cylindrical surface and is therefore a reasonable approximation to a small sphere:

$$D_s = 0.054\left[\frac{\eta_s}{\Delta\rho}\right]^{1/3}\left[\left\{\frac{u}{C}\right\}\exp -\left\{\frac{(D_sC/u)}{(r+(D_sC/4u))}\right\}\right]^{4/3} \qquad (12)$$

where D_s is the interface diffusion coefficient, η_s is the kinematic viscosity at the interface, $\Delta\rho$ is the fractional density difference in the melt, r is the sphere radius and C is a concentration parameter equal to $(c_s - c_i)/(1-c_sV_i)$. The kinematic viscosity was calculated using the method of Shaw (1972) with an appropriate correction for the pressure dependence of the viscosity of alkali basaltic melts (Scarfe, 1981). Melt densities were calculated by the method of Herzberg (1985). The interface diffusion coefficient, calculated by iteration in this method because D_s also appears in the exponential term, may be converted to a diffusion coefficient at any point on the profile by using a correction for the variation in viscosity according to the Stokes-Einstein relationship.

The results of these calculations are also shown in Table 10. While the diffusivities calculated by the method of Cooper and Kingery (1964) are systematically higher than those calculated by the method of Smith et al. (1955), the apparent dependence of cation diffusivity on dissolution rate is still evident. The

estimation of the viscosities and densities most probably accounts for the discrepancies in the absolute diffusivities between the two methods.

F. Discussion

Crystal/melt textural relationships

It is to be expected that a crystal not in equilibrium with a melt may exhibit a reaction relationship with the melt. Many natural examples of reaction coronas around crystals in disequilibrium with a melt have been attributed to magma mixing, assimilation or contamination processes (e.g., Hibbard, 1981; Sakuyama, 1981; Gerlach and Grove, 1982; Tsuchiyama, 1985a; b; c).

The reaction textures produced by the dissolution of olivine, orthopyroxene, clinopyroxene, spinel and garnet in an alkali basalt have been documented at superliquidus temperatures and at three different pressures (Table 7). The crystal/melt textural relationships observed in this study may be grouped into three categories:

(1) Type A dissolution (simple dissolution of Tsuchiyama, 1985a) characterized by the reaction:

$$\text{Crystal} + \text{melt}_1 \rightarrow \text{melt}_2$$

(2) Type B dissolution (partial dissolution of Tsuchiyama, 1985a) characterized by the reaction:

$$\text{Crystal}_1 + \text{melt}_1 \rightarrow \text{crystal}_2 + \text{melt}_2$$

(3) Type C dissolution characterized by the presence of quench spinifex textures.

Type A dissolution occurs at all three pressures studied (e.g., olivine at 5 and 12 kbar, garnet at 30 kbar). Type B dissolution occurs at 5 kbar (e.g., orthopyroxene) and 12 kbar (e.g., garnet). Type C dissolution occurs only at 30 kbar.

The presence of crystal/melt textures at superliquidus temperatures may be discussed with reference to the liquidus phase diagram of KR-13 alkali basalt (Fig. 11). Unfortunately, subliquidus phase relationships have not been determined for this alkali basalt composition, thus precluding a detailed examination of relative mineral stabilities with textures. However, phase equilibria of similar compositions indicate that at low pressure the crystallization sequence may be olivine --> clinopyroxene + plagioclase $\pm$ orthopyroxene and at higher pressure clinopyroxene --> olivine + plagioclase $\pm$ orthopyroxene (Basaltic Volcanism Study Project, 1981).

At 5 kbar, olivine shows no reaction texture both because it is the liquidus phase and because it is more Mg-rich than the equilibrium olivine composition (Tsuchiyama, 1985b). All other phases are less stable and therefore exhibit reaction textures. The initial reaction of clinopyroxene, orthopyroxene and spinel to chromite suggests that the Cr_2O_3 released from these mineral phases during dissolution causes local saturation of chromite in the melt. The lack of chromite crystallization after this stage may be due to the change in melt composition and/or to the reduction in oxygen fugacity caused by the encapsulating graphite. Further dissolution of clinopyroxene is of Type A, suggesting that clinopyroxene is relatively stable. The crystallization of olivine by dissolution of orthopyroxene also indicates that olivine is the most stable phase at this pressure.

The absence of reaction textures during the dissolution of olivine, orthopyroxene and clinopyroxene at 12 kbar suggests that these three phases are stable at or just below the liquidus. Garnet is clearly not stable at this pressure and crystallizes a variety of minerals as it dissolves. The initial rapid release of Mg from the garnet probably causes olivine saturation. Thereafter, the transport of other cations away from the interface results in the crystallization of orthopyroxene and spinel. Hunter and Taylor (1982) have

observed the reaction pyrope --> spinel + clinopyroxene + orthopyroxene in a symplectitic intergrowth with glass ± olivine in a natural kimberlite. This reaction is very similar to the dissolution reaction documented here.

At 30 kbar, spinifex textures are present around all the dissolving phases except garnet, which dissolves simply at this pressure. Spinifex textures, formed as a result of quenching, have been documented in many experimental studies at high pressure (e.g., Elthon and Scarfe, 1984; Takahashi and Scarfe, 1985). However, the spinifex textures formed in this study occur only in the volume of melt between the original and final crystal/melt interface, indicating the more Mg-rich composition of this zone.

Tsuchiyama (1985a) has conducted a detailed experimental study of the reaction relationships between plagioclase crystals and compositions in the synthetic diopside-albite-anorthite system at 1 bar. Tsuchiyama defined two different dissolution processes characterized by the presence or absence of reaction textures: (1) simple dissolution (no reaction) in which a crystal dissolves in a melt which is undersaturated with respect to the mineral phase, (2) partial dissolution in which a crystal dissolves by a complex reaction forming a mantle around the edge of the crystal. Tsuchiyama (1985b) conducted a similar

experimental study of reaction relationships between olivine and both boninite and andesite compositions. In this latter study, it was found that olivine more Mg-rich than the equilibrium olivine in the boninite composition dissolved by simple dissolution above the olivine liquidus. In the andesite composition, however, olivine dissolution produced a complex reaction texture. These results imply that olivine is relatively stable in the boninite melt, because it is the liquidus phase of the boninite at 1 bar, but is unstable in the andesite.

Donaldson (1984b) has studied the textures produced by the dissolution of several silicate minerals in a tholeiitic melt at 1 bar. No deep embayments in the crystals were observed and a variety of reaction coronas around the crystals were found, indicating that different minerals produce different textures. Donaldson (1984c) investigated the stability and decomposition of pyrope garnet at 1 bar at subliquidus temperatures and found that garnet decomposed at a rapid rate to a corona of orthopyroxene (or olivine) $\pm$ glass. The absence of this type of texture around pyrope megacrysts was used as evidence that either the host magma cooled extremely rapidly or that the host magma was considerably cooler than was previously believed (Chapman, 1976).

Dissolution rates

The dissolution rates of olivine, orthopyroxene, clinopyroxene, spinel and garnet determined in this study are shown in Fig. 20 together with other data relevant to the dissolution of mafic minerals in mafic melts at various pressures (Kutolin and Agafonov, 1978; Scarfe et al., 1980; Kuo and Kirkpatrick, 1985). The data of Thornber and Huebner (1985) and Donaldson (1984a) have been omitted from Fig. 20 for clarity.

Dissolution at one bar

The dissolution rates of upper mantle minerals in an alkalic melt have been determined at 1 bar by Kutolin and Agafonov (1978). Their results show that the order of dissolution at small degrees of superheating is garnet > clinopyroxene > orthopyroxene > olivine, and that olivine of $Fo_{,,}$ composition dissolves at a slower rate than does olivine of $Fo_{,,}$ composition. It may therefore be concluded that the mineral phase which is stable on the liquidus dissolves at the slowest rate and that the equilibrium olivine composition (presumably less Mg-rich than $Fo_{,,}$) may dissolve at a faster rate than more Mg-rich olivine compositions. This latter statement was confirmed by Donaldson (1984a), who concluded that phenocryst olivines dissolve faster than olivines which are more

Figure 20. Logarithm of the dissolution rate versus reciprocal temperature at 1 bar and high pressure. Lines on the high pressure diagram from this study are taken from Fig. 16.

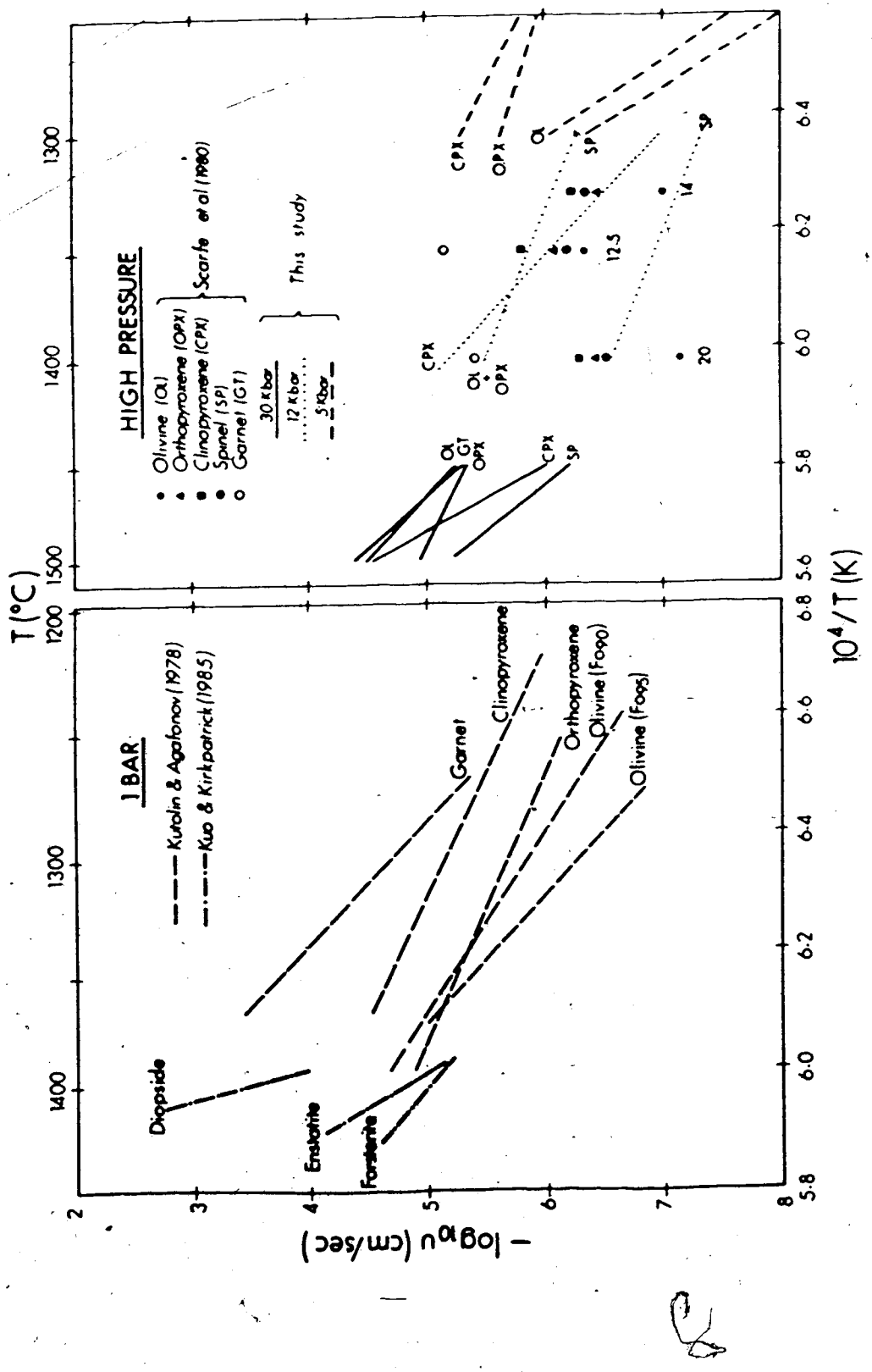
T (°C)
1200
1300
1400
1500
1300
1400
1500
1 BAR
Kutolin & Agafonov (1978)
Kuo & Kirkpatrick (1985)
Diopside
Enstatite
Forsterite
Garnet
Clinopyroxene
Orthopyroxene
Olivine (Fo90)
Olivine (Fo95)
HIGH PRESSURE
Olivine (Ol)
Orthopyroxene (OPX)
Clinopyroxene (CPX)
Spinel (SP)
Garnet (GT)
Scarfe et al (1980)
30 Kbar
12 Kbar
5 Kbar
This study
CPX
OPX
Ol
SP
GT
12.5
14
20
− log10 u (cm/sec)
2
3
4
5
6
7
8
10⁴/T (K)
5.8
6.0
6.2
6.4
6.6
6.8
5.6
5.8
6.0
6.2
6.4

magnesian. The preferential dissolution of equilibrium olivine compositions relative to Mg-rich olivines may be explained by considering the simple forsterite-fayalite binary loop. At isothermal conditions above the liquidus, more Mg-rich olivines experience a smaller degree of superheating and are thus likely to dissolve at a slower rate.

Kutolin and Agafonov (1978) also showed that garnet is not stable and therefore dissolves at a much faster rate than olivine or pyroxene. In addition, because olivine has a higher activation energy than pyroxene (200 kcal/mole vs 125 kcal/mole), it appears that the dissolution rates of olivine and pyroxene converge at larger degrees of superheating (Fig. 20).

In a related study, Kuo and Kirkpatrick (1985) showed that the relative dissolution rates of forsterite, enstatite and diopside in a melt in the system forsterite-diopside-silica can be qualitatively explained by the relative driving forces for dissolution. This is illustrated schematically in Fig. 21. The ratio of the dissolution rates of anorthite and diopside u(An)/u(Di) in the eutectic melt composition is approximately equal to the distance Y/X. This explanation can not easily be used quantitatively in a complex natural system. However, it can be demonstrated qualitatively that the liquidus phase relationships of a complex melt govern the relative dissolution rates at

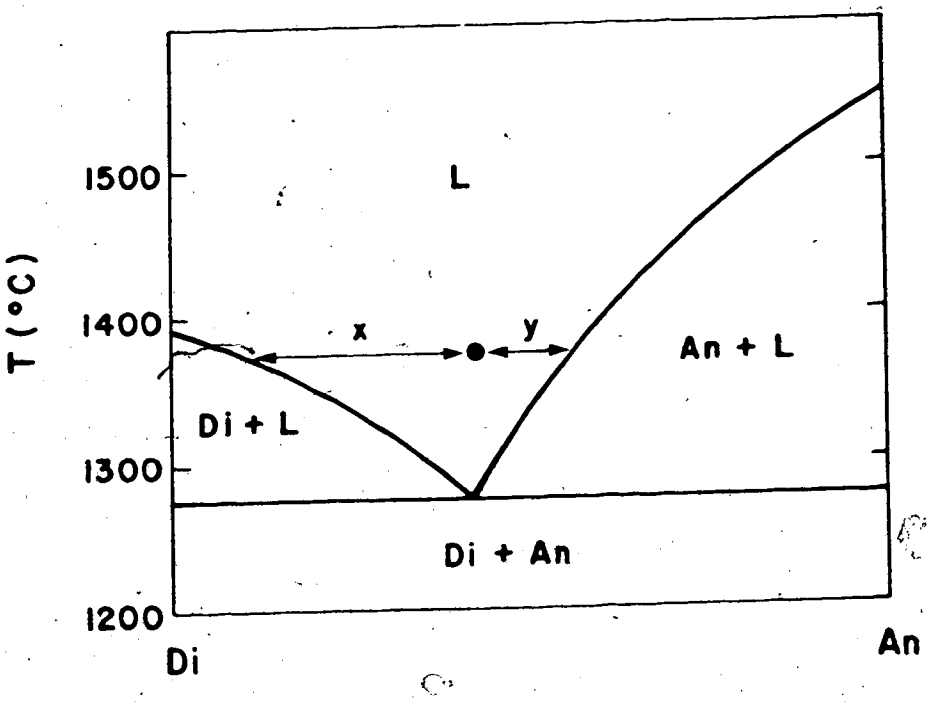

Figure 21. The binary system diopside-anorthite used to illustrate that the relative driving forces for dissolution of anorthite u(An) versus diopside u(Di) in the eutectic melt composition at 1375°C is related to the distance between the melt composition and the respective liquidus surfaces. Here u(An)/u(Di) is approximately equal to Y/X.

least at small degrees of superheating.

Dissolution at high pressure

High pressure experimental determinations of the dissolution rates of upper mantle minerals are limited to those presented here and those determined by Scarfe et al. (1980).

The results of this study may be used to discuss several points. Firstly, the relative dissolution rates of the silicate mineral phases at any given pressure appear to be governed by the liquidus phase relationships of the melt composition. This may be illustrated at each of the three pressures studied with reference to the phase diagram of the alkali basalt (Figs. 11, 20). At 30 kbar and 12 kbar, where clinopyroxene is the liquidus phase of the basalt, the dissolution rate of clinopyroxene is the slowest at small degrees of superheating with olivine and orthopyroxene dissolving at a faster rate. At 5 kbar, where olivine is the liquidus phase, olivine has the slowest dissolution rate and pyroxenes dissolve at a faster rate.

Secondly, the relative rates of dissolution at high pressure appear to converge at large degrees of superheating and the "stable" mineral dissolves more rapidly than the other phases at temperatures between 50-100°C above the liquidus. This is a direct function

of the higher activation energy of dissolution of the mineral which is the liquidus phase. Those minerals which are less stable in the melt at that pressure have a lower activation energy, implying that it is energetically more favourable to dissolve a mineral which is not stable at any given pressure. The same conclusion is implicit in the 1 bar results of Kutolin and Agafonov (1978).

Thirdly, the dissolution rates, at upper mantle pressures and temperatures above the liquidus of the host basalt, are sufficiently high to raise questions about the preferential dissolution of peridotite relative to pyroxenite xenoliths. This will be addressed in a later section.

Scarfe et al. (1980) also determined the dissolution rates of upper mantle minerals in an alkali basalt melt that was multiply saturated with olivine, orthopyroxene and clinopyroxene at 12.5 kbar (Takahashi, 1980b). Their results showed that olivine is the slowest and garnet the fastest phase to dissolve at each pressure studied (12.5, 14 and 20 kbar). The dissolution rates of the pyroxenes were intermediate between the two in each case. The results are shown in Fig. 20. Because Scarfe et al. (1980) present their data as a constant function of the change of volume of the sphere with time, their results have been recalculated using an average sphere radius of 0.05cm.

Unfortunately, Scarfe et al. (1980) only determined the dissolution rates at a single temperature at each pressure, thus evaluation of the dependence of the dissolution rate on degree of superheating is not possible and the results are difficult to apply to the previous discussion. However, the apparently lower dissolution rate of olivine relative to clinopyroxene at 20 kbar, at which pressure clinopyroxene is the liquidus phase (Takahashi, 1980b), may be due to the fact that the dissolution of clinopyroxene has a higher activation energy than olivine. Therefore, the temperature at which the dissolution rates crossover has been exceeded.

Scarfe et al. (1980) also attempted to determine the effect of a pseudoinvariant point on the relative dissolution rates of olivine, orthopyroxene and clinopyroxene. The discussion of the relative stabilities of the minerals would imply that at low superheatings the dissolution rates of these three minerals would be very similar. However, this does not appear to be the case at a superheating of 40°C (Fig. 20). Kuo and Kirkpatrick (1985) determined that the relative dissolution rates of diopside, forsterite and enstatite in a peritectic melt (coexisting with forsterite + diopside + pigeonite$_{ss}$) could be explained by their relative stabilities even considering that diopside dissolves an order of magnitude faster than

the other two phases. Such a geometric evaluation is not possible in a system as complex as that studied by Scarfe et al. (1980) or that discussed here.

Cation diffusivities

Chemical diffusivities of cations in melts adjacent to dissolving crystals have been determined by a number of workers (e.g., Cooper and Kingery, 1964; Watson, 1982; Harrison and Watson, 1983; 1984; Chekhmir and Epel'baum, 1985; Rapp and Watson, 1985). A recent review of diffusivities obtained from dissolution experiments has been provided by Watson (1985). However, only Chekhmir and Epel'baum (1985) have done a detailed study of the cation diffusivities adjacent to dissolving crystals of different composition in the same melt.

Harrison and Watson (1984) investigated the diffusivity of phosphorus in a granitic melt adjacent to dissolving apatite and Rapp and Watson (1985) determined the diffusivity of phosphorus in a granitic melt adjacent to dissolving monazite. The diffusivity of P calculated for apatite and monazite is 1.0×10^{-10} and 7.29×10^{-12}, respectively, for conditions of 1200°C, 8 kbar and 1% H_2O in the melt. It is also important to note that the dissolution of monazite is much slower than that of apatite. For example, under identical conditions, a crystal of apatite 100 μm in

diameter takes 125 years to completely dissolve, whereas a crystal of monazite 50 μm in diameter takes 0.7Ma. Harrison and Watson (1984) also observed that because the diffusivity of P is much slower than that of Ca, the diffusivity of Ca is limited by the slower P diffusivity during stoichiometric dissolution of apatite, indicating that the diffusivity of P is the rate-limiting step in apatite dissolution.

Chekhmir and Epel'baum (1985) reported cation diffusivities for dissolution experiments conducted in an albite-H_2O melt. Interestingly, the diffusivity of each cation appears to be related to the mineral which is dissolving. Chekhmir and Epel'baum (1985) do not present any dissolution rates, thus evaluation of the relationship between diffusivity and dissolution rate is not possible. However, some qualitative conclusions can be drawn from their data. The diffusion coefficient calculated for CaO adjacent to dissolving anorthite is more than three orders of magnitude less than that for wollastonite under identical conditions. Anorthite is likely to be more stable in an albite-H_2O melt than wollastonite and is therefore likely to dissolve at a much slower rate. Similarly, the diffusivity of Al_2O_3 is two orders of magnitude slower adjacent to dissolving anorthite than adjacent to dissolving cordierite. Thus, it seems clear that there is an intimate relationship between the dissolution rate and

diffusivity which is ultimately determined by the relative stabilities of the respective minerals in the melt. The same conclusions can be drawn from the cation diffusivities determined in this study. Chekhmir and Epel'baum (1985) attributed the differing diffusivities to the fact that the molecules released into the melt on dissolution of a particular mineral have a fixed mobility and therefore that the diffusivity is due to the mobility of the diffusing species. The implication is that the dissolving mineral exerts a control on the species released into the melt and hence on the diffusivity of the "cations", and that in complex systems, single component diffusivities are not appropriate to describe the transport of the diffusing species.

The conclusion to be drawn from the data presented here is that while a knowledge of the speciation of the diffusing complex is important, the dominant factor in determining the mobility of species in the melt during a dissolution process is the stability of the mineral; hence, there appears to be a structural or surface energy control which determines the ability of the mineral components to diffuse away from the crystal/melt interface. It is also likely that, if dissolution is stoichiometric, the diffusivity of the least mobile cation or species (i.e. Al or Si) has an effect on the mobility of the faster network-modifying

cations (Harrison and Watson, 1984). We conclude that cation diffusivities obtained from dissolution experiments must be treated with caution because the apparent diffusivities depend on both the stability of the dissolving mineral (dissolution rate) and on the diffusivity of the least mobile diffusing species. The speciation and multicomponent effects involved in the diffusion process are also important characteristics which need to be quantified.

G. The dissolution of ultramafic xenoliths in alkali basalt magmas: a model

The dissolution rates of olivine and clinopyroxene in alkali basalt melts shown in Figs. 16, 20 were used to formulate a model to predict the dissolution rate of ultramafic xenoliths as a function of xenolith radius, magma superheating and ascent time (Fig. 22). Because the depth of generation of alkali basalt magmas is likely to be variable (Yoder 1976; Eggler, 1978; Takahashi, 1980b; Takahashi and Kushiro, 1983), the xenolith dissolution rates have been calculated for a magma generated at 10, 20 and 30 kbar.

The model is based on the high pressure dissolution rates obtained in this study with the following assumptions: (1) the dissolution rates of olivine and clinopyroxene are representative of peridotite and pyroxenite, respectively; (2) the dissolution rates at

Figure 22. Model calculations for the dissolution of peridotite (olivine) and pyroxene (clinopyroxene) xenoliths (see text for assumptions). Numbers on the lines represent the initial radius of the xenolith (in cm). Lines are shown for 25° and 75° superheating and 25° undercooling for magmas generated at 10, 20 and 30 kbar. Lines shown for 10 km/hr and 5 km/hr are limits of realistic ascent rates for alkali basalt magmas (Kushiro et al., 1976; Fujii and Scarfe, 1982).

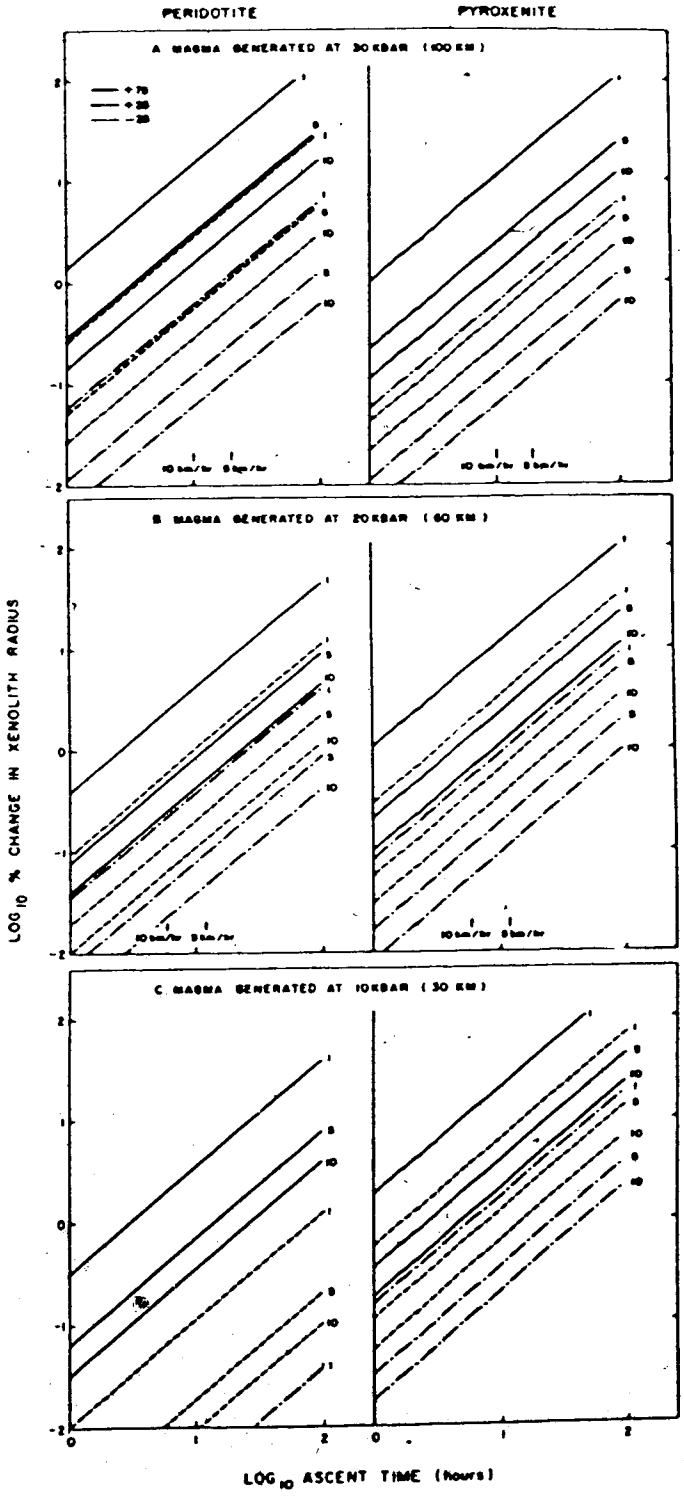
PERIDOTITE
PYROXENITE
A MAGMA GENERATED AT 30 KBAR (100 KM)
B MAGMA GENERATED AT 20 KBAR (60 KM)
C MAGMA GENERATED AT 10 KBAR (30 KM)
LOG10 % CHANGE IN XENOLITH RADIUS
LOG10 ASCENT TIME (hours)

5 kbar are representative up to 10 kbar, those at 12 kbar are valid from 10 to 20 kbar, and those at 30 kbar are valid from 20 to 30 kbar; (3) the ascent rate of the magma is constant; (4) the xenoliths are spherical; (5) melt percolation along grain boundaries in the xenolith is negligible; (6) the magma is superheated by a constant amount during its ascent or that it cools at a constant rate during ascent until it attains a temperature 25° below the liquidus at the surface.

In order to model the effect of cooling of a basalt magma during its ascent to the surface, the temperature-depth profiles of a magma for three depths of generation have also been estimated (Fig. 23), following the non-adiabatic model of Spera (1984). Because alkali basalt magmas containing xenoliths are largely aphyric when they reach the surface (Spera, 1984), the three temperature-depth profiles of the magma have been constrained to attain an undercooling of 25° at the surface. This produces ascent rates of approximately 1 km/hr, 3 km/hr and 10 km/hr for magmas generated at 30, 60 and 100 km, respectively. These ascent rates are within the accepted limits for the ascent of alkali basalt magmas (10^{-2} to 10 m/s; Kushiro et al., 1976; Fujii and Scarfe, 1982; Spera, 1984). The results of these calculations are shown in Fig. 24. All the curves in Fig. 24 are constructed for xenoliths initially 1cm in radius. Similar curves may be drawn

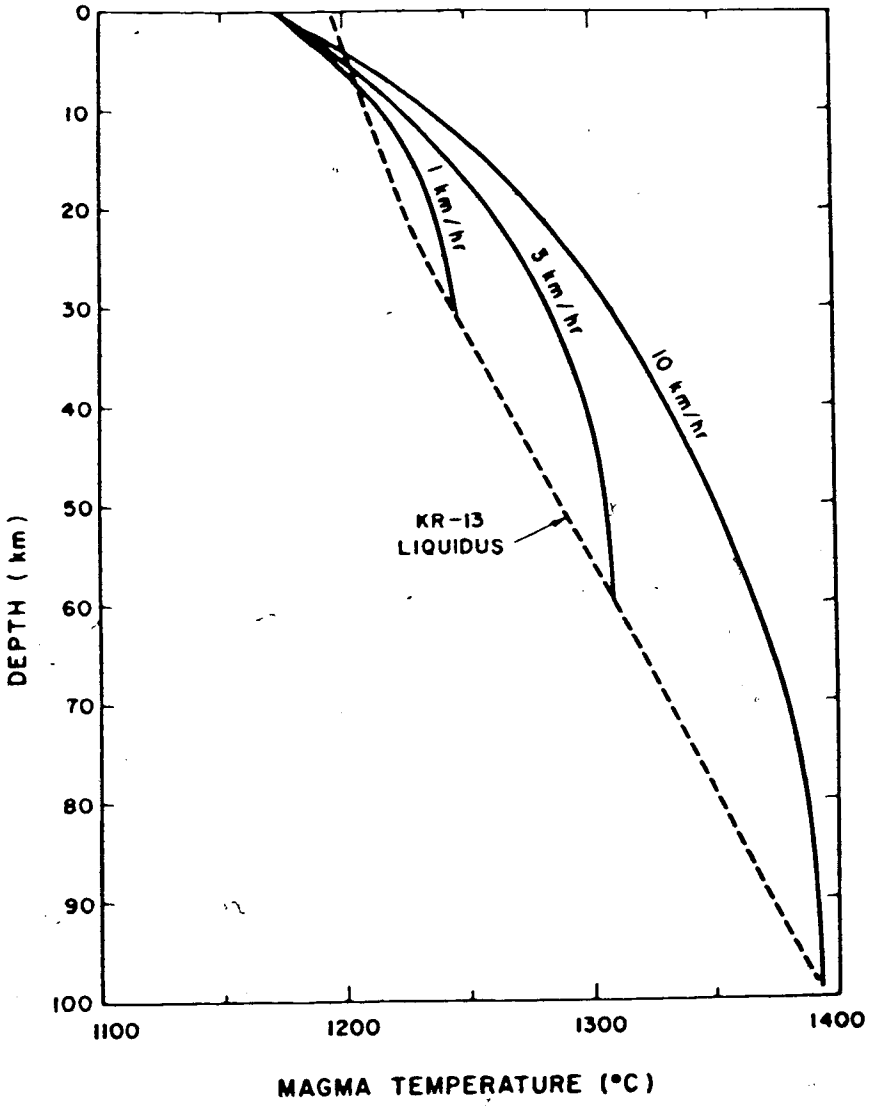

Figure 23. Temperature-depth profiles for the ascent of an alkali basalt magma in a conduit 5m in diameter generated from 30, 60 and 100 km depth (after Spera, 1984). Liquidus temperature-depth profile of KR-13 alkali basalt from Fig. 11. See text for further explanation.

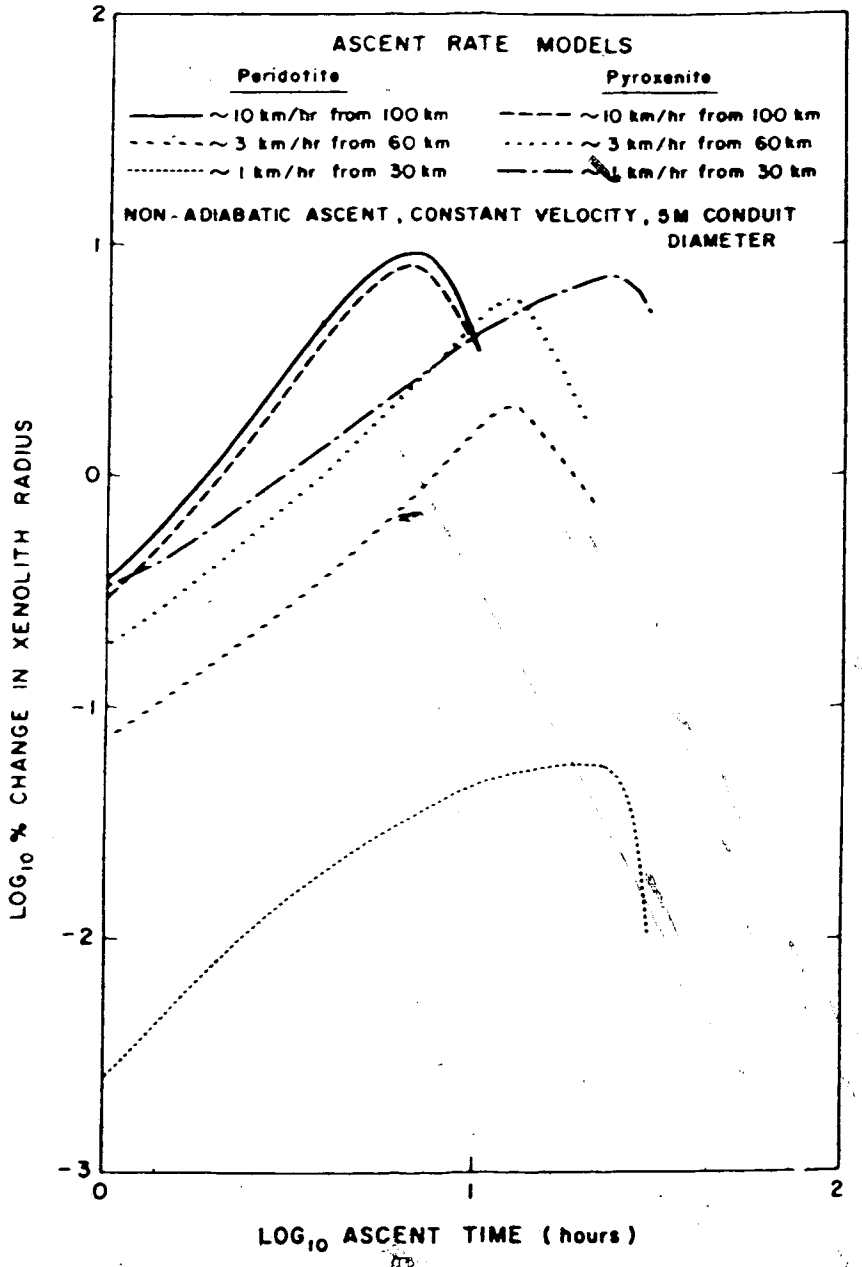

Figure 24. Dissolution behaviour of xenoliths assuming cooling rates shown on the curves. Calculations are based on the model of Spera (1984) and Fig. 20. Ascent rates are constrained by assuming a 25° undercooling at the time of eruption. All curves show a maximum where the competing effects of cooling rate and dissolution rate are equal.

for xenoliths of different radii, larger xenoliths being displaced to the negative side on the vertical axis.

Magma generation at 30 kbar

For an alkali basalt magma generated at 30 kbar, the dissolution rates of peridotite and pyroxenite xenoliths are likely to be similar and the effective dissolution of the xenolith will be small. For example, a xenolith of 1cm radius or greater and at a constant superheating of 25°, will only show 1-5% decrease in its radius during transit to the surface. The ascent and cooling rate model calculations show that for this depth of magma generation, the xenolith dissolution will reach a maximum of close to 10% decrease in xenolith radius before decreasing as the magma cooling rate becomes dominant over the dissolution rate of the xenolith.

Magma generation at 20 kbar

An alkali basalt magma generated at 20 kbar may preferentially dissolve pyroxenite xenoliths relative to peridotite xenoliths, because the pressure-integrated dissolution rate of olivine is less than that of clinopyroxene. At a superheating of 25° there will be a 1-5% decrease in the radius of a pyroxenite xenolith, but less than 1% decrease in a

peridotite xenolith. The ascent and cooling rate model also shows that there will be a slight preferential dissolution of pyroxenite relative to peridotite and that the maximum dissolution will be 6% for pyroxenite and 2% for peridotite.

Magma generation at 10 kbar

An alkali basalt magma generated at 10 kbar will almost certainly preferentially dissolve pyroxenite relative to peridotite xenoliths provided that the xenoliths are small and the magma is superheated by 50° or more. The pressure-integrated dissolution rate of olivine is much less than that of clinopyroxene. For a xenolith 1cm in radius, there will be a 1-5% reduction in the radius of a pyroxenite xenolith; whereas it will be <1% for a peridotite at a superheating of 25°. However, at a superheating of 75°, a pyroxenite xenolith 1cm in radius will have 5-10% reduction in the xenolith radius versus 1-2% for a peridotite xenolith. The cooling model basically enhances the preferential dissolution of pyroxenite over peridotite.

In summary, according to the model, the effects of dissolution in nature are only likely to be significant if the xenolith is small, the magma is superheated by 50°C or more, or the ascent rate of the magma is slower than predicted. Grain boundaries within the xenolith

will accelerate dissolution because they provide pathways through which the magma can percolate and thus expose a greater surface area. Convection within the magma will also enhance the dissolution of a xenolith. Therefore, because the model is based on experiments in which convection is relatively unimportant, it describes minimum dissolution rates for ultramafic xenoliths in alkali basalt magmas. Because, in the model, rapid ascent rates and undercooling of 25°C or less have been considered, it is unlikely that there will be sufficient crystals present in the melt to induce non-Newtonian effects (McBirney and Murase, 1984).

The results of the model are in accord with the observations of many natural examples, where it has been concluded that xenolith dissolution is minimal (e.g., Wilshire and Binns, 1961; Kutolin and Frolova, 1970). The relative difference between the pressure-integrated dissolution rates of olivine and clinopyroxene is negligible, unless the xenoliths are small, the magma is considerably superheated and is generated at relatively low pressure. However, the preferential dissolution of pyroxene relative to olivine observed in some xenoliths (Kutolin and Frolova, 1970; unpublished data) may occur because the xenoliths are incorporated in the ascending magma at relatively low pressures (<20 kbar), where olivine is

more stable in the magma than pyroxene.

Therefore, it is likely that in alkali basalts the proportions of peridotite and pyroxenite xenoliths observed at the Earth's surface are generally representative of the composition of the underlying upper mantle. This conclusion depends on the depth of magma generation, ascent time, superheating and magma composition. The applicability of the model to other magma compositions generated in the upper mantle must be extended by dissolution experiments on melts of picrite, komatiite and kimberlite composition.

H. Conclusions

The dissolution rates of the upper mantle minerals olivine, orthopyroxene, clinopyroxene, spinel and garnet have been determined in an alkali basalt melt at three different pressures. It is apparent that the relative stabilities of the minerals in the melt at each pressure govern the relative rates of dissolution. Spinel is the slowest mineral to dissolve at each pressure. At low pressure, where olivine is the liquidus phase of the basalt, olivine is more stable than the other silicate minerals. At higher pressures, clinopyroxene is the liquidus phase and dissolves more slowly than olivine, orthopyroxene or garnet. The instability of garnet at pressures lower than 25-30 kbar in a melt results in very rapid dissolution at 12

kbar. The dissolution rates at each pressure have been used to construct a model to predict the dissolution rates of ultramafic xenoliths in alkali basalt magmas. The results of the model indicate that there will only be preferential dissolution of pyroxenite xenoliths relative to peridotite xenoliths at low pressure (<10 kbar) and that the proportions of these types of xenolith we observe at the surface are probably representative of their proportions in the upper mantle. Therefore, the abundance of pyroxene-rich eclogites and pyroxenite xenoliths at some localities is attributed to their local abundance in the upper mantle.

Cation diffusivities calculated from concentration profiles in the glass adjacent to dissolving crystals are dependent on the dissolution rate of the mineral, indicating that the stability of the mineral exerts some control on the diffusivities. Thus, diffusivities obtained from dissolution experiments should be treated with caution until the species involved in the diffusion process and the effects of multicomponent diffusion are evaluated for a complex natural system.

VII. Summary and Conclusions

A. Summary of Results

The petrology of ultramafic xenoliths from two localities in the Canadian Cordillera and one locality in western Alaska have been discussed along with an experimental study of the dissolution rates of ultramafic xenoliths in alkali basalt magmas. The following is a brief summary of the results.

The suite of ultramafic xenoliths from Summit Lake is dominantly comprised of spinel lherzolite. However, both chrome diopside-bearing (Group I) and aluminous augite-bearing (Group II) xenoliths are present, indicating that the upper mantle is mineralogically heterogeneous. The Group I xenoliths have a mineralogy of olivine (Fo_{91}), orthopyroxene (En_{91}), clinopyroxene ($Wo_{47}En_{50}Fs_3$) and spinels with variable Cr_2O_3 and Al_2O_3 content. Equilibration temperatures range from 1080-1100°C, suggesting that these xenoliths are derived from greater depth than other xenoliths in the Cordillera and/or that the geotherm is variable.

At Lightning Peak, pargasitic amphibole has been observed in a spinel lherzolite xenolith. This represents the first documentation of a hydrous mineral in the upper mantle beneath the Canadian Cordillera. The amphibole is in textural and chemical equilibrium with the other phases in the xenolith and may have

formed as a result of metasomatism of the upper mantle beneath this region. Melting textures observed within the amphibole may be evidence of in-situ partial melting in the upper mantle or may be due to melting during decompression and incorporation of the xenolith within the host basalt. Partial melting of an amphibole-bearing spinel lherzolite may be one method of generating the Late Cenozoic alkali basaltic magmas in the Canadian Cordillera.

A preliminary investigation of a suite of ultramafic xenoliths from western Alaska suggests that the upper mantle beneath this locality is anhydrous and is dominated by depleted spinel lherzolite. However, two xenoliths have been observed, in which each of the four mineral phases are more iron-rich than normal. These xenoliths may either be high pressure cumulates or represent upper mantle which has exchanged with a metasomatic fluid. The latter origin is favoured because of the pervasive metasomatism documented at Nunivak Island.

An experimental study of the dissolution rates of the major anhydrous upper minerals in an alkali basalt melt at high pressure indicates that the relative dissolution rates of the minerals at any pressure are governed by the liquidus phase relationships of the basalt. At low pressure, olivine dissolves most slowly; at high pressure clinopyroxene has the slowest

dissolution rate. Dissolution is a steady-state process in these experiments and is brought about by diffusion of mineral components away from the crystal/melt interface. However, diffusion coefficients calculated from the concentration profiles in the glass appear to depend on the dissolution rate of the mineral. Thus, a knowledge of the speciation involved in melt diffusion is important for obtaining diffusivities from dissolution experiments in such a complex system. A model that predicts the dissolution rates of peridotite and pyroxenite xenoliths in alkali basalt magmas indicates that there is little xenolith digestion during the supposed rapid ascent of alkali basalt magmas, and there is only likely to be preferential dissolution of pyroxenite relative to peridotite only if the magma is generated at low pressure.

B. Conclusions

The nature of the Cordilleran upper mantle

The evidence from ultramafic xenolith studies indicate that the upper mantle beneath the Canadian Cordillera is heterogeneous on a scale of centimeters to meters (e.g., Fujii and Scarfe, 1982; Scarfe et al., 1982). The composition of the upper mantle is predominantly anhydrous chrome diopside-bearing spinel

lherzolite, with minor proportions of dunite, harzburgite, wehrlite, pyroxenite and websterite (e.g., Littlejohn and Greenwood, 1974; Fiesinger and Nicholls, 1977; Fujii and Scarfe, 1982; Nicholls et al., 1982). Amphibole has only been discovered at only one locality in southern British Columbia. The range in chemical compositions of the constituent minerals are olivine ($Fo_{\sim 90}$), orthopyroxene ($En_{\sim 90}$), chrome diopside (Na_2O > 1.0 wt%, TiO_2 < 1.0 wt%, Al_2O_3 2.0-7.0 wt%), aluminous augite (Na_2O < 0.5 wt%, TiO_2 > 1.0 wt%, Al_2O_3 > 10.0 wt%), spinel (Cr_2O_3 0-40.0 wt%, Al_2O_3 25.0-64.0 wt%, Mg/(Mg+Fe) 0.7-0.85).

Equilibration temperatures calculated using the empirical two-pyroxene geothermometer of Wells (1977) range from 850-1150°C. The temperatures of the xenoliths from the Yukon, northern and southern British Columbia are relatively constant (950-1000°C); whereas those in central British Columbia are extremely variable. The conclusion to be drawn is that the temperatures in the northern and southern Cordillera represent the predominant geotherm and that the xenoliths are incorporated within the host magmas from a restricted depth range. This may also indicate that many of the magmas are generated from a common depth. The variable temperature distribution recorded by the xenoliths from central British Columbia may be rationalized either by local perturbations in the

geotherm as a result of recent volcanism in that area or by magmas sampling a different depth range at each locality. The lack of a suitable geobarometer for spinel-bearing xenoliths precludes a definitive answer to the problem.

Ultramafic xenolith survival

Ultramafic xenoliths have been commonly used in experimental studies to determine both the subsolidus high pressure phase relationships of the upper mantle and the pressure and temperature of origin of basalts and their compositions (e.g., Takahashi and Kushiro, 1983; Fujii and Scarfe, 1985). Therefore, it is important to have a knowledge of the stability of ultramafic xenoliths (the mantle sample) as they are brought to the surface in magmas.

The results determined in this thesis indicate that the mineralogical varieties of ultramafic xenoliths that are observed at the surface are generally representative of their relative proportions in the upper mantle. However, this statement depends on a number of criteria being met:

1. the ascending magma is not superheated to a great degree
2. The ascent rate of the magma is rapid (>1km/hr)
3. the magma is not generated at low pressure (<10 kbar).

In many cases, these three restrictions may be satisfied; however, this work should be extended to other melt compositions, both alkali basalts and other mantle-derived melts in order to quantify the survival of the mantle sample. Further work is also required on the ascent rates, times and cooling regimes of magmas as they rise to the Earth's surface.

Bibliography

Aoki, K. and Kushiro, I. (1968) Some clinopyroxenes from ultramafic inclusions in Dreiser Weiher, Eifel. Contrib. Mineral. Petrol. 18, 326-337.

Bailey, D.K. (1982) Mantle metasomatism - continuing chemical change within the Earth. Nature 296, 525-530.

Basaltic Volcanism Study Project (1981) Basaltic Volcanism on the Terrestrial Planets. Pergamon Press, New York.

Best, M.G. (1974) Mantle-derived amphibole within inclusions in alkalic-basaltic lavas. J. Geophys. Res. 79, 2107-2113.

Boettcher, A.L., O'Neil, J.R., Windom, K.E., Stewart, D.G. and Wilshire, H.G. (1979) Metasomatism of the upper mantle and the genesis of kimberlites and alkali basalts. In The mantle sample: inclusions in kimberlites and other volcanics. (Boyd, F.R. and Meyer, H.O.A. eds.), Amer. Geophys. Union, Washington, D.C., pp. 173-182.

Boettcher, A.L. and O'Neil, J.R. (1980) Stable isotope,

chemical and petrographic studies of high-pressure amphiboles and micas: evidence for metasomatism in the mantle source regions of alkali basalts and kimberlites. Amer. J. Sci. 280-A, 594-621.

Bond, W. (1951) Making small spheres. Rev. Sci. Instrum. 22, 344-345.

Boyd, F.R. and England, J.L. (1960) Apparatus for phase equilibria measurements at pressures up to 50 kilobars and temperatures to 1750°C. J. Geophys. Res. 65, 741-748.

Brearley, M., Fujii, T. and Scarfe, C.M. (1982) The petrology and geochemistry of ultramafic nodules from Summit Lake, near Prince George, British Columbia. Geol. Assoc. Canada/Min. Assoc. Canada, Progr. Abstr. 7, 40.

Bultitude, R.J. and Green, D.H. (1971) Experimental study of crystal-liquid relationships at high pressures in olivine nephelinite and basanite compositions. J. Petrol. 12, 121-147.

Carmichael, I.S.E., Turner, F.J. and Verhoogen, J. (1974) Igneous Petrology. McGraw-Hill, New York.

Carslaw, H.S. and Jaeger, J.C. (1959) Conduction of Heat in Solids. Oxford University Press.

Carswell, D.A. and Dawson, J.B. (1970) Garnet peridotite xenoliths in South African kimberlite pipes and their petrogenesis. Contrib. Mineral. Petrol. 25, 163-184.

Chapman, N.A. (1976) Inclusions and megacrysts from undersaturated tuffs and basanites, East Fife, Scotland. J. Petrol. 16, 472-498.

Chekhmir, A.S. and Epel'baum, M.B. (1985) Experimental study of the diffusion processes in magmatic melts. In Physical Chemistry of Magmas (Perchuk, L.L. and Kushiro, I. Eds.) (in press)

Cooper, A.R. (1962) Effect of moving boundary on molecular diffusion controlled dissolution or growth kinetics. Trans. Farad. Soc. 58, 2468-2472.

Cooper, A.R. and Kingery, W.C. (1964) Dissolution in ceramic systems: I, molecular diffusion, natural convection, and forced convection of sapphire dissolution in calcium aluminum silicate. J. Amer. Ceram. Soc. 47, 37-43.

Cooper, A.R. and Schut, R.J. (1980) Analysis of transient dissolution in $CaO-Al_2O_3-SiO_2$. Metall. Trans. 11B, 373-376.

Crank, J. (1975) The Mathematics of Diffusion. (2nd. Ed.) Oxford University Press.

Dawson, J.B. (1980) Kimberlites and Their Xenoliths. Springer-Verlag, Berlin.

Dawson, J.B. (1981) The nature of the upper mantle. Mineral. Mag. 44, 1-18.

Dawson, J.B. and Smith, J.V. (1982) Upper-mantle amphiboles: a review. Mineral. Mag. 45, 35-46.

Delaney, J.S., Smith, J.V., Carswell, D.A. and Dawson, J.B. (1980) Chemistry of micas from kimberlites and xenoliths - II. Primary- and secondary-textured micas from peridotite xenoliths. Geochim. Cosmochim. Acta 44, 857-872.

Dodson, M.H. (1973) Closure temperature in cooling geochronological and petrological systems. Contrib. Mineral. Petrol. 40, 259-274.

Donaldson, C.H. (1984a) Crystal dissolution rates in a

basaltic melt. In Progress in Experimental Petrology. N.E.R.C., 174-175.

Donaldson, C.H. (1984b) Textures resulting from partial crystal dissolution in basaltic melt. In Progress in Experimental Petrology N.E.R.C., 175-177.

Donaldson, C.H. (1984c) Kinetics of pyrope megacryst reactions in ascending basaltic magma -relevance to high-pressure magmatic crystallization at Elie Ness, East Fife. Geol. Mag. 121, 615-620.

Eggler, D.H. (1978) The effect of CO_2 upon partial melting of peridotite in the system Na_2O-CaO-Al_2O_3-MgO-SiO_2-CO_2 to 35 kb, with an analysis of melting in a peridotite-H_2O-CO_2, system. Amer. J. Sci. 278, 305-343.

Elthon, D. and Scarfe, C.M. (1984) High-pressure phase equilibria of a high magnesia basalt and the genesis of primary oceanic basalts. Amer. Mineral. 69, 1-15.

Epstein, P.S. and Plesset, M.S. (1950) On the stability of gas bubbles in liquid-gas solutions. J. Chem. Phys. 18, 1505-1509.

Evans, B.W. (1982) Amphiboles in metamorphosed ultramafic rocks. In Amphiboles: Petrology and Experimental Phase Relations (Veblen, D.R. and Ribbe, P.H. eds.) Reviews in Mineralogy, 9B. Min. Soc. Amer., Washington, D.C., pp. 98-113.

Fiesinger, D.W. (1975) Petrology of the Quaternary volcanic centers in the Quesnel Highlands and Garibaldi Provincial Park areas, British Columbia. Ph.D. thesis, Univ. Calgary, Calgary, Alberta.

Fiesinger, D.W. and Nicholls, J. (1977) Petrography and petrology of Quaternary volcanic rocks, Quesnel Lake region, East-Central British Columbia. In Volcanic Regimes in Canada. (Baragar, W.R.A. et al. eds.) Geol. Assoc. Canada Spec. Pap., 16, pp. 25-38.

Francis, D.M. (1976a) The origin of amphibole in lherzolite xenoliths from Nunivak Island, Alaska. J. Petrol. 17, 357-378.

Francis, D.M. (1976b) Amphibole pyroxenite xenoliths: cumulate or replacement phenomena from the upper mantle, Nunivak Island, Alaska. Contrib. Mineral. Petrol. 58, 51-61.

Frey, F.A. and Prinz, M. (1978) Ultramafic inclusions from San Carlos, Arizona: Petrologic and geochemical data bearing on their petrogenesis. Earth Planet. Sci. Lett. 38, 129-176.

Fujii, T. (1976) Solubility of Al_2O_3 in enstatite coexisting with forsterite and spinel. Carnegie Inst. Wash. Yb. 75, 566-571.

Fujii, T. (1977) Pyroxene equilibria in spinel lherzolite. Carnegie Inst. Wash. Yb. 76, 569-572.

Fujii, T. and Scarfe, C.M. (1982) Petrology of ultramafic nodules from West Kettle River, near Kelowna, southern British Columbia. Contrib. Mineral. Petrol. 80, 297-306.

Fujii, T. and Scarfe, C.M. (1985) Composition of liquids coexisting with spinel lherzolite at 10 kbar and the genesis of MORBs. Contrib. Mineral. Petrol. 90, 18-28.

Gerlach, D.C. and Grove, T.L. (1982) Petrology of the Medicine Lake Highland volcanics: characterization of the endmembers of magma mixing. Contrib. Mineral. Petrol. 80, 147-159.

Gilbert, M.C., Helz, R.T., Popp, R.K. and Spear, F.S. (1982) Experimental studies of amphibole stability. In Amphiboles: Petrology and Experimental Phase Relations. (Veblen, D.R. and Ribbe, P.H. eds.) Reviews in Mineralogy, 9B, Min. Soc. Amer., Washington, D.C. pp. 229-346.

Green, T.H. and Ringwood, A.E. (1968) Genesis of the calc-alkaline igneous rock suite. Contrib. Mineral. Petrol. 18, 105-162.

Hamilton, T.S. (1981) Late Cenozoic alkaline volcanics of the Level Mountain Range, northwestern British Columbia: geology, petrology and paleomagnetism. Ph.D. thesis, Univ. Alberta, Edmonton, Alberta.

Harris, D.M. (1981) The microdetermination of H_2O, CO_2, and SO_2 in glass using a 1280°C microscope vacuum heating stage, cryopumping, and vapor pressure measurements from 77 to 273 K. Geochim. Cosmochim. Acta 45, 2023-2036.

Harrison, T.M. and Watson, E.B. (1983) Kinetics of zircon dissolution and zirconium diffusion in granitic melts of variable water content. Contrib. Mineral. Petrol. 84, 66-72.

Harrison, T.M. and Watson, E.B. (1984) The behavior of apatite during crustal anatexis: equilibrium and kinetic considerations. Geochim. Cosmochim. Acta 48, 1467-1477.

Hawkesworth, C.J. and Norry, M.J. (1983) Continental Basalts and Mantle Xenoliths. Shiva Publishing, Cheshire, U.K.

Henry, D.T. and Medaris, L.G. (1980) Application of pyroxene and olivine-spinel geothermometers to spinel peridotites in southwestern Oregon. Amer. J. Sci. 280-A, 211-231.

Herzberg, C.T. (1985) Internal structures of the Earth and terrestrial planets: constraints from ultrahigh pressure magma density and phase equilibrium relations. In Silicate Melts: their Properties and Structure applied to problems in Geochemistry, Petrology, Economic Geology and Planetary Geology. (Scarfe, C.M. ed.) Min. Assoc. Short Course Handbook (in prep.)

Hibbard, M.J. (1981) The magma mixing origin of mantled feldspars. Contrib. Mineral. Petrol. 76, 158-170.

Holloway, J.R. (1973) The system pargasite-H_2O-CO_2: a

model for melting of a hydrous mineral with a mixed-volatile fluid - I. Experimental results to 8 kbar. Geochim. Cosmochim. Acta 37, 651-666.

Hunter, R.H. and Taylor, L.A. (1982) Instability of garnet from the mantle: glass as evidence of metasomatic melting. Geology 10, 617-620.

Irvine, T.N. and Baragar, W.R.A. (1971) A guide to the chemical classification of the common volcanic rocks. Can. J. Earth Sci. 8, 523-548.

Irving, A.J. (1980) Petrology and geochemistry of composite ultramafic xenoliths in alkalic basalts and implications for magmatic processes within the mantle. Amer. J. Sci. 280-A, 389-426.

Ito, E., Harris, D.M. and Anderson, A.T. (1983) Alteration of oceanic crust and geologic cycling of chlorine and water. Geochim. Cosmochim. Acta 47, 1613-1624.

Jackson, E.D. and Wright, T.L. (1970) Xenoliths in the Honolulu Volcanic Series, Hawaii. J. Petrol. 11, 405-430.

Jenkins, D.M. (1983) Stability and composition

relations of calcic amphiboles in ultramafic rocks. Contrib. Mineral. Petrol. 83, 375-384.

Kuno, H. and Aoki, K. (1970) Chemistry of ultramafic nodules and their bearing on the origin of basaltic magmas. Phys. Earth Planet. Inter. 3, 273-301.

Kuo, L-C. and Kirkpatrick, R.J. (1985) Kinetics of crystal dissolution in the system diopside-forsterite-silica. Amer. J. Sci. 285, 51-90.

Kushiro, I., Yoder, H.S. and Mysen, B.O. (1976) Viscosities of basalt and andesite melts at high pressures. J. Geophys. Res. 81, 6351-6356.

Kutolin, V.A. and Agafonov, L.V. (1978) Composition of the upper mantle in light of the relative stability of ultramafic nodules. Geologiya i Geofiz. 19(5), 3-13.

Kutolin, V.A. and Frolova, V.M. (1970) Petrology of ultrabasic inclusions from basalts of Minusa and Transbaikalian regions (Siberia, USSR). Contrib. Mineral. Petrol. 29, 163-79.

Leake, B.E. (1978) Nomenclature of amphiboles. Can. Mineral. 16, 501-520.

Lindsley, D.H. (1983) Pyroxene thermometry. Amer. Mineral. 68, 477-493.

Lindsley, D.H. and Andersen, D.J. (1983) A two-pyroxene thermometer. Proc. 13th. Lunar Planet. Sci. Conf., J. Geophys. Res. 88, A887-9.

Lindsley, D.H., Grover, J.E. and Davidson, P.M. (1981) The thermodynamics of the $Mg_2Si_2O_6$-$CaMgSi_2O_6$ join: a review and an improved model. In Thermodynamics of Minerals and Melts (Newton, R.C. et al. eds.) Springer, New York, pp 149-176.

Littlejohn, A.L. and Greenwood, H.J. (1974) Lherzolite nodules in basalts from British Columbia, Canada. Can. J. Earth Sci. 11, 1288-1308.

Maaløe, S. and Printzlau, I. (1979) Natural partial melting of spinel lherzolite. J. Petrol. 20, 727-741.

MacDonald, G.A. and Katsura, T. (1964) Chemical composition of Hawaiian lavas. J. Petrol. 5, 82-133.

McBirney, A.R. and Murase, T. (1984) Rheological properties of magmas. Ann. Rev. Earth Planet. Sci. 12, 337-357.

Mercier, J.C. (1976) Single-pyroxene geothermometry and geobarometry. Amer. Mineral. 61, 603-615.

Mercier, J.C. (1980) Single-pyroxene thermobarometry. Tectonophysics 70, 1-37.

Mercier, J.C. and Nicolas, A. (1975) Textures and fabrics of upper mantle peridotites as illustrated by xenoliths from basalts. J. Petrol. 16, 454-487.

Min, S. (1985) Sr isotopic study of ultramafic nodules from Neogene alkaline lavas of British Columbia, Canada and Josephine Peridotite, southwestern Oregon, U.S.A. M.Sc. thesis, Univ. British Columbia, Vancouver, British Columbia.

Mori, T. and Kanehira, K. (1984) X-ray energy spectrometry for electron-probe analysis. Jour. Geol. Soc. Japan 90, 271-285.

Nickel, K.G., Brey, G.P. and Ryabchikov, I. (1985) High-pressure geothermobarometry for natural systems. EOS Trans. Amer. Geophys. Union 66, 413.

Nickel, K.G. and Green, D.H. (1985) Empirical geothermobarometry for garnet peridotites and implications for the nature of the lithosphere, kimberlites and diamonds. Earth Planet. Sci. Lett. 73, 158-170.

Nicholls, J., Stout, M.Z. and Fiesinger, D.W. (1982) Petrologic variations in Quaternary volcanic rocks, British Columbia, and the nature of the underlying mantle. Contrib. Mineral. Petrol. 79, 201-218.

Nixon, P.H. and Boyd, F.R. (1979) Garnet-bearing lherzolites and discrete nodule suites from the Malaita alnoite, Solomon Islands, South West Pacific, and their bearing on oceanic mantle composition and geotherm. In The mantle samples inclusions in kimberlites and other volcanics. (Boyd, F.R. and Meyer, H.O.A. eds.). Amer. Geophys. Union, Washington, D.C. pp. 400-423.

Ozawa, K. (1983) Evaluation of olivine-spinel geothermometry as an indicator of thermal history for peridotites. Contrib. Mineral. Petrol. 82, 52-65.

Ranalli, G. (1980) Rheological properties of the upper

mantle in Canada from olivine microrheology. Can. J. Earth Sci. 17, 1499-1505.

Rapp, R.P. and Watson, E.B. (1985) Solubility and dissolution behavior of monazite and LREE diffusion in a hydrous granitic melt, EOS Trans. Amer. Geophys. Union 66, 416.

Reed, S.J.B. and Ware, N.G. (1973) Quantitative electron microprobe analysis using a lithium drifted silicon detector. X-ray Spectrom. 2, 69-74.

Roden, M.F., Frey, F.A. and Francis, D.M. (1984) An example of consequent mantle metasomatism in peridotite inclusions from Nunivak Island, Alaska. J. Petrol. 25, 546-577.

Ross, J.V. (1983) The nature and rheology of the Cordilleran upper mantle of British Columbia: inferences from peridotite xenoliths. Tectonophysics 100, 321-357.

Sakuyama, M. (1981) Petrological study of the Myoko and Kurohime volcanoes, Japan: crystallization sequence and evidence for magma mixing. J. Petrol. 22, 553-583.

Scarfe, C.M. (1981) The pressure dependence of the viscosity of some basic melts. Carnegie Inst. Wash. Yb. 80, 336-339.

Scarfe, C.M., Takahashi, E. and Yoder, H.S. (1980) Rates of dissolution of upper mantle minerals in an alkali-olivine basalt melt at high pressures. Carnegie Inst. Wash. Yb. 79, 290-296.

Scarfe, C.M., Fujii, T. and Brearley, M. (1982) Heterogeneities in the upper mantle beneath south and central British Columbia. EOS Trans. Amer. Geophys. Union 63, 463.

Shaw, H.R. (1972) Viscosities of magmatic liquids: an empirical method of prediction. Amer. J. Sci. 272, 870-893.

Sinclair, P.D., Tempelman-Kluit, D.J. and Medaris, L.G. (1978) Lherzolite nodules from a Pleistocene cinder cone in central Yukon. Can. J. Earth Sci. 15, 220-226.

Smith, D. and Roden, M.F. (1981) Geothermometry and kinetics in a two-spinel peridotite nodule, Colorado Plateau. Amer. Mineral. 66, 334-346.

Smith, D.G.W. (1976) Quantitative energy dispersive microanalysis. In Short Course in Microbeam Techniques. (Smith, D.G.W. ed.) Min. Assoc. Canada Short Course Handbook 1, 63-106.

Smith, D.G.W. and Gold, C.M. (1979) EDATA2: A FORTRAN IV computer program for processing wavelength- and/or energy-dispersive microprobe analyses. In Proc. 14th Ann. Conf. Microbeam Anal. Soc., San Antonio, Texas. (Newbury, D.E. ed.) pp. 273-278.

Smith, J.V., Delaney, J.S., Hervig, R.L. and Dawson, J.B. (1981) Storage of F and Cl in the upper mantle: geochemical implications. Lithos 14, 133-147.

Smith, V.G., Tiller, W.A. and Rutter, J.W. (1955) A mathematical analysis of solute redistribution during solidification. Can. J. Phys. 33, 723-745.

Sneeringer, M., Hart, S.R. and Shimizu, N. (1984) Strontium and samarium diffusion in diopside. Geochim. Cosmochim. Acta 48, 1589-1608.

Souther, J.G. (1977) Volcanism and tectonic environments in the Canadian Cordillera - a second look. In Volcanic Regimes in Canada. (Baragar,

W.R.A. et al. eds.), Geol. Assoc. Canada Spec. Pap. 16, 3-24.

Spera, F.J. (1984) Carbon dioxide in petrogenesis III: role of volatiles in the ascent of alkaline magma with special reference to xenolith-bearing mafic lavas. Contrib. Mineral. Petrol. 88, 217-232.

Swanson, S.E., Turner, D.L., Forbes, R.B. and Hopkins, D.M. (1981) Petrology and geochronology of Tertiary and Quaternary basalts from the Seward Peninsula, western Alaska. Geol. Soc. Amer. Progr. Abstr., 13, 563.

Swanson, S.E., Mahlburg Kay, S.M., Brearley, M. and Scarfe, C.M. (1985) Mantle xenoliths - Pacific Plate and surrounding regions - Kurile-Kamchatka and western Alaska. In Mantle Xenoliths (Nixon, P.H. ed.) (in press)

Takahashi, E. (1980a) Thermal history of lherzolite xenoliths-I. Petrology of lherzolite xenoliths from the Ichinomegata Crater, Oga peninsula, North East Japan. Geochim. Cosmochim. Acta 44, 1643-1658.

Takahashi, E. (1980b) Melting relations of an

alkali-olivine basalt to 30 kbar and their bearing on the origin of alkali basalt magmas. Carnegie Inst. Wash. Yb. 79, 271-276.

Takahashi, E. and Kushiro, I. (1983) Melting of a dry peridotite at high pressures and basalt magma genesis. Amer. Mineral. 68, 859-879.

Takahashi, E. and Scarfe, C.M. (1985) Melting of peridotite to 14 GPa and the genesis of komatiite. Nature 315, 566-568.

Thompson, R.N. and Kushiro, I. (1972) The oxygen fugacity within graphite capsules in piston-cylinder apparatus at high pressures. Carnegie Inst. Wash. Yb. 71, 615-616.

Thornber, C.R. and Huebner, J.S. (1985) Dissolution of olivine in basaltic liquids: experimental observations and applications. Amer. Mineral. 70, 934-945.

Tsuchiyama, A. (1985a) Dissolution kinetics of plagioclase in the melt of the system diopside-albite-anorthite, and the origin of dusty plagioclase in andesites. Contrib. Mineral. Petrol. 89, 1-16.

Tsuchiyama, A. (1985b) Experimental study of olivine-melt reaction and its petrological implications. J. Geophys. Res. (submitted)

Tsuchiyama, A. (1985c) Melting and dissolution kinetics: some petrological applications. J. Volc. Geotherm. Res. (submitted)

Varne, R. (1968) The petrology of Moroto Mountain, Eastern Uganda, and the origin of nephelinites. J. Petrol. 9, 169-190.

Varne, R. (1970) Hornblende lherzolite and the upper mantle. Contrib. Mineral. Petrol. 27, 45-51.

Watson, E.B. (1982) Basalt contamination by continental crust: some experiments and models. Contrib. Mineral. Petrol. 80, 73-87.

Watson, E.B. (1985) Chemical diffusion in magmas: an overview of experimental results and geochemical applications. In Physical Chemistry of Magmas (Perchuk, L.L. and Kushiro, I. Eds.) (in press)

Wells, P.R.A. (1977) Pyroxene thermometry in simple and complex systems. Contrib. Mineral. Petrol. 68, 129-139.

Wilkinson, J.F.G. and Binns, R.A. (1977) Relatively iron-rich lherzolite xenoliths of the Cr-diopside suite: a guide to the primary nature of anorogenic tholeiitic andesite magmas. Contrib. Mineral. Petrol. 65, 199-212.

Wilshire, H.G. and Binns, R.A. (1961) Basic and ultrabasic xenoliths from volcanic rocks of New South Wales. J. Petrol. 2, 185-208.

Wilshire, H.G. and Shervais, J.W. (1975) Al-augite and Cr-diopside ultramafic xenoliths in basaltic rocks from Western United States. In Physics and Chemistry of the Earth. (Ahrens, L.H. et al. eds.) Pergamon Press. 9, pp. 257-272.

Wilshire, H.G., Pike, J.E.N., Meyer, C.E. and Schwarzmann, E.C. (1980) Amphibole-rich veins in lherzolite xenoliths, Dish Hill and Deadman Lake, California. Amer. J. Sci. 280-A, 576-593.

Wilson, A.D. (1960) The micro-determination of ferrous iron in silicate minerals by a volumetric and colorimetric method. Analyst 85, 823-828.

Wood, B.J. and Banno, S. (1973) Garnet-orthopyroxene and orthopyroxene-clinopyroxene relationships in

simple and complex systems. Contrib. Mineral. Petrol. 42, 109-124.

Yoder, H.S. (1976) Generation of Basaltic Magma. National Academy of Sciences, Washington, D.C.